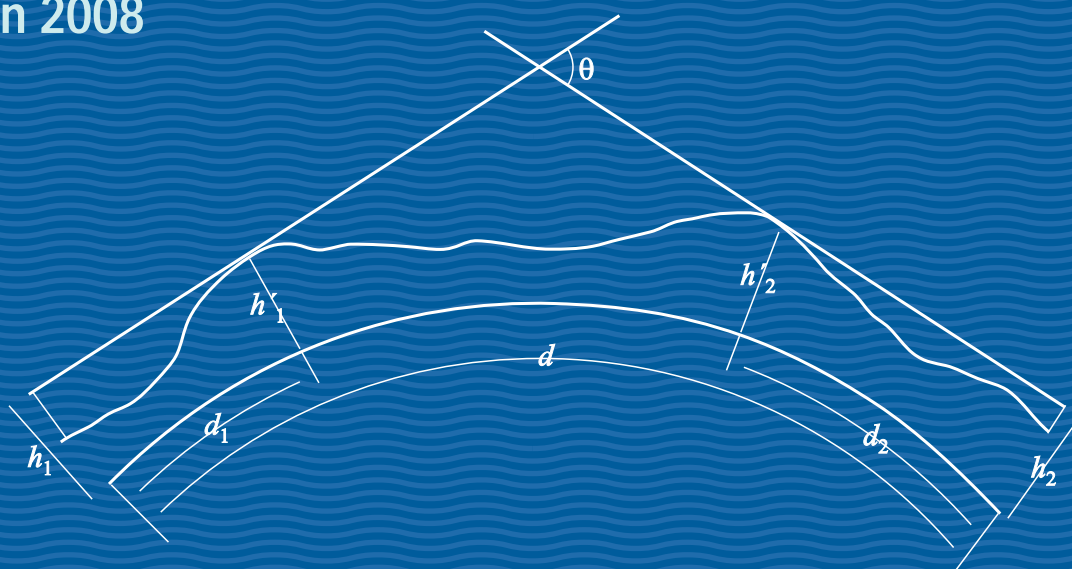


# Handbook

RADIOWAVE PROPAGATION INFORMATION  
FOR DESIGNING TERRESTRIAL  
POINT-TO-POINTS LINKS

Edition 2008



## THE RADIOCOMMUNICATION SECTOR OF ITU

The role of the Radiocommunication Sector is to ensure the rational, equitable, efficient and economical use of the radio-frequency spectrum by all radiocommunication services, including satellite services, and carry out studies without limit of frequency range on the basis of which Recommendations are adopted.

The regulatory and policy functions of the Radiocommunication Sector are performed by World and Regional Radiocommunication Conferences and Radiocommunication Assemblies supported by Study Groups.

### **Inquiries about radiocommunication matters**

*Please contact:*

ITU  
Radiocommunication Bureau  
Place des Nations  
CH -1211 Geneva 20  
Switzerland

Telephone:	+41 22 730 5800
Fax:	+41 22 730 5785
E-mail:	brmail@itu.int
Web:	<a href="http://www.itu.int/itu-r">www.itu.int/itu-r</a>

### **Placing orders for ITU publications**

*Please note that orders cannot be taken over the telephone. They should be sent by fax or e-mail.*

ITU  
Sales and Marketing Division  
Place des Nations  
CH -1211 Geneva 20  
Switzerland

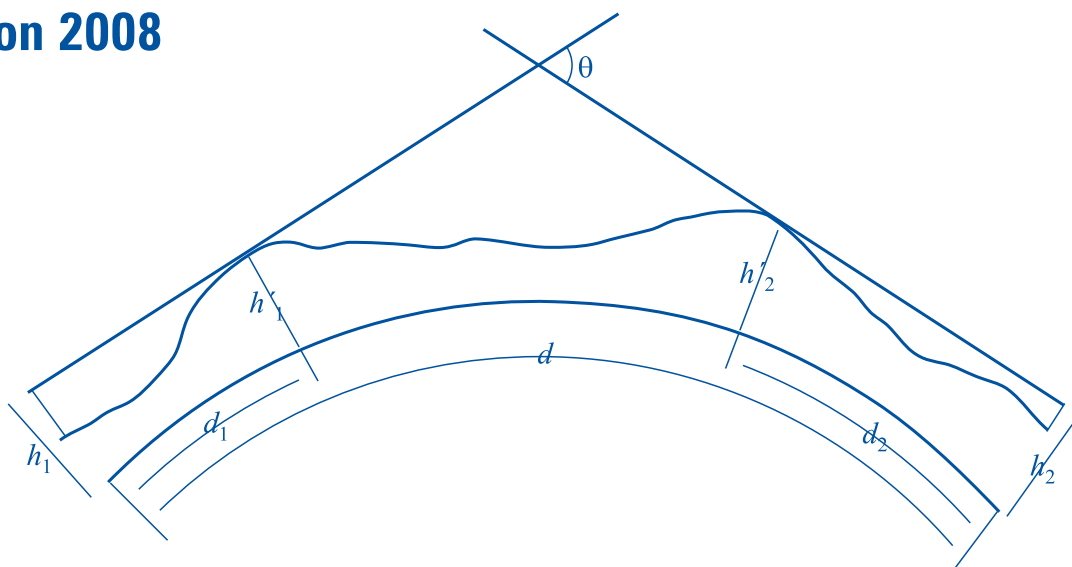
<b>Fax:</b>	<b>+41 22 730 5194</b>
<b>E-mail:</b>	<b><a href="mailto:sales@itu.int">sales@itu.int</a></b>

<b>The Electronic Bookshop of ITU:</b>	<b><a href="http://www.itu.int/publications">www.itu.int/publications</a></b>
--	---

# Handbook

RADIOWAVE PROPAGATION INFORMATION  
FOR DESIGNING TERRESTRIAL  
POINT-TO-POINTS LINKS

Edition 2008





## **FOREWORD**

Terrestrial radio links are forming a vital part of the telecommunications infrastructure in most countries of the world. Correct dimensioning with respect to radiowave propagation effects is of crucial importance for the performance of the network and quality of services supported, and of vital economical value by using the electromagnetic spectrum in the most efficient manner.

This Handbook provides background information, scientific references and guide material on radiowave propagation effects for line-of-sight links, troposcatter and trans-horizon links as well as free-space optical links. It is intended to be used in conjunction with the Recommendations that are maintained by Radiocommunication Study Group 3 to assist in the design of terrestrial point-to-point links.

Bertram Arbesser-Rastburg

Chairman, Radiocommunication Study Group 3



## TABLE OF CONTENTS

		<i>Page</i>
FOREWORD.....		iii
INTRODUCTION.....		1
ACKNOWLEDGEMENTS .....		2
 <b>PART 1 – LINE-OF-SIGHT LINKS</b> .....		 3
1	INTRODUCTION.....	3
2	TYPICAL APPLICATIONS .....	3
3	BASIC PROPAGATION EFFECTS .....	4
3.1	Free-space loss.....	4
3.2	Attenuation due to atmospheric gases .....	4
3.3	Diffraction fading and path clearance.....	5
3.3.1	Basis of the prediction method for diffraction loss.....	5
3.3.2	Basis of procedures for determining path clearance .....	5
3.4	Scintillation fading.....	7
3.5	Summary of propagation mechanisms associated with multipath fading.....	7
4	ATTENUATION DUE TO PRECIPITATION AND OTHER ATMOSPHERIC PARTICLES...	8
4.1	Attenuation due to precipitation .....	8
4.1.1	Basis of the prediction method for rain attenuation.....	8
4.1.2	Specific attenuation .....	9
4.1.3	Effective path length.....	10
4.1.4	Application examples .....	10
4.1.5	Prediction of combined rain and wet snow.....	11
4.1.6	Long-term frequency and polarization scaling of rain attenuation statistics .....	14
4.1.6.1	Single-frequency scaling .....	14
4.1.6.2	Polarization scaling.....	14
4.1.7	Statistics of duration and rate of rain induced fading .....	14
4.1.8	Seasonal variations – worst-month .....	15
4.1.9	Discussion of model evaluation (testing).....	16
4.1.10	Example of calculation .....	16
4.2	Tandem and convergent links .....	17
4.2.1	Correlated fading on tandem paths .....	17
4.2.2	Convergent paths .....	18
4.3	Paths with passive repeaters .....	19
5	MULTIPATH FADING AND ENHANCEMENT AT A SINGLE FREQUENCY .....	19
5.1	Prediction of the fading/enhancement distribution .....	19
5.1.1	Basis and accuracy of Methods 1 and 2.....	19
5.1.1.1	The full distribution derived from the tail .....	19

	<i>Page</i>
5.1.1.2	Determining the multipath fading distribution tail ..... 20
5.1.1.3	Accuracy of the method for deep fade distribution tail ..... 22
5.1.2	Basis and accuracy of the method for shallow fading ..... 23
5.1.3	Basis and accuracy of the method for enhancement range ..... 23
5.1.4	Application examples ..... 24
5.2	Statistics on fade number and duration ..... 25
5.2.1	Estimation procedures ..... 25
5.2.2	Experimental basis of the estimation procedures ..... 26
5.3	Rate of change of signal level ..... 26
5.4	Short paths ..... 26
5.5	Short periods of time ..... 27
5.6	Tandem links ..... 28
6	PROPAGATION-INDUCED DISTORTION ..... 28
6.1	Multipath propagation models ..... 28
6.1.1	Hypothetical ray models ..... 29
6.1.2	Polynomial models ..... 29
6.1.3	Parametric models ..... 29
6.2	Performance calculation ..... 29
6.2.1	Signature curve methods ..... 30
6.2.2	Fade margin methods ..... 32
6.2.3	Method using linear amplitude dispersion (LAD) statistics ..... 32
7	REDUCTION IN CROSS-POLARIZATION DISCRIMINATION ..... 34
7.1	Channel model ..... 34
7.1.1	Nominal received field ..... 36
7.1.2	XPI due to propagation (1 ray approach) ..... 36
7.1.2.1	Clear air conditions ..... 37
7.1.2.2	Rain conditions ..... 37
7.1.3	XPI due to multipath propagation (2 rays) ..... 38
7.1.4	Co-polar attenuation dependence ..... 38
7.2	Prediction of XPD statistics during clear air conditions ..... 39
7.2.1	Description of Method $Q$ ..... 40
7.2.2	Application examples ..... 41
7.3	Prediction of XPD statistics during precipitation conditions ..... 42
7.3.1	Basis of prediction methods of XPD during precipitation ..... 42
7.3.2	Application examples ..... 43
7.4	Relative effects of XPD deterioration in clear-air and rain conditions ..... 43
7.5	Cross-polarization due to sand and dust storms ..... 44

8	MULTIPATH-PROPAGATION RELATED ALLEVIATION TECHNIQUES .....	44
8.1	Non-diversity strategies and techniques .....	44
8.1.1	Increasing path inclination.....	45
8.1.2	Reduction of the effect of surface reflections .....	45
8.1.2.1	Shielding of the reflection point .....	46
8.1.2.2	Moving of reflection point to poorer reflecting surface.....	46
8.1.2.3	Optimum choice of antenna heights .....	46
8.1.2.4	Choice of vertical polarization.....	46
8.1.2.5	Use of antenna discrimination .....	46
8.1.3	Reduction of path clearance.....	47
8.2	Diversity techniques .....	47
8.2.1	Space diversity .....	48
8.2.2	Antenna spacing in space diversity systems .....	48
8.2.3	Angular spacing in angle-diversity and combined space/angle-diversity systems ...	48
8.2.4	Space-diversity improvement in narrow-band systems .....	50
8.2.5	Frequency diversity .....	50
8.2.5.1	Frequency-diversity improvement factor for narrow-band 1 + 1 systems.....	50
8.2.5.2	Frequency-diversity improvement factor for narrow-band multi-channel switched ( $n + 1$ ) etc. systems .....	51
8.2.5.3	Application examples .....	51
8.2.6	Polarization-diversity improvement factor for wideband systems .....	52
8.2.7	Relative merits of the various diversity techniques and their combinations.....	53
8.3	Diversity techniques for alleviating reductions in XPD .....	53
	REFERENCES .....	54
	<b>PART 2 – TRANS-HORIZON LINKS .....</b>	<b>61</b>
1	INTRODUCTION.....	61
2	TYPICAL APPLICATIONS .....	61
3	BASIC THEORY .....	61
3.1	Diffraction.....	62
3.1.1	Diffraction over a smooth spherical Earth.....	62
3.1.2	Diffraction over isolated obstacles .....	63
3.1.3	Diffraction over multiple obstacles.....	63
3.1.4	Diffraction over irregular terrain .....	63
3.2	Tropospheric scatter.....	64
4	PREDICTION OF TRANSMISSION LOSS.....	66
4.1	Diffraction loss .....	67
4.1.1	Diffraction over a spherical Earth.....	67
4.1.2	Knife-edge diffraction .....	68
4.1.3	Single rounded obstacle .....	68
4.1.4	Double knife-edges.....	69

	<i>Page</i>
4.1.5 Multiple isolated obstacle .....	69
4.1.6 Application examples .....	69
4.1.6.1 Spherical earth path .....	69
4.1.6.2 Diffraction over a single obstacle .....	70
4.1.6.3 Diffraction over several obstacles .....	71
4.2 Troposcatter transmission loss .....	73
4.2.1 Path antenna gain .....	74
4.2.2 Application example .....	75
4.2.3 Testing results .....	77
4.2.4 Combined loss and its variability .....	77
4.2.4.1 Effect of frequency .....	77
4.2.4.2 Long-term and short-term transmission loss variations .....	77
4.2.4.3 Seasonal and diurnal variations .....	78
5 PROPAGATION INDUCED DISTORTION .....	79
6 DIVERSITY TECHNIQUES .....	80
6.1 Space diversity .....	80
6.2 Frequency diversity .....	81
6.3 Angle diversity .....	81
6.4 Polarization diversity .....	82
6.5 Time diversity .....	82
6.6 Combining techniques .....	82
6.7 Diversity gain .....	82
REFERENCES .....	84
<b>PART 3 – FREE-SPACE OPTICAL LINKS</b> .....	<b>87</b>
1 INTRODUCTION .....	87
2 INITIAL CONSIDERATIONS IN DESIGNING AN FSO LINK .....	87
3 GEOMETRICAL ATTENUATION .....	88
4 ATMOSPHERIC ATTENUATION DUE TO ABSORPTION AND SCATTERING .....	88
4.1 Clear air attenuation .....	89
4.2 Excess attenuation .....	89
4.2.1 Mie scattering (estimation of fog attenuation) .....	91
4.2.2 Rain attenuation .....	92
4.2.3 Snow attenuation .....	93
5 SCINTILLATION EFFECTS .....	94
6 AMBIENT LIGHT ATTENUATION .....	95
7 OTHER ISSUES .....	96
8 APPLICATION EXAMPLE .....	97
REFERENCES .....	99

## INTRODUCTION

The ITU-R Handbook – Radiowave Propagation Information for Designing Terrestrial Point-to-Point Links supplies background and supplementary information on radiowave propagation effects, and serves as a companion volume and guide to the Recommendations that have been developed by Radiocommunication Study Group 3 to assist in the design of terrestrial communication systems. The relevant ITU-R Recommendations, listed below, contain impairment prediction methods and engineering advice on radiowave propagation for terrestrial line-of-sight (LoS) systems and for trans-horizon radio-relay systems.

This Handbook is one of six Handbooks prepared by Radiocommunication Study Group 3 and is intended to be used in conjunction with the published P-Series ITU-R Recommendations to assist the user in the application of those Recommendations. Listed below are the other Study Group 3 ITU-R Handbooks which cover propagation over the Earth's surface, radiometeorology, Earth-space and land mobile systems, as follows:

- Curves for Radiowave Propagation over the Surface of the Earth.
- Radiometeorology.
- Radiowave Propagation Information for Predictions for Earth-to-space Path Communications.
- Ionosphere and its Effects on Radiowave Propagation.
- Terrestrial land mobile radiowave propagation in the VHF/UHF bands.

Users of the ITU-R Recommendations are advised to consult the appropriate Handbook for their specific requirements.

The terrestrial point-to-point links Handbook is intended for use with P-Series ITU-R Recommendations for LoS systems, trans-horizon radio-relay systems and free-space optical systems. The key ITU-R Recommendations that are referred to throughout this Handbook are:

Recommendation ITU-R P.530-12: Propagation data and prediction methods required for the design of terrestrial line-of-sight systems.

Recommendation ITU-R P.617-1: Propagation prediction techniques and data required for the design of trans-horizon radio-relay systems.

This ITU-R Handbook is linked to the above Recommendations and uses the same terminology, notation, equation numbers, etc. Duplication of the propagation data from those Recommendations is intentionally minimal and the prediction methods themselves are found in the Recommendations. It is recommended of course to use the latest version of the Recommendations for all system calculations.

Proper application of the ITU-R Recommendations for the terrestrial systems requires radiometeorological input and other data from additional ITU-R Recommendations. The other ITU-R Recommendations referred to in this Handbook are:

Recommendation ITU-R P.310-9: Definitions of terms relating to propagation in non-ionized media.

Recommendation ITU-R P.311-12: Acquisition, presentation and analysis of data in studies of tropospheric propagation.

Recommendation ITU-R P.525-2: Calculation of free-space attenuation.

Recommendation ITU-R P.526-10: Propagation by diffraction.

Recommendation ITU-R P.453-9: The radio refractive index: its formula and refractivity data.

Recommendation ITU-R P.676-7: Attenuation by atmospheric gases.

Recommendation ITU-R P.834-6: Effects of tropospheric refraction on radiowave propagation.

Recommendation ITU-R P.837-5: Characteristics of precipitation for propagation modelling.

Recommendation ITU-R P.310-9: Definitions of terms relating to propagation in non-ionized media.

Recommendation ITU-R P.838-3: Specific attenuation model for rain for use in prediction methods.

Recommendation ITU-R P.1814: Prediction methods required for the design of terrestrial free-space optical links”.

## ACKNOWLEDGEMENTS

The Handbook was put together by ITU-R Working Party 3M and based on a number of contributions and open source material, in particular the project COST 235 Final Report. The following persons have in particular been contributors:

ARAPOGLOU, Pantelis-Daniel

ASSIS, Mauro

MIRANDA, Erasmus Couto Brazil de

OLSEN, Roderic L.

ORDANO, Luciano

SATO, Akio

SILVA MELLO, Luiz A.R. da

SIZUN, Herve

TANEM, Torbjørn

TJELTA, Terje

VENTOURAS, Spiridon

ZAFFARONI, Maurizio

ZHANG, Minggao.

**Handbook Editors:** Luiz A.R. da Silva Mello and Terje Tjelta.

*Editor Part 1* – Line-of-sight links: Roderic L. Olsen.

*Editor Part 2* – Trans-horizon links: Mauro Assis.

*Editor Part 3* – Free-space optical links: Spiridon Ventouras.

## PART 1

### LINE-OF-SIGHT LINKS

#### 1 Introduction

This Part of the ITU-R Handbook supplies guidance on propagation-related aspects for the design and operation of line-of-sight radio-relay systems. For more details about system aspects such as principles, design, and operation of line-of-sight radio-relay systems, the ITU-R Handbook – Digital radio-relay systems should be used.

First, a short overview of the typical applications of such radio systems is given. The following sections provide background information on the various prediction methods for line-of-sight (LoS) links as given in the associated Recommendation ITU-R P.530. Similar to the latter Recommendation, the information is arranged according to the propagation effects that must be considered.

In addition, the Handbook provides selected alternative prediction methods to those given in Recommendation ITU-R P.530 for predicting the multipath fading at a single frequency and for the propagation induced distortion.

#### 2 Typical applications

Line-of-sight radio-relay systems have existed for several decades, both for transmission in the telecommunication network and for distribution in broadcasting systems. The first radio-relay systems were analogue systems where the carrier was frequency modulated. The first digital radio-relay systems in the plesiochronous digital hierarchy (PDH), introduced around 1970, were working with bit rates from 1.5 Mbit/s and up to 140 Mbit/s. In the synchronous digital hierarchy (SDH), digital line-of-sight radio-relay systems can be used as an integrated part of the network together with optical fibres and other transmission equipments. These radio-relay systems have a capacity varying from 52 to 622 Mbit/s for each radio channel. In the last years, digital radio-relay systems with Gbit/s capacity have been introduced.

Digital line-of-sight radio-relay systems may operate in the frequency range from about 1 GHz to 90 GHz. In the ITU-R Recommendations pertaining to Radiocommunication Study Group 5, the specific frequencies and channel bandwidths for different radio-relay systems are given.

For propagation problems due to signal fading, rain attenuation, diffraction, some new propagation conditions were introduced by the large bandwidth of digital transmissions. The distortion due to the frequency dependence of amplitude and group delay becomes significant during clear-air multipath conditions. To alleviate the effects of multipath fading and distortion, adaptive equalizers as well as different types of diversity techniques can be used, such as frequency, space, angle or polarization diversity.

Due to the propagation losses, the restricted transmitter power and limited antennas gain, the usable path length is limited. The maximum path length for higher frequencies (> about 10 GHz) depends mainly on rain precipitation, which increases with the frequency, but depends also on the path profile and performance objectives. For lower frequencies (< about 10 GHz), the effects of rain precipitation are less significant when compared to signal distortion due to multipath fading. As for examples: for frequencies lower than 11 GHz the typical path length is approximately 40 to 60 km; for frequencies between 13 and 15 GHz, approximately 20 to 30 km; and for 18 GHz approximately 15 km; however, local variations can be quite significant.

Usually one linear polarization only, horizontal or vertical, is used for the transmission. To increase channel capacity (e.g. 622 Mbit/s or more) without increasing bandwidth, orthogonal polarization may be used independently for transmission on the same frequency channel over the same path. However, in this case cross-polar interference cancellers (XPIC) should be used to reduce the effect of co-channel interference.

The main applications for future digital line-of-sight radio-relay systems are high capacity point-to-point transport systems and broadband metropolitan area networks using wireless access. These and other existing applications take advantage of the reliability, capacity and speed of digital radio systems at an ever decreasing cost and short time to market.

### 3 Basic propagation effects

The propagation mechanisms that must be taken into account in the design of terrestrial LoS links can be divided into two groups depending on the presence, or not, of their effect on outage, at least for the typical applications discussed in § 2. Multipath fading is the major outage causing mechanism below about 10 GHz on links longer than a few kilometres. Precipitation attenuation is the major outage causing mechanism above 10 GHz. Because of their importance, methods for predicting the fading and attenuation statistics due to these mechanisms and techniques for alleviating them are discussed separately in the following sections.

The principal role of the current chapter is to discuss the other fundamental propagation effects that must be taken into account in system design but which do not have a significant effect on outage. These include free space loss, attenuation due to atmospheric absorption, diffraction loss, loss due to antenna decoupling, and scintillation fading. These are discussed in § 3.1 to § 3.5. However, because of their role in several sections dealing with the effects and alleviation of multipath fading, the phenomena associated with multipath fading are briefly summarized in § 3.6. A more detailed account of the physical phenomena associated with all these propagation effects are presented in the associated Study Group 3 ITU-R Handbook – Radiometeorology.

#### 3.1 Free-space loss

Free-space loss is primarily caused only by beam divergence, i.e., signal energy spreading over larger areas at increased distances from the source. It can be defined as the signal attenuation that would be observed if all absorbing, diffracting, obstructing, refracting, scattering, and reflecting influences were sufficiently removed so as to have no effect on propagation. Recommendation ITU-R P.525 gives the equation to be used in the calculation of free-space loss:

$$L_{bf} = 20 \log \left( \frac{4\pi d}{\lambda} \right) \quad (1)$$

where:

- $L_{bf}$ : free-space loss
- $d$ : path length
- $\lambda$ : wavelength in the same unit as  $d$ .

Expressing the equation (dB) and using frequency instead of wavelength:

$$L_{bf} \text{ (dB)} = 32.4 + 20 \log f + 20 \log d \quad (2)$$

where:

- $L_{bf}$ : free-space basic transmission loss (dB)
- $d$ : path length (km)
- $f$ : frequency (MHz).

#### 3.2 Attenuation due to atmospheric gases

Some attenuation due to absorption by oxygen and water vapour is always present, and should be included in the calculation of total propagation loss at frequencies above about 10 GHz. The attenuation on a path of length  $d$  (km) is given by:

$$A_a = \gamma_a d \quad \text{dB} \quad (3)$$

The specific attenuation  $\gamma_a$  (dB/km) is obtained using Recommendation ITU-R P.676.

NOTE 1 – On paths longer than 10 km at frequencies above about 20 GHz, it may be desirable to take into account known statistics of water vapour density and temperature in the vicinity of the path. Information on water vapour density is given in Recommendation ITU-R P.836.

### 3.3 Diffraction fading and path clearance

Reductions in the vertical atmospheric refractivity gradient along the path sufficiently below the median value of approximately  $-40$  N units/km can cause the path of the direct wave to be bent towards the Earth. If the atmosphere is sufficiently "subrefractive", the wave will intercept the Earth's surface resulting in a loss due to diffraction (sometimes also referred to as obstruction loss or loss due to Earth bulge). The amount of diffraction loss that is judged to be acceptable is the factor that determines the path clearance.

The amount of refractive bending is normally described by the effective Earth's radius or  $k$ -factor. To avoid having to calculate the path curvature when designing a link, the effective Earth radius can be used instead of the actual Earth radius. In this modified geometry, the difference between the path of the direct wave and the Earth's curvature becomes constant and the path of the direct wave can be plotted as a straight line, helping to identify possible obstructions by the terrain profile or Earth's surface. The  $k$ -factor is the ratio between the effective and actual Earth's radius, which has a median value of about  $4/3$  for a standard radio atmosphere, lower values under subrefractive conditions and higher values under superrefractive conditions (when the refractivity gradient approaches a value of  $-157$  N units/km, the  $k$ -factor approaches infinity). The equation for the  $k$ -factor is given in Recommendation ITU-R P.834.

In this section, the origin of the equation of Recommendation ITU-R P.530 for determining diffraction loss statistics is first presented along with the procedures for determining the path clearances of the main and diversity antennas. Application examples are then given.

#### 3.3.1 Basis of prediction method for diffraction loss

The formula included in Recommendation ITU-R P.530 for determining the diffraction loss statistics is based on measurements over average terrain in the United States of America [Vigants, 1981]. In its application, the probability that a given diffraction fade depth is exceeded is assumed to be identical with that does not exceed the effective  $k$ -factor giving the corresponding normalized clearance  $h/F_1$ , where  $h$  is the height of the most significant path blockage and  $F_1$  is the radius of the first Fresnel zone.

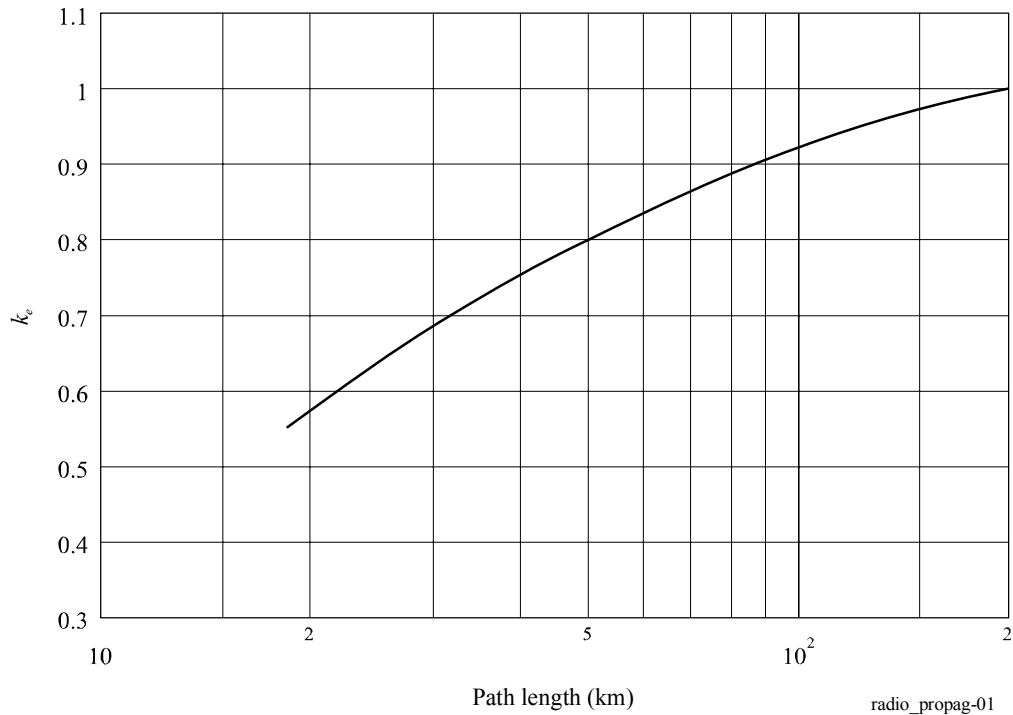
#### 3.3.2 Basis of procedures for determining path clearance

The procedures of Recommendation ITU-R P.530 for determining the path clearances of the main and space-diversity antennas were developed in the absence of an accurate worldwide path clearance procedure that makes a known allowance for diffraction fading. Figure 1, reproduced from Recommendation ITU-R P.530, is based on path measurements obtained in a continental temperate climate [Boithias and Battesti, 1967].

The 99.9% figure attached to the curve is still somewhat uncertain. Application of the value of the effective  $k$ -factor obtained from the curve of this figure has been found to give acceptable clearance for non-diversity links or for the main antenna with space-diversity links longer than 45 km with  $0.6 F_1$  radius. However, as noted in Recommendation ITU-R P.530, smaller fractions of  $F_1$  may be acceptable for frequencies of less than 2 GHz in order to avoid unacceptably large antenna heights.

Regional techniques have been developed for setting path clearance on the basis of a known amount of diffraction loss [Kalinin, 1979; Nadenenko, 1981; Schiavone, 1981; Vigants, 1981 and Olsen and Segal, 1992], and may provide the basis in the future for an accurate worldwide procedure.

FIGURE 1  
Value of  $k$ , exceeded for approximately 99.99% of the worst month  
(continental temperate climate)



**Calculation example:**

Example parameters:

Path length: 30 km

Climate Tropical

Operating frequency: 15 GHz

Highest knife edge obstacle located 10 km from the transmitter.

Highest obstacle height: 30 m.

No available data on median  $k$ -factor.

Desired clearance:  $1.0 F_1$ .

The steps presented below follow the procedure described in § 2.2.2.1 of Recommendation ITU-R P.530 and use the information to estimate the necessary antenna heights.

*Step 1:* Determine the antenna height required for the appropriate median value of the point  $k$ -factor (in the absence of any data, use  $k = 4/3$ ) and  $1.0 F_1$  clearance over the highest obstacle (temperate and tropical climates):

$$F_1 = 17.3 \sqrt{\frac{d_1 d_2}{fd}} = 17.3 \sqrt{\frac{10 \cdot 20}{15 \cdot 30}} = 17.3 \sqrt{0.44} = 11.5 \text{ m} \quad (4)$$

Calculation of the Earth bulge at the point of dominant obstacle for  $k = 4/3$ , yields:  $b = 11.8$  m with Earth radius = 6360 km.

Assuming the same height for the transmitting and receiving antennas, this result leads to antenna height higher than  $30 + 11.5 + 11.8 = 53.3$  m.

*Step 2:* Obtain the value of  $k_e$  (99.9%) from Fig. 1 for the path length in question.

Using Fig. 1, the value of  $k_e$  is readily available:

$$k_e = 0.69$$

*Step 3:* Repeating the calculations shown above using  $k = k_e = 0.69$ , the Earth bulge is  $b = 22.8$  m. The value of  $0.6 F_1 = 6.9$  m yields to an antenna height equal to  $30 + 6.9 + 22.8 = 59.7$  m.

*Step 4:* Choosing the highest of the antenna height the final result is 59.7 m.

### 3.4 Scintillation fading

Turbulent irregularities of the refractive index can give rise to amplitude scintillations and angle of arrival variations of the received signal. These effects are present on all LoS paths at microwave frequencies and above, but can be masked by multipath fading and related phenomena.

The variance of the logarithm of the amplitude of the received signal due to scintillations is given by Tatarskii [1967]:

$$\sigma_x^2 = 42.25 \left( \frac{2\pi}{\lambda} \right)^{7/6} \int C_n^2(r) r^{5/6} dr \quad (5)$$

where:

$\sigma_x$ : standard deviation of the logarithm of the received power

$\lambda$ : wavelength (m)

$C_n^2$ : refractive index structure function ( $\text{m}^{-2/3}$ )

$r$ : distance along the path.

$C_n^2$  is a macroscopic parameter that varies in space and time, primarily with height. Values at a given height may vary by several orders of magnitude over time periods of tens of minutes. The highest values of  $C_n^2$  are found at the planetary boundary layer (extending from the surface to a height varying from 1 to 2 km, depending on climate region, season and time of the day). Typical values are in the range of  $10^{-14}$  to  $10^{-12}$  [COST 1996], but may vary from  $10^{-25}$  to  $10^{-10} \text{ m}^{-2/3}$  [Gossard, 1977].

The amplitude scintillation effect is more significant in satellite links. Measurements [Crane, 1976] at 7 GHz and elevation angles above  $3^\circ$  show signal fluctuations at levels between 0.1 dB and about 1 dB, depending on elevation angle and conditions. At 100 GHz, the levels scale in frequency to lie correspondingly between 0.4 dB and 3.8 dB.

### 3.5 Summary of propagation mechanisms associated with multipath fading

Under normal propagation conditions, there should be only one propagation path between the two antennas on a line-of-sight radio-relay link. In practice, for some percentage of time, more than one propagation path (multipath) may exist and interference between the signals received over these paths may give rise to significant fading.

Fading due to multipath propagation is the most severe of the various clear-air mechanisms. Due to the fact that multipath fading is frequency selective, the distortion induced (see § 6) at all amplitude levels in a wideband digital link can be a major outage source.

The propagation mechanisms that give rise to severe fading and phase effects on horizontal and low-angle slant path are due to the occurrence of multipath propagation conditions during which the additional unwanted rays interfere with the normal direct signal.

Multipath conditions are generally due to reflection from:

- the ground, water or other surface structures; or
- large negative values of the refractivity gradient in the lower atmosphere (see ITU-R Handbook – Radiometeorology) or
- combinations of ground reflections and tropospheric layers.

While investigating fading phenomena, a distinction must be made between the slow non-selective fading caused by single path propagation effects, which also occurs during stratified atmospheric conditions associated with the formation of ducts (ITU-R Handbook – Radiometeorology) and more rapid frequency-selective fading caused by layers with large negative refractivity gradients situated below the path, and is highest when the centre of the layer is just below the path [Olsen *et al.*, 1987]. Frequently, combinations of these various fading mechanisms occur.

## 4 Attenuation due to precipitation and other atmospheric particles

### 4.1 Attenuation due to precipitation

Attenuation due to rainfall along a path may be calculated by integrating the specific attenuation over the path length if the rainfall rate variation along the path is known.

Rainfall rate is inhomogeneous in space and time. Various precipitation models that have been developed to deal with these complexities are described in the ITU-R Handbook – Radiometeorology. Rain cells are known to cluster frequently within rain regions sometimes called small mesoscale areas [Segal, 1979 and Crane, 1979]. Rain gauge records show short intervals of higher rain rate imbedded in longer periods of lighter rain. Weather radar observations show small areas of higher rain rate imbedded in larger regions of lighter rain. Terrestrial links exceeding 10 km may, therefore, pass through more than one rain cell within a rain region. In addition, influence of the lower intensity rainfall surrounding the cell must be taken into account in the attenuation calculations. The linear extent of these regions increases with decreasing rain intensity and may be as large as several tens of kilometres.

The main difference in the various methods developed for predicting rain attenuation statistics from rainfall rate measurements is in the models used to describe the time-space structure of rainfall rate.

The "synthetic storm method" generates attenuation statistics by converting rain rate/time profiles recorded at a point to rain rate/distance profiles, using the translation velocity of the rain pattern, this is estimated as the wind speed [Drufuca, 1974; Bertok *et al.*, 1977 and Segal, 1982].

All other methods make use of cumulative distributions of rainfall rate measured at a point. Some methods derive the statistical profile of rain along the path assuming a single cell of suitable shape [Misme and Fimbel, 1975] or a statistical distribution of sizes for cells of a particular shape [Capsoni *et al.*, 1987]. Other methods characterize the statistical rain profile simply by a reduction coefficient which may be derived from the spatial correlation function of rainfall or from measurements using rapid response rain gauges spaced along a line [Harden *et al.*, 1978 and Crane, 1980] or from a semi-empirical law [Battesti and Boithias, 1978]. Multiplying point rain rate by this reduction coefficient gives the equivalent path-averaged rain rate.

An alternative procedure is to apply the reduction coefficient to the actual path length, which yields an equivalent path length over which the rain intensity may be assumed to be constant [Lin, 1975; Garcia-Lopez and Peiro, 1983; Moupfouma, 1984 and Dissanayake and Allnut, 1992]. This type of procedure is currently adopted in the methodology of Recommendation ITU-R P.530.

#### 4.1.1 Basis of prediction method for rain attenuation

The rain attenuation prediction procedure currently adopted in Recommendation ITU-R P.530 was derived from an analysis of concurrent rainfall rate and propagation measurements obtained primarily in Europe, with some additional data from Japan and the United States of America. It uses the concept of effective path length to take into account the non-uniform profile of rain intensity along the actual path. The method is

based on the estimation of the attenuation exceeded at 0.01% of the time ( $A_{0.01}$ ) from the rainfall rate exceeded at the same time percentage ( $R_{0.01}$ ). For a given value of  $R_{0.01}$  the specific attenuation is calculated and multiplied by the effective path length to produce the corresponding value of  $A_{0.01}$ :

$$A_{0.01} = \gamma_R \cdot d \cdot \frac{1}{1 + d/d_0} \quad (6)$$

where:

$\gamma_R$ : specific attenuation

$d$ : path length

$d_0$ : equivalent rain cell length.

Empirical equations are used for scaling to other time percentages ( $p$ ), in order to provide the complete attenuation distribution. These equations have been derived based on experimental data. For radio links located in latitudes equal to or greater than  $30^\circ$  (North or South):

$$\frac{A_p}{A_{0.01}} = 0.12 p^{-(0.546 + 0.043 \log_{10} p)} \quad (7)$$

For radio links located at latitudes below  $30^\circ$  (North or South):

$$\frac{A_p}{A_{0.01}} = 0.07 p^{-(0.855 + 0.139 \log_{10} p)} \quad (8)$$

Both equations have been derived for percentages of time between 1% and 0.001% and their use should be limited to this range. The concept of equi-probability is not consistent with meteorological information and is not entirely satisfactory from a theoretical point of view. Also, as the method uses only one point on the rain rate distribution, it will produce the same attenuation distribution for two sites with different rain rate distributions but the same value of  $R_{0.01}$ . However, it has been observed that the attenuation distributions have a greater tendency to be parallel to one another than rain rate distributions. In any case, the accuracy obtained with the prediction method for terrestrial links is consistent with the quality and variability of available rain intensity data.

#### 4.1.2 Specific attenuation

The specific attenuation  $\gamma_R$  (dB/km) at a given frequency may be obtained from the rainfall rate derived from the knowledge of the complex index of refraction of water at the temperature of the raindrops, the terminal velocity and the size distribution of the raindrops [Ryde and Ryde, 1945; Medhurst, 1965 and Setzer, 1970]. Because of the non-spherical shape of the raindrops, horizontally polarized waves suffer greater attenuation than vertically polarized waves [Morita *et al.*, 1974 and Chu, 1974]. In some climates the difference in attenuation may reach values as high as 35% [Fedi *et al.*, 1977 and Fimbel and Juy, 1977]. Specific attenuation for vertical and horizontal polarizations, for frequencies of up to 100 GHz, may be obtained from extensive calculations that take into account the non-spherical shape of the raindrops [Oguchi and Hosoya, 1974; Chu, 1974 and Oguchi, 1977].

For practical applications the relationship between specific attenuation  $\gamma_R$  (dB/km) and rain rate  $R$  (mm/h) can be approximated by the power-law [Olsen *et al.*, 1978]:

$$\gamma_R = k R^\alpha \quad (9)$$

Considering the assumption of spherical drops, values of  $k$  and  $\alpha$  have been calculated at a number of frequencies in the range of 1 to 1000 GHz for several drop temperatures and drop size distributions [Olsen *et al.*, 1978].

Recent works carried out by Gibbins and Walden [2003] presented results from a comprehensive study on the nature of the  $k$  and  $\alpha$  parameters. These results were the basis for Recommendation ITU-R P.838.

Values for the coefficients  $k$  and  $\alpha$  are determined as functions of frequency,  $f$  (GHz), in the range from 1 to 1 000 GHz, from the equations of Recommendation ITU-R P.838, which have been developed from curve-fitting to power-law coefficients derived from scattering calculations.

Values for the constants to be used in the calculation of coefficients  $k_H$ ,  $k_V$ ,  $\alpha_H$  and  $\alpha_V$ , required for the calculation of  $k$  and  $\alpha$ , can be obtained from Recommendation ITU-R P.838.

A more detailed discussion of the relation between specific attenuation and rain rate is given in the ITU-R Handbook – Radiometeorology.

#### 4.1.3 Effective path length

The effective path length in terrestrial links is the length of a hypothetical path obtained from radio data by dividing the total attenuation exceeded at 0.01% of time by the specific attenuation exceeded for the same percentage of time.

The path reduction factor  $r$  is given by:

$$r = \frac{1}{1 + d/d_0} \quad (10)$$

This equation was derived based on two assumptions:

- the spatial structure of rain can be modelled by an equivalent rain cell with a rectangular cross-section of equivalent length  $d_0$  in the plane of the path;
- the rectangular rain cell cross-section may assume any position with respect to the path with equal probability.

The effective path length  $d_{eff} = dr$  corresponds to the average length of the intersection between the terrestrial path and the randomly positioned equivalent rain cell of length  $d_0$  at 0.01% exceedence.

The length  $d_0$  of the equivalent rain cell was initially assumed to be constant but the model has been subsequently improved by assuming a dependence on rainfall intensity [Yamada *et al.*, 1987]:

$$d_0 = 35 e^{-0.015 R_{0.01}} \quad (11)$$

For  $R_{0.01} > 100$  mm/h, the value 100 mm/h shall be used in place of  $R_{0.01}$ .

Although this equation has been derived based on slant path rain attenuation data, it has been successfully tested with results of rain attenuation measurements on terrestrial links.

#### 4.1.4 Application examples

Location: Rio de Janeiro, BRA

Latitude: 22° 50' S

Longitude: 317° 00' E

Frequency:  $f = 13$  GHz

Path length:  $d = 20$  km

Linear polarization:  $\tau = 90^\circ$ .

*Step 1:* By applying Recommendation ITU-R P.837 (global maps of rain rate) for this location, one obtains  $R_{0.01} = 59.67$  mm/h for the rain rate exceeded for 0.01% of the time.

*Step 2:* Specific attenuation  $\gamma_R$  is evaluated using Recommendation ITU-R P.838 for the frequency, polarization and rain rate of interest. As a result  $\gamma_R$  is equal to 2.82 dB/km.

*Step 3:* In Step 3, the computation of the effective path length is carried out  $d_{eff} = d \times r = 20 \times 0.42 = 8.34$  km, which enables the derivation of an estimate of the path attenuation exceeded for 0.01% of the time:

$$A_{0.01} = \gamma_R d_{eff} = 23.4 \quad \text{dB} \quad (12)$$

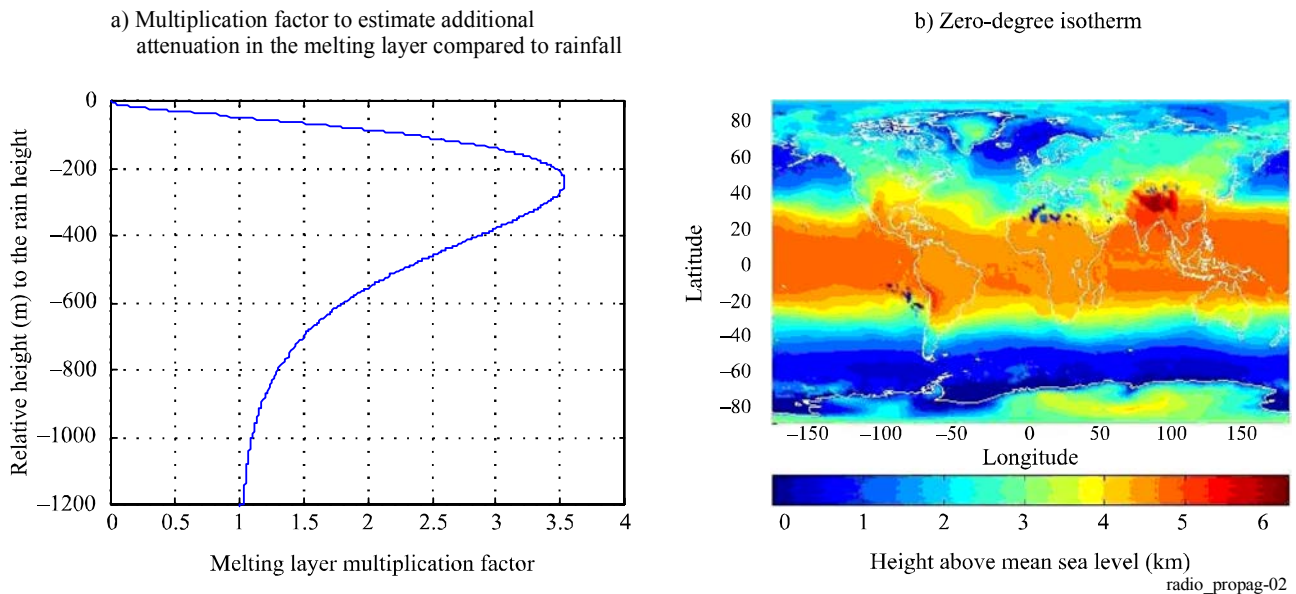
Finally, employing the formula that corresponds to radio links below  $30^\circ$ , the rain attenuation exceeded for 0.001%, 0.01%, 0.1% and 1% is  $A_{0.001} = 33.9$  dB,  $A_{0.01} = 23.4$  dB,  $A_{0.1} = 8.5$  dB and  $A_1 = 1.6$  dB, respectively.

#### 4.1.5 Prediction of combined rain and wet snow

The method in Recommendation ITU-R P.530 is based on a proposal made in 2002 by Bacon and Eden and further developments with an approximate implementation as given by Tjelta *et al.* [2005]. The method makes use of a global map for the rain height and indirect information to make an estimate of the amount of wet snow and an average attenuation profile to obtain excess attenuation in the melting layer. It further assumes a certain distribution of the height of rainfall, or zero-degree isotherm, as well as a fixed shape of the melting layer excess attenuation as a function of the position in the layer. With this information it is possible to predict the attenuation distribution on any link taking both rain and wet snow into consideration.

The melting layer consists of a mixture of ice, water and air. Falling ice hydrometeors melt, coalesce and then separate into raindrops. Hydrometeor precipitation in the form of wet snow may occur along the propagation path when the air temperature is around  $0^\circ$  C. The theory of rain attenuation is well understood and reasonably well modelled for the frequency ranges in use today. Theoretical extinction coefficients have been established for various particle sizes and forms, and simplified specific attenuation models established depending on radio wave frequency and polarisation, and the path angle with respect to the major axis of large non-spherical raindrops. In contrast, wet snow particles cause significantly greater difficulties when modelling, but certain attempts have been done. Theoretical analyses of radio wave propagation through the melting layer use models of the melting ice particles. It has been found that wet snow particles have larger extinction coefficients than raindrops with the same amount of liquid water, causing excess specific attenuation compared to rain (see [Jain and Watson, 1985 and Kuznetov *et al.*, 2000] for a recent analysis). The radar terminology used is “bright band”, due to the observed strong radar echoes from this layer. In addition to co-polar attenuation, the anisotropic nature of the wet snow particles may also result in some depolarisation.

FIGURE 2



The prediction method for combined rain and wet snow presented in this paper uses a simplified approximation. A multiplication factor is introduced to describe whether the specific attenuation is different from rain. The factor is 1 for rain and higher than 1 for wet snow with a maximum slightly higher than 3.5, and 0 for dry snow or ice. The model given by equation (18) is shown graphically in Fig. 2a) where the multiplication factor is given as a function of the vertical position of the melting layer from the top of the rain.

The multiplication factor is given by  $\Gamma(h)$ :

$$\Gamma(h) = \begin{cases} 0 & 0 < h \\ \frac{a(1 - e^{h/b})^2}{\left(1 + \left(1 - e^{-(h/c)^2}\right)^2 \left(a(1 - e^{h/b})^2 - 1\right)\right)} & h \leq 0 \end{cases} \quad (13)$$

where the constants  $a = 4$ ,  $b = 70$ , and  $c = 600$ . As a crude indication the three coefficients have an impact on the maximum multiplication factor, its position relative to the top and the depth of the layer, respectively. The function goes asymptotic to 1 for large negative  $h$  values, in practical term it is 1 for  $h < -1400$  with  $a$ ,  $b$ , and  $c$  as indicated.

The actual multiplication factor to use in prediction is made up as an integral of the multiplicative factors weighted with the relative melting layer height probability density function along the path. The multiplication factor is made relative to the zero degree isotherm height.

The combined rain, wet snow, and dry snow or ice prediction method is simple and uses the following assumptions:

- The precipitation rate is known, for example from the map in Recommendation ITU-R P.837;
- The precipitation is classified into rain, wet snow and dry snow or ice using the rain height, as shown in the map found in Recommendation ITU-R P.839, and a melting layer model as described above;
- The combined rain and snow precipitation attenuation distribution is the same distribution as for rain only.

The key of the method is to establish a multiplication factor taking into account the contribution of wet and dry snow. If all the precipitation is observed as rain this factor will be 1 and there will be no change to the results of the current procedure (see Recommendation ITU-R P.530) gives. However, if all the precipitation is observed as dry snow or ice the factor will be 0 and no attenuation can be estimated. This is obviously quite different to the existing method. The realistic case is, since the zero degree height varies over the year and that most of the precipitation will be rain, with some wet and some dry snow. In wet snow the attenuation may be significantly worse than that for rain. Thus, when making the summation of all the possibilities, the likely factor will be larger than 1 so that some additional margin has to be allowed for wet snow.

Two features have to be established and used in the procedure: the mean rain height derived from the zero degree isotherm height, and its variation or distribution. Rain height data are given in Recommendation ITU-R P.839. The zero degree height data are shown in Fig. 2b). The rain height is assumed to follow a normal distribution of mean zero with an 800 m standard deviation. It is currently taken to have the same distribution all over the world. The attenuation,  $A_p$ , exceeded for time percentage,  $p$ , given in the previous sub-section, is valid for link paths through which only liquid rain falls. Recommendation ITU-R P.530 provides a step-by-step procedure.

Figure 3 shows an example of the procedure for selected cities from the Equator to the North Pole. Up to 10 dB additional attenuation due to wet snow is estimated with  $p = 0.001$  % for an average year.

FIGURE 3  
**Estimated attenuation due to wet snow estimated at  $p = 0.001\%$  of an average year for some selected cities from the Equator to the North Pole**

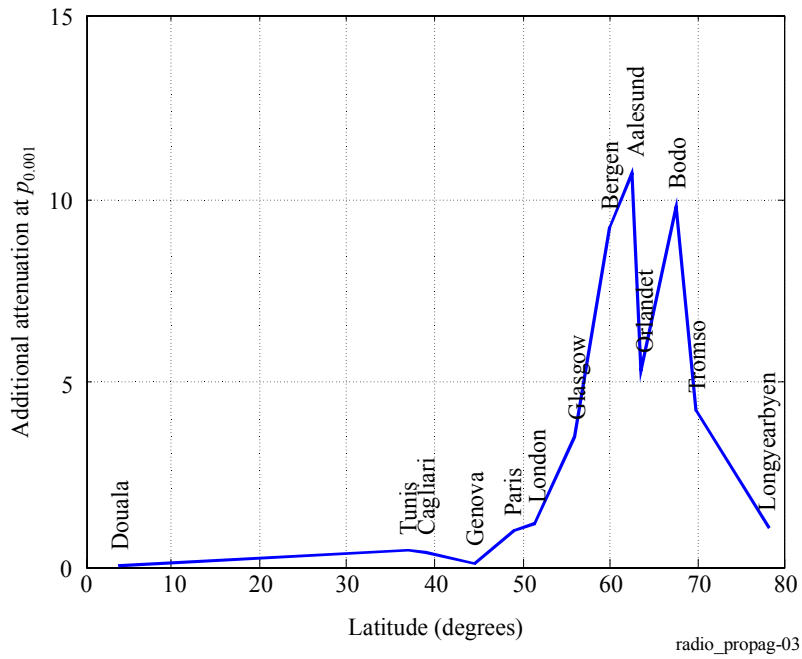
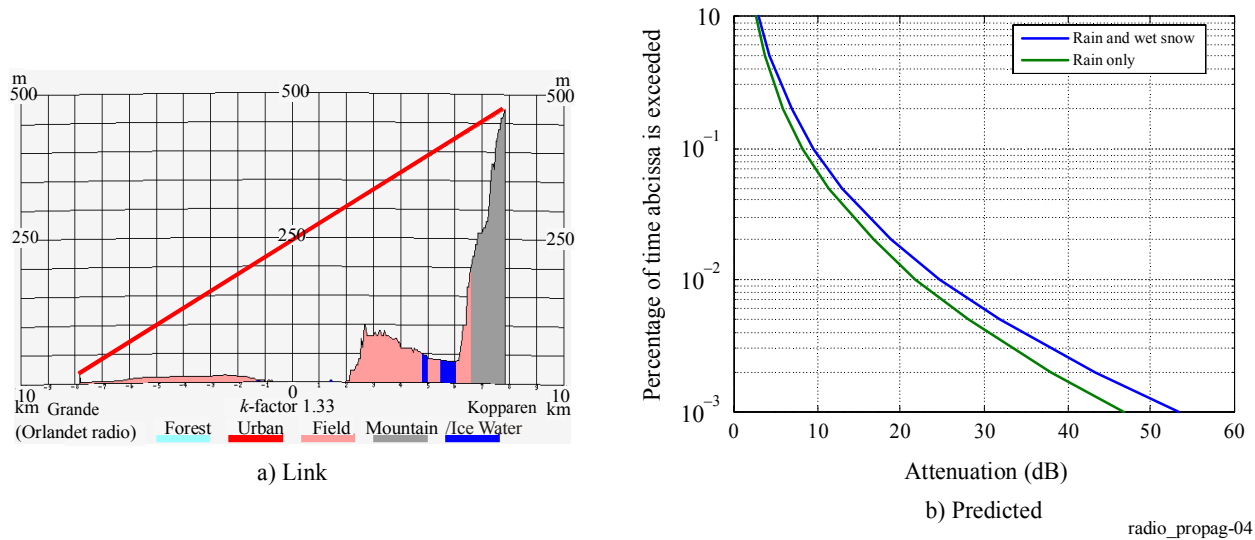


FIGURE 4  
**Prediction example for a coastal link in Norway [Tjelta *et al.*, 2006] deploying an averaged multiplication factor for an inclined path**



There are no testing results for the time being. In a number of publications there are measurements indicating excess attenuation due to wet snow. Such data cover Japan, Canada, the United Kingdom and Norway, see [Takada and Nakamura, 1966; Nishitsuji, 1971; Hendry *et al.*, 1981; Gutteberg, 1983; Kharadly *et al.*, 1983; Kharadly and Owen, 1988; Thurai and Woodroffe, 1997; Walden *et al.*, 2003; Tjelta *et al.*, 2005 and Tjelta *et al.*, 2006].

#### 4.1.6 Long-term frequency and polarization scaling of rain attenuation statistics

##### 4.1.6.1 Single-frequency scaling

If only attenuation data measured at one frequency are available, the empirical formula in Recommendation ITU-R P.530, giving an attenuation ratio directly as a function of frequency and attenuation, may be applied for frequency scaling on the same path in the frequency range 7 to 50 GHz (and tentatively, up to 100 GHz):

$$A_2 = A_1 (\Phi_2 / \Phi_1)^{1 - H(\Phi_1, \Phi_2, A_1)} \quad (14)$$

where:

$$\Phi(f) = \frac{f^2}{1 + 10^{-4} f^2} \quad (15)$$

$$H(\Phi_1, \Phi_1, A_1) = 1.12 \times 10^{-3} (\Phi_2 / \Phi_1)^{0.5} (\Phi_1 A_1)^{0.55} \quad (16)$$

Here,  $A_1$  and  $A_2$  are the equiprobable values of the excess rain attenuation at frequencies  $f_1$  and  $f_2$  GHz, respectively.

The formula was found to be the best empirical fit to the available scaling data [Boithias, 1989]. As the accuracy of this procedure is well within 10%, a frequency scaling technique should normally be employed when a long-term distribution is available from measurements.

Frequency scaling is examined in greater detail in the ITU-R Handbook – Radiometeorology which gives, as an alternative another method that makes use of the  $k$  and  $\alpha$  constants and is therefore more appropriate where polarization scaling is required. Some other methods use attenuation statistics measured at two frequencies or information on the elevation angle to predict the attenuation at another frequency.

##### 4.1.6.2 Polarization scaling

If only attenuation data measured at one polarization (either vertical or horizontal) are available, equations (37) and (38) of Recommendation ITU-R P.530 [Boithias, 1983] may be applied for polarization scaling of equi-probable values of rain attenuation, within the range of path length and frequency of the attenuation prediction method.

The polarization scaling is to be applied only to measurements or calculations of attenuation due to rain. Additional attenuation due to gaseous absorption must be added. The expressions given in Recommendation ITU-R P.530 are in general agreement with experimental results and with estimates using the specific attenuation coefficients of Recommendation ITU-R P.838:

$$A_V = \frac{300 A_H}{335 + A_H} \quad \text{dB} \quad (17)$$

or

$$A_H = \frac{335 A_V}{300 - A_V} \quad \text{dB} \quad (18)$$

These expressions are considered to be valid in the range of path length and frequency for the rain attenuation prediction method. It should be noted, however, that calculations of polarization scaling ratios using radar data suggest they are larger for convective rain than that for stratiform rain. This may produce some climatic dependence.

#### 4.1.7 Statistics of duration and rate of rain induced fading

The procedures for determining the statistics of duration of rain induced fades can be found in Recommendation ITU-R P.530.

Although there is little information as yet on the overall distribution of fade duration, there are some data and an empirical model for specific statistics such as mean duration of a fade event and the number of such events. An observed difference between the average and median values of duration indicates, however, a skewness of the overall distribution of duration. Also, there is strong evidence that the duration of fading events in rain conditions is much longer than those during multipath conditions.

An attenuation event is here defined to be the exceedance of attenuation  $A$  for a certain period of time (e.g., 10 s or longer). The relationship between the number of attenuation events  $N(A)$ , the mean duration  $D_m(A)$  of such events, and the total time  $T(A)$  for which attenuation  $A$  is exceeded longer than a certain duration, is given by:

$$N(A) = T(A) / D_m(A) \quad (19)$$

The total time  $T(A)$  depends on the definition of the event. The event usually of interest for application is one of attenuation  $A$  lasting for 10 s or longer. However, events of shorter duration (e.g., a sampling interval of 1 s used in an experiment) are also of interest for determining the percentage of the overall outage time attributed to unavailability (i.e., the total event time lasting 10 s or longer).

The number of fade events exceeding attenuation  $A$  for 10 s or longer can be represented by:

$$N_{10s}(A) = a A^b \quad (20)$$

where  $a$  and  $b$  are coefficients that are expected to depend on frequency, path length, and other variables such as climate.

On the basis of one set of measurements for an 18 GHz, 15 km path on the Scandinavian peninsula, values of  $a$  and  $b$  estimated for a one-year period are:

$$a = 5.7 \times 10^5 \quad b = -3.4 \quad (21)$$

Once  $N_{10s}(A)$  has been obtained from equation (20), the mean duration of fading events lasting 10 s or longer can be calculated by inverting equation (19).

Based on the noted set of measurements (from an 18 GHz, 15 km path on the Scandinavian peninsula), 95-100% of all rain events greater than about 15 dB can be attributed to unavailability. With such a fraction known, the availability can be obtained by multiplying this fraction by the total percentage of time that a given attenuation  $A$  is exceeded as obtained from the method presented in Recommendation ITU-R P.530.

#### 4.1.8 Seasonal variations – worst month

System planning often requires the attenuation value exceeded for the time percentage  $P_w$  of the "worst month" (see Recommendation ITU-R P.581).

The conversion from annual statistics to "worst month" statistics is discussed in detail in Recommendation ITU-R P.841. The relationship between  $P_w$  and the annual percentage of time,  $P$ , can be expressed as:

$$P = Q_1^{\frac{1}{1-\beta}} P_w^{\frac{1}{1-\beta}} \quad (22)$$

The above expression is applicable for the probability range ( $0.001\% < P < 3\%$ ). Values of  $Q_1$  and  $\beta$  found in various locations and for several propagation effects are given in Recommendation ITU-R P.841. For global planning purposes, a single "average" relationship may be preferable, using  $Q_1 = 2.85$  and  $\beta = 0.13$ , which yields:

$$P = 0.3 P_w^{1.15} \quad (23)$$

Measurements obtained in a variety of climates indicate that the ratio of average yearly worst-month time percentage to average yearly time percentage depends somewhat on the climate. The above equation corresponds to climates with relatively small seasonal variations in rainfall intensity. For the Mediterranean and Northwest Europe, and other regions that exhibit similar seasonal variations in rainfall, the above value for  $P$  has to be reduced by 20%, while in the more extreme cases the above value for  $P$  has to be reduced by 30%.

#### 4.1.9 Discussion of model evaluation (testing)

Testing criteria for comparing prediction methods, including the definition of a test variable for comparing rain attenuation predictions, are provided in Recommendation ITU-R P.311.

Extensive tests performed on the basis of available methods and data have suggested the adoption of the method of § 2.4.1 of Recommendation ITU-R P.530 and shown that the accuracy obtainable is of about 25%-30% on a global basis for percentages of time of 0.001% and 0.1%. Long-term statistical data, especially from tropical regions, are needed to improve the prediction accuracy.

For time percentages in excess of 0.1%, it is worth to remind that rain intensity measurements tend to become increasingly inaccurate as rain rate decreases. In particular, gaseous absorption may become non-negligible at these time percentages and should be added to the predicted rain attenuation.

#### 4.1.10 Example of calculation

As an example, the rain attenuation distribution will be calculated for a link with the following characteristics:

Operation frequency: 18 GHz

Mid-point latitude: 12° 00' 00"

Mid-point longitude: 44° 00' 00"

Path length: 10 km

Polarization: Vertical.

*Step 1:* The rain rate  $R_{0.01}$  exceeded for 0.01% of the time (with an integration time of 1 min) shall be obtained, preferably, from local sources of long-term measurements. If this is not available, an estimate can be obtained from the information given in Recommendation ITU-R P.837. This Recommendation provides figures for a quick estimate of  $R_{0.01}$  and a method for a more accurate calculation of this parameter, in such a case, one obtains  $R_{0.01} = 50$  mm/h. It should be noted that, although the use of the geographic coordinates of the link mid-point is indicated, the use of the coordinates of one of its extreme points will not introduce significant error in the calculation.

*Step 2:* The specific attenuation,  $\gamma_R$  (dB/km) is computed using Recommendation ITU-R P.838.

$$\log_{10} k = \sum_{j=1}^4 a_j \exp \left[ - \left( \frac{\log_{10} f - b_j}{c_j} \right)^2 \right] + m_k \log_{10} f + c_k \quad (24)$$

$$\alpha = \sum_{j=1}^5 a_j \exp \left[ - \left( \frac{\log_{10} f - b_j}{c_j} \right)^2 \right] + m_\alpha \log_{10} f + c_\alpha \quad (25)$$

where:

$f$ : frequency (GHz)

$k$ : either  $k_H$  or  $k_V$

$\alpha$ : either  $\alpha_H$  or  $\alpha_V$ .

The coefficients  $a_j$ ,  $b_j$ ,  $c_k$ ,  $m_k$ ,  $c_\alpha$  and  $m_\alpha$  are given in Recommendation ITU-R P.838. The coefficients  $k$  and  $\alpha$  may have a horizontal (H) or vertical polarization (V). Using these equations one obtains, for vertical polarization,  $\alpha(18 \text{ GHz}) = 1.002505$  and  $k(18 \text{ GHz}) = 0.077076$ . The specific attenuation is:

$$\gamma_R = k R_{0.01}^\alpha = 3.89 \quad \text{dB/km} \quad (26)$$

Step 3: Computation of the effective path length  $d_{eff}$ :

$$d_0 = 35 \exp(-0.015 R_{0.01}) = 16.53 \text{ km} \quad (27)$$

$$r = \frac{1}{1 + d/d_0} = 0.623 \quad (28)$$

$$d_{eff} = d \cdot r = 6.23 \text{ km} \quad (29)$$

Step 4: Estimation of the path attenuation exceeded for 0.01% of the time:

$$A_{0.01} = \gamma_R d_{eff} = 24.2 \text{ dB} \quad (30)$$

Step 5: Conversion for other percentages of time:

$$\frac{A_p}{A_{0.01}} = 0.12 p^{-(0.546 + 0.043 \log_{10} p)} \quad (31)$$

$p$ (%)	$A_p$ (dB)
1	2.9
0,1	9.2
0,01	24.2
0,01	51.7

Step 6: If worst-month statistics are desired, calculate the annual time percentages  $p$  corresponding to the worst-month time percentages  $p_w$  using climate information specified in Recommendation ITU-R P.841. For global planning purposes:

$$p(\%) = 0.30 p_w(\%)^{1.15} \quad (32)$$

For this example one obtains:

$p_w$ (%)	$p$ (%)	$A_p$ (dB)
1	0.3	5.5
0,1	0.021	18.1
0,01	0.0015	45.9

## 4.2 Tandem and convergent links

### 4.2.1 Correlated fading on tandem paths

The overall transmission performance of a tandem system is largely influenced by the propagation characteristics of the individual links. For long hops and small outage probabilities, the likelihood of joint fading in two or more hops is usually negligible. Under these circumstances, the overall outage probability

for a tandem series will equal the sum of outage probabilities for the individual links [Peroni and Fedi, 1974], as indicated in Recommendation ITU-R P.530:

$$P_T = \sum_{i=1}^n P_i \quad (33)$$

where  $P_i$  is the  $i$ th outage probability of the total number  $n$  of links.

In case of short hop lengths (i.e. comparable with dimensions of the attenuating rainfall structure), the adjacent links may be affected simultaneously giving an overall outage probability less than the sum of the individual probabilities. As indicated in Recommendation ITU-R P.530:

$$P_T = K \sum_{i=1}^n P_i \quad (34)$$

where  $K$  is a reduction factor that includes the overall effect of rainfall correlation.

Measurements in Japan over a series of 4.5 km links have demonstrated this condition. Reduction factors of about 0.8 for the outage over two hops and 0.7 for four hops were observed for single link outage probabilities of 0.03% [Sasaki *et. al.*, 1976 and Morita and Higuti, 1978].

Calculations based on the spatial correlation function for rainfall observed over widely spaced locations in Canada indicate that similar reduction factors apply for longer hop lengths consisting of ten tandem hops of 10 to 20 km each. For even longer hop lengths simultaneous fading is significant only at large probabilities of occurrence [Segal, 1982].

Based on these experiments and calculations, Recommendation ITU-R P.530 provides graphs of the modification factor  $K$  as a function of the number of hops of equal path length for various path lengths, and for various percentages of time considering a path length of 4.6 km.

#### 4.2.2 Convergent paths

Information on the diversity improvement factor for converging paths in the lower EHF range of the spectrum can be found in Recommendation ITU-R P.1410. Although developed for point-to-area applications, it can be used to give some general indication of the improvement afforded by such elements of a point-to-point route-diversity (or mesh) network.

Due to the random temporal and spatial distribution of the rainfall rate, convergent point-to-point links will instantaneously experience different depths of attenuation. As a result, there may be a degradation in the carrier-to-interference ratio  $C/I$  between links from users in different angular sectors whenever the desired signal is attenuated by rain in its path and the interfering signal is not.

The differential rain attenuation cumulative distribution for two convergent links operating at the same frequency can be estimated by (see Note 1):

$$A_{12}(p) = [A_1(p) - 0.34 A_2(p)] \left( 2.65 |\theta|^{0.23} + 0.004 |\Delta d|^{2.25} \right) f^{-0.4} \quad \text{dB} \quad (35)$$

where:

$p$ : percentage of time, between 0.01% and 1%

$f$ : frequency (GHz)

$\Delta d$ : path length difference (km)

$\theta$ : angle (rad) between the links, from  $0^\circ$  to  $180^\circ$

$A_1(p)$  and  $A_2(p)$ : values of rain attenuation in the individual links exceeded during  $p\%$  of the time, calculated using the method given in Recommendation ITU-R 530.

NOTE 1 – Equation (35) is based on the results of measurements on 36 pairs of convergent links with frequencies in the range from 15 to 38 GHz and path lengths in the range of 1 to 23 km.

### 4.3 Paths with passive repeaters

Recommendation ITU-R P.530 gives procedures for extension of the single-hop procedures to passive repeater hops with two or more legs, based on the work of Karl and Persson [1998].

In the case of plane reflectors, the procedure is simple and consists in the insertion of the total path length into equation (32) of the mentioned Recommendation for the distance reduction factor. This approach is most accurate if the legs of the hop are approximately parallel to one another. Deviation from parallel legs will have the overall effect of increasing the uniformity of the rain over the entire path since the distance between the end points is reduced relative to the size of a rain cell. This will in turn cause the attenuation to be underestimated since the reduction factor will be underestimated. An untested approach for approximately eliminating this effect is indicated in the above mentioned Recommendation.

In the case of back-to-back antenna repeaters with identical polarizations on the legs, the procedure is identical to that for plane reflectors. For alternating vertical and horizontal polarizations, the attenuation is calculated over the entire path for one polarization and then the other, and then a simple weighted average is calculated based on the actual length of the path for each polarization.

## 5 Multipath fading and enhancement at a single frequency

Distributions of multipath fading at a single frequency or in a narrow bandwidth are the sole means of estimating outages due to this phenomenon on analogue links. They are also a fundamental ingredient in virtually all techniques for estimating outages on digital links. Distributions of enhancement during multipath conditions are important for interference calculations and receiver saturation calculations (see ITU-R Handbook – Digital Radio-Relay Systems).

In this chapter, the basis and accuracy of prediction methods given in Recommendation ITU-R P.530 for estimating the single frequency fading and enhancement distributions are presented in § 5.1. To aid in the application of these methods, this is followed by worked examples on actual links. Although prediction procedures for the average number and duration of fades are not yet available, estimation procedures based on the limited experimental data available are given in § 5.2. Data available on the rate of change of signal level are discussed in § 5.3. Finally, the multipath fading on tandem links is discussed in § 5.4.

Because of its particular importance on digital radio links, the distortion associated with the frequency selective nature of multipath fading is discussed separately in § 6. Since diversity techniques are an important means of reducing both the occurrence of multipath fading and the associated distortion, they are discussed separately in § 8.

### 5.1 Prediction of the fading/enhancement distribution

Four complementary methods designed for predicting various parts of the fading/enhancement distribution for the average worst month at any location in the world are given in Recommendation ITU-R P.530. Two methods are provided for the deep fading range of the distribution, Method 1 intended for detailed link design and Method 2 for initial planning or licensing purposes. These methods provide the calculation basis for the interpolation method for the shallow fading range and the method for the enhancement range. The basis of each of these methods is described in § 5.1.1-5.1.3 along with a summary of test results. Examples employing all methods are presented in § 5.1.4.

#### 5.1.1 Basis and accuracy of Methods 1 and 2

##### 5.1.1.1 The full distribution derived from the tail

The deep faded signal follows a Rayleigh-distribution. It has been accepted for a very long time [Pearson, 1965; Morita *et al.*, 1974 and Barnett, 1972], and the more detailed study of measurement data supported this view [Tjelta *et al.*, 1990].

A common approach has been to assume that each link and climate/terrain variable contributes independently to the deep fading range. Therefore a power-law model of the deep fading region has been adopted. In a general form, the probability  $p_w$  (often calculated in percent) that the fade depth  $A$  is exceeded is given by:

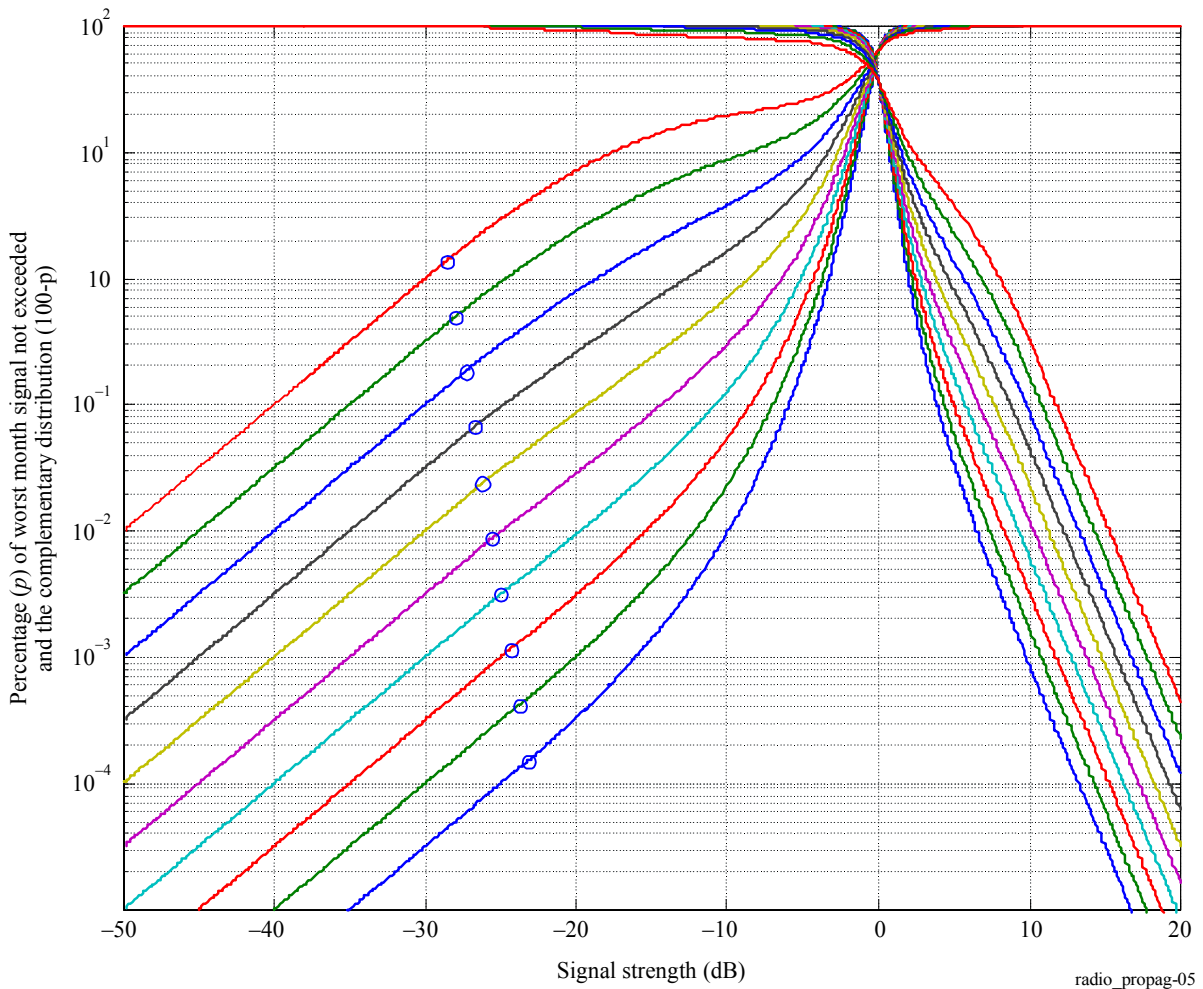
$$p_w = \prod_i g_i(x_i) 10^{-A/10} \tag{36}$$

where  $i$  is the  $i$ th link and the predictor variables  $x_i$  and  $g_i$  are functions of it. Exponential functions of the variables have been common where the exponent gives a direct indication of the predictor's importance.

The full distribution is easily drawn as soon as the deep fade tail has been found. Figure 5 presents a family of multipath fading and enhancement distributions. The small circle on each curve indicates where the Rayleigh slope ends. Between this specific point and 0 dB at 67.7 % and an interpolation is used. In the enhancement region, the distribution follows fixed slope above 10 dB, based on empirical analyses of measurement data [Tjelta and Tanem, 1992] and an interpolation between 0 dB and 10 dB.

FIGURE 5

Example of a family of multipath fading and enhancement distributions



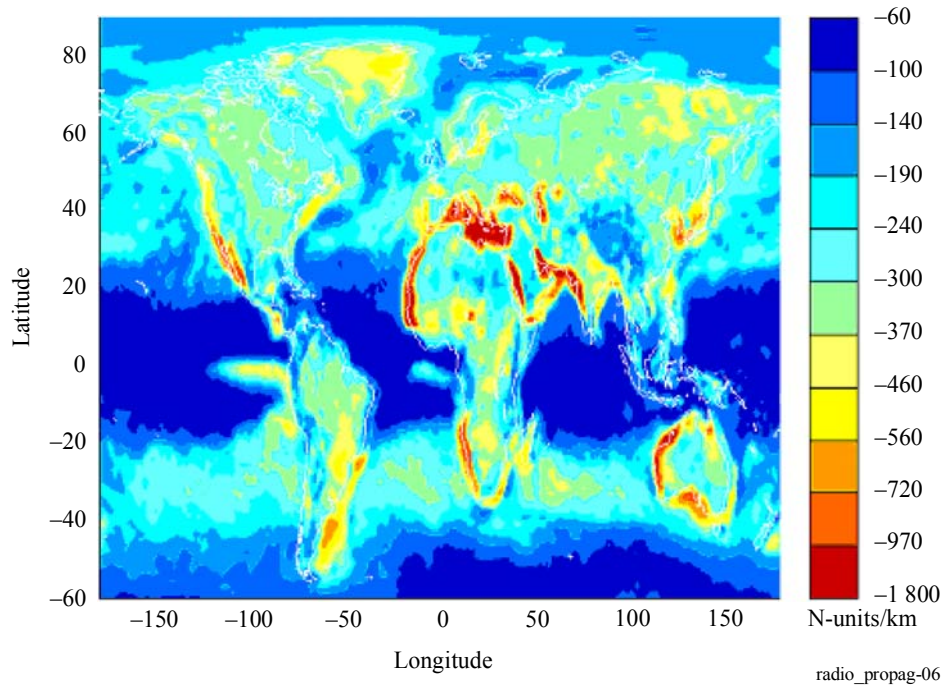
### 5.1.1.2 Determining the multipath fading distribution tail

There are two proposed ITU-R methods in Recommendation ITU-R P.530. Both split the method in (1) into one part describing the climate, a geoclimatic parameter  $K$ , and another taking care of the link variables. The climate part is based on the likelihood of strong negative refractive gradients in an area where the most exact method also makes use of area roughness. Figure 6 shows a map of the refractivity gradients not exceeded

for 1% of an average year [Tjelta *et al.*, 1998]. A table of these data at any wanted location of the Earth is available in Recommendation ITU-R P.453.

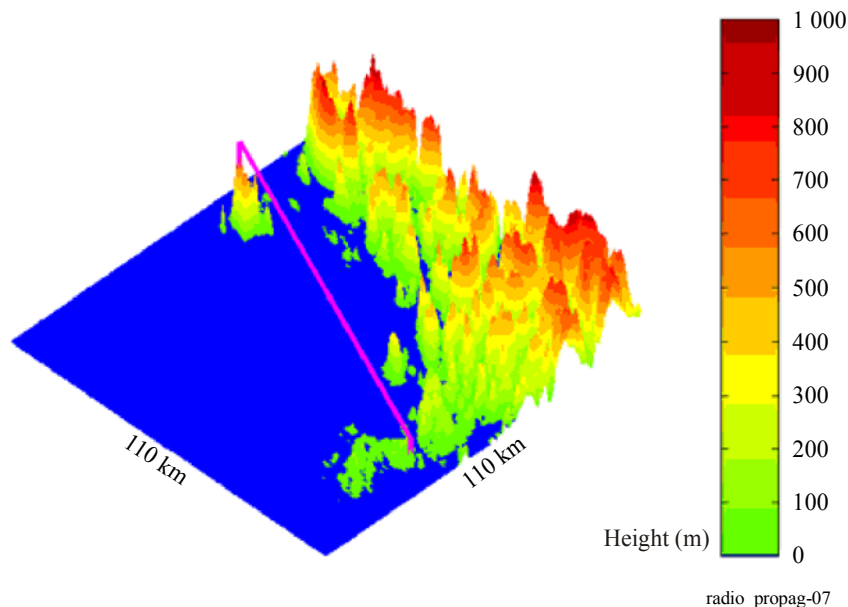
Methods along these lines have been investigated and commonly adopted by the propagation community [Crombie, 1984, Tjelta *et al.*, 1990].

FIGURE 6  
**Negative refractivity gradient in the lowest 65 m of the atmosphere  
 not exceeded for 1% of an average year  
 (see Recommendation ITU-R P.453)**

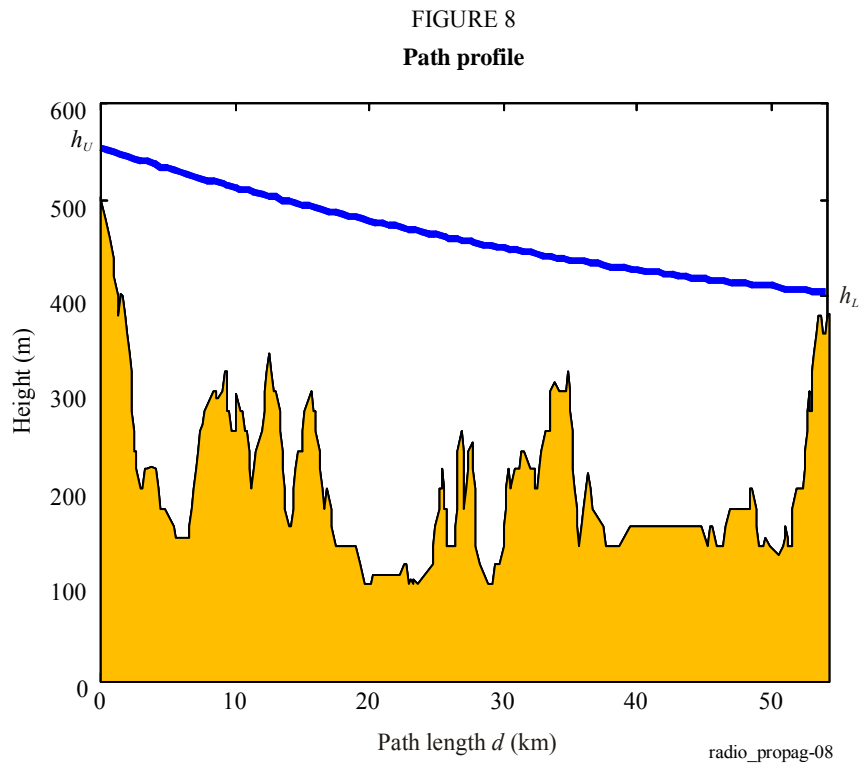


The area roughness is used in the most accurate method and digital data is required covering a 110 km by 110 km area where the link is located in the middle. The area surface roughness,  $s_a$ , is simply the standard deviation of all heights in the square.

FIGURE 7  
**Example of a 110 km by 110 km surface to calculate area roughness  $s_a$**



The mentioned methods employ slightly different functions with respect to the link variables of path length  $d$ , path inclination  $\varepsilon_p$ , lowest antenna height  $h_L$  and frequency  $f$ . Figure 8 illustrates a flat Earth plot of the path profile indicating the path length and the antenna heights to derive the path inclination, with the lowest antenna height and path length highlighted.



The basic methodology of deriving the empirical equations in Methods 1 and 2 for the percentage of time  $p$  of exceeding fade depth  $A$  was established using a multiple regression analysis technique on fading data for 47 paths in North Western Europe [Tjelta *et al.* 1990]. A later approach using maps of refractivity gradient statistics is actually a generalization for worldwide use based on an approach initially developed for use in Canada [Olsen and Segal, 1992]. Bases for the new ITU-R methods and an extensive analysis of the commonly used regional methods have been provided by [Olsen and Tjelta, 1999 and Olsen *et al.*, 2003]. In deriving the geoclimatic factors for Methods 1 and 2, the refractivity gradient data is necessary, which was obtained from numerical atmospheric data [Tjelta *et al.*, 1998]. The same article also provides the systematic regression and correlation method leading to the predictors. The actual coefficients used in Recommendation ITU-R P.530 originate from input documents to the ITU-R.

The methods are now very easy to implement in software as they do not leave users with manual or subjective judgment on classification. Clearly, the earlier methods gave accurate results for a trained user, but the move towards more software based tools make the method in Recommendation ITU-R P.530 more suitable.

### 5.1.1.3 Accuracy of the method for deep fade distribution tail

The path length,  $d$ , and the path inclination,  $\varepsilon_p$ , remain strong predictors for a good reason, the longer is the link, the more likely it is to be included in duct structures. By the same token, the more inclined the path is, the more likely it will not be affected by the typical horizontal layered duct structures. This seems reasonable with the lower antenna height as a predictor. It indicates surface based layers as a prime caused of multipath fading and enhancement. The lower the antenna, the more likely the path will be located in the ducts. It is more problematic to find an explanation for the frequency term, and it is only fair to indicate that it is a fairly weak predictor in multiple regression equations. But correlation between variables may mask out real dependencies, such as the obvious negative correlation between path lengths and frequency.

The overall standard deviations of prediction errors using Methods 1 and 2 are 5.7 dB and 5.9 dB, respectively (including the contribution from year-to-year variability). Within the wide range of paths included in these figures, a minimum standard deviation of error of 5.2 dB applies to overland paths for which  $h_L < 700$  m, and a maximum value of 7.3 dB for overwater paths. The small difference between the overall standard deviations, however, does not accurately reflect the improvement in predictions that is available using Method 1 for links over very rough terrain (e.g. mountains) or very smooth terrain (e.g. overwater paths). For example, standard deviations of error for mountainous links ( $h_L > 700$  m) are reduced by 0.6 dB, and individual errors for links over high mountainous regions by up to several decibels.

Methods 1 and 2 were derived from multiple regressions on fading data for 251 links in various geoclimatic regions of the world with path length  $d$  in the range of 7.5 to 185 km, frequencies  $f$  in the range from 450 MHz to 37 GHz, path inclinations  $|\epsilon_P|$  up to 37 mrad, lower antenna altitudes  $h_L$  in the range from 17 to 2300 m, refractivity gradients  $dN_1$  in the range from  $-860$  to  $-150$  N-unit/km, and area surface roughness  $s_a$  in the range from 6 to 850 m (for  $s_a < 1$  m, use a lower limit of 1 m). The results of a semi-empirical analysis indicate that the lower frequency limit of validity is inversely proportional to path length.

### 5.1.2 Basis and accuracy of the method for shallow fading

The method given in Recommendation ITU-R P.530 for predicting fade depths at various percentages of time combines an empirical interpolation procedure between the deep fading range of the distribution and 0 dB, with Method 1 or 2 discussed in the preceding section. The method was partly based on a fit of data in the 7-95 km path length range and the 2-37 GHz frequency range.

Nevertheless, it may also be valid for the wider ranges suggested for Methods 1 and 2 in the previous section.

All data available in the ITU-R database Table I-2 are used, i.e., all data with the required variables for the prediction methods Table 1 summarises test results of the prediction method in Recommendation ITU-R P.530 for the worst month multipath fading distribution where observed data where less than 20 dB faded. At 10% all available data has less fading than 20 dB, at 1% almost all has less. However, at 0.1% half of the worst month data are faded less than 20 dB and at 0.01% only a few, and finally, at 0.001% none. The tests show reasonably low mean errors and standard deviations of errors for percentages at and above 0.1%.

TABLE 1

Tests against the worst month shallow fading data observed less than 20 dB

Percentage of time	Number of observations	Mean error (dB)		Standard deviation (dB)	
		Method 1	Method 2	Method 1	Method 2
10	11	-1.0	-1.0	1.7	1.7
1	49	-1.2	-1.4	1.6	1.7
0.1	63	-0.2	-0.48	4.1	3.9
0.01	9	5.4	5.3	2.9	2.9

### 5.1.3 Basis and accuracy of the method for the enhancement range

The enhancement method is based on an analysis of available data found in [Tjelta and Tanem, 1992]. The approach is based on the assumption that the same atmospheric layers or ducting structures causing deep fading can also cause strong enhancement. If a link in an area exhibits much multipath fading it also exhibits much strong enhancement. Using the scarce data available, a simple fit was done to relate enhancement with the multipath fading tail. It also seems that the examples found in the concerned literature show that the strong tail of the enhancement distribution slope is about 3.5 dB per decade. The data suggested a fixed slope from the 10 dB enhancement level and onwards. Between 10 dB and 0 dB, a similar interpolation procedure as in the case for multipath fading is used.

The percentages ranging from 90% to 99.999%, correspond to 10% to 0.001% enhancement exceeded. All data used are those for which it is possible to predict.

TABLE 2  
Test results of the prediction methods for the worst enhancement

Percentage of time	Number of observations	Mean error (dB)		Standard deviation (dB)	
		Method 1	Method 2	Method 1	Method 2
99.999	4	-0.8	-0.6	2.8	2.7
99.99	8	-0.2	-0.1	3.1	3.0
99.9	10	-0.9	-0.8	1.8	1.8
99	10	-0.6	-0.6	2.0	2.0
90	3	-1.4	-1.4	0.8	0.8

The results indicate low mean and standard deviation for both methods, but there are few data available.

#### 5.1.4 Application examples

Location: Athens, GRC

Latitude: 38° 50' N

Longitude: 23° 40' E

Frequency:  $f = 6$  GHz

Path length:  $d = 60$  km

Transmitter antenna height:  $h_t = 45$  m

Receiver antenna height:  $h_r = 30$  m.

*Step 1:* For the given path location, the value of the point refractivity gradient ( $dN_1$ ) in the lowest 65 m of the atmosphere not exceeded for 1% of an average year, is  $-594.75$  N-unit/km. To obtain this result, the  $1.5^\circ$  grid in latitude and longitude in Recommendation ITU-R P.453 is applied.

*Step 2:* Then, the geoclimatic factor  $K$  for the average worst month is determined. To do so, the following quick calculation equation is used:

$$K = 10^{-4.2 - 0.0029 dN_1} = 0.00335 \quad (37)$$

*Step 3:* The corresponding simplified equation is used in the calculation of the multipath occurrence factor:

$$p_0 = Kd^{3.0} (1 + |\epsilon_p|)^{-1.2} \times 10^{0.033f - 0.001h_L} = 814.57\% \quad (38)$$

where:

$h_e$  and  $h_r$ : antenna heights (m) (above sea level)

$$|\epsilon_p| = |h_r - h_e| / d$$

$h_L$ : altitude of the lower antenna.

*Step 4:* The fade transition depth  $A_t$ , that is the transition between the deep- and the shallow-fading distribution, is given by:

$$A_t = 25 + 1.2 \log p_0 = 28.49 \quad \text{dB} \quad (39)$$

Step 5: Table 3 illustrates the percentage of time,  $p_w$  that various fade depths  $A$  (dB) are exceeded in the average worst month.

TABLE 3  
Percentage of exceedance of fade depth levels

Fade depth, $A$ (dB)	Percentage of exceedance, $p_w$ (%)
2	36.054
5	23.246
10	16.986
30	0.815

## 5.2 Statistics on fade number and duration

The planning and engineering of radio-relay systems are based on requirements concerning both availability and performance.

Unavailability is defined as the performance of the signal below a chosen threshold (as  $\text{BER} \geq 10^{-3}$  for a digital system) for more than 10 consecutive seconds, and/or whenever the signal is totally interrupted.

It is therefore necessary to know the statistics about the number and duration of fades in order to predict the probability of a radio system becoming unavailable.

Additionally, these statistics (as for the statistics of the rate of change of fades) are of great importance for the designers of protection switching systems for radio-relay systems.

### 5.2.1 Estimation procedures

For fade depths,  $A$ , greater than about 15 dB, the average number of fades per hour,  $N$ , and the average fade duration,  $t$ , at frequency,  $f$ , are usually estimated from:

$$N = C_1 10^{-\alpha_1 A f \beta_1} \quad (40)$$

and

$$t = C_1 10^{-\alpha_2 A f \beta_2} \quad (41)$$

TABLE 4  
Values for the equation (40) determined experimentally

Location	$\alpha_1$	$\alpha_2$	$\beta_1$	$\beta_2$	$\beta_1 + \beta_2$	$C_1$	$C_1$
France	0.5	0.5	1.4	-1	0.4	-	-
Denmark	0.67	0.33	-	-	-	$\sim 0.7^{(1)}$	-
United States	0.5	0.5	1.32	-0.50	0.82	-	$56.6 \sqrt{d}$
Switzerland	0.41	0.59	1.38	-1.38	0	-	-

<sup>(1)</sup> Based on an assumed value for  $\beta_1$  of 1.4.

Although it is not yet possible to give a general set of rules for the parameters of equations (40) and (41), the values listed in Table 4 above were determined experimentally by several administrations for overland paths and can be used for guidance.

### 5.2.2 Experimental basis of the estimation procedures

Measurements of the average number and duration of fades have been carried out by several administrations at frequencies between 4 and 15 GHz [Boithias, 1981]. Equations (40) and (41) are based on data for overland paths obtained in France [Boithias, 1981], Denmark [Stephansen and Mogensen, 1979], the United States of America [Lin, 1971; Vigants, 1971; Bullington, 1971 and Barnett, 1972], and Switzerland. The constants of proportionality,  $C_1$  and  $C_2$ , depend on the period under consideration, path length, climate, etc., however, until now these dependencies are not accurately known. There is some evidence suggesting that  $N$  (and therefore  $C_1$ ) tends to increase with increasing path length. Measurements in former USSR suggested that  $t$  decreases with path length and with path clearance.

In each case of the aforementioned table, the sum of the exponents  $\alpha_1$  and  $\alpha_2$  is equal to 1, since the product  $N \cdot t$  represents the total fade duration, which for deep fades is proportional to the received power.

The distribution of fade duration, for which the average value is given by equation (41), has been observed to follow a lognormal law [Boithias, 1981]. The standard deviation of fade duration has been observed to decrease with fade depth from 13.5 to 15 GHz and increase somewhat with frequency [Nadenenko and Sviatogor, 1972 and Stephansen and Mogensen, 1979]. It appears to exhibit only a slight dependence on the geometrical characteristics of the path and the climatic conditions [Nadenenko and Sviatogor, 1972].

Over sufficiently flat paths, the number of multipath related fades has been observed to increase with increasing path clearance. On coastal paths, the number of fades was found to be substantially higher than on inland paths. For example, the number of measured multipath related fades on overseas paths was found to be five to ten times higher than that on overland paths with a flat region in the vicinity of the ground reflection point [Nadenenko and Sviatogor, 1972].

Measurements on a 22 km overseas path off the West coast of France showed a decrease in the median value of the fade duration as well as in the standard deviation, with an increase in frequency from 2 to 15 GHz.

### 5.3 Rate of change of signal level

The rate of change of signal level has been measured in one of the two following ways: either as a change in signal level within a specified time interval, or as a time interval associated with a specified small change in level. In general, the few experimental data available have shown that this rate increases with frequency and fade depth (consistent with the behaviour of  $t$  in equation (41)) and increases with path length.

Measurements over one year in France on a 53 km overland link operating at 13 GHz showed the rates of change in signal level to have lognormal distributions with the same standard deviation for average fade depths of 20 and 30 dB over 10 dB intervals. The median values were 5 dB/s around 20 dB and 20 dB/s around 30 dB. The ratio of the rates of change over a standard deviation interval was 5.4 [Derrennes, 1979].

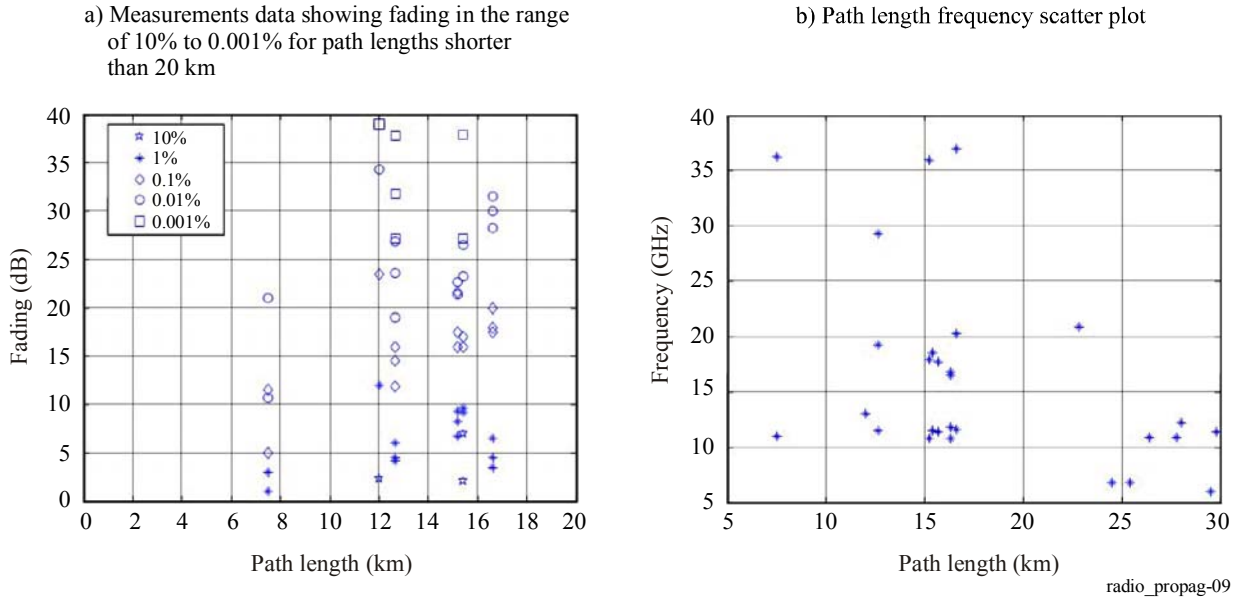
Also in France, it was observed on a 53 km overland path that the rates of change of signal level at four fixed frequencies between 11.25 GHz and 11.65 GHz had approximately lognormal distributions for fade depths exceeding 12 dB. The rates of change exceeded in 0.1% of cases were above 100 dB/s. The ratio of the rates of change over a standard deviation interval was roughly 2.7 [Martin, 1983].

On an overseas path in the former USSR, fading rates of 5 dB/s at 2 GHz and rates above 100 dB/s observed at 15 GHz were measured with 10 dB interval [Gavzilina *et al.*, 1986].

### 5.4 Short paths

Measurement data indicate significant fading even for paths as short as 10 km, but no multipath data for paths shorter than 7 km have been reported. From Fig. 9a) it is noted that at about 7 km the data indicates even 20 dB fading at 0.01% of the time. It seems that there might be some multipath fading data at even shorter lengths. On the other hand, for very short paths, ducting mechanisms seem not to create deep fading.

FIGURE 9



## 5.5 Short periods of time

The prediction methods for fading and enhancement due to multipath and its related mechanisms given in Recommendation ITU-R P.530 are based on statistics of long term propagation measurements and are adequate for planning of line-of-sight radio-relay links.

However, methods of predicting reliability and performance indicators over short intervals of time are important, particularly for bringing a system into service according to Recommendation ITU-R F.1330. In Recommendation ITU-R P.530, only general guidance on this subject is given, as the information available about short term fading measurements is limited to particular regions of the world.

The most detailed studies reported were carried out in the frequency range 3.7-8 GHz on 25 radio-relay hops of length from 36.3 to 166.3 km located in different climatic regions in the central, north-western and southern regions of the European part of Russia, the Baltic coast, Ukraine, Belarus, Crimea and the Black Sea coast in the Caucasus [Minkin and Nadenenko, 1998]. The statistics of fading over short periods of time (15 min, 1 h, 3 h, 6 h, 1 day, 4 days and 7 days) were obtained through the processing of continuous round-the-clock signal level recordings during the summer months. A total of 23 000 h of experimental data for short test periods were processed.

Based on those results, and for particular regions of the world, the following empirical equations were proposed for converting worst-month fading distributions to distributions for shorter periods of time.

For relatively flat paths:

$$p_{sw} = p_w \cdot \left( 89.34T^{-0.854} + 0.676 \right) \% \quad \text{for } 1 \text{ h} \leq T \leq 720 \text{ h} \quad (42)$$

For hilly coastal paths:

$$p_{sw} = p_w \cdot \left( 119T^{-0.78} + 0.295 \right) \% \quad \text{for } 1 \text{ h} \leq T \leq 720 \text{ h} \quad (43)$$

For hilly land paths:

$$p_{sw} = p_w \cdot \left( 119.85T^{-0.834} + 0.175 \right) \% \quad \text{for } 1 \text{ h} \leq T \leq 720 \text{ h} \quad (44)$$

## 5.6 Tandem links

As in the case of rain attenuation, the correlation between deep fades in individual hops of tandem links is usually considered negligible. The overall outage probability for a tandem series will then equal the sum of outage probabilities for the individual links:

$$P_T = \sum_{i=1}^n P_i \quad (45)$$

where  $P_i$  is the outage probability for the  $i$ th of the total  $n$  links.

In measurements made in Japan for five consecutive links, the simultaneous probability of occurrence of a given fade depth for two consecutive links was always less than 10% of the probability for each individual link. Measurements made in 18 pairs of adjacent hops in Brazil [Silva Mello *et. al.*, 2005] indicate that a higher correlation can be observed in tropical and equatorial climates. The results indicate a strong correlation between the joint distribution attenuation value and the smaller value of attenuation in the individual links distribution for the same percentage of time.

## 6 Propagation induced distortion

The primary cause of distortion on LoS links in the UHF and SHF bands is the frequency dependence of amplitude and group delay during clear-air multipath conditions. Such distortion, which usually is called frequency selective fading, increases with increasing system bandwidth and depends on the amplitude and relative delay for the individual paths between the transmitter and the receiver. Multipath induced distortion is likely to be the limiting factor for high capacity digital radio links for systems operating at frequencies below about 15 GHz. At higher frequencies the effects of the induced distortion must also be taken into account. However, one has to consider that, usually, the precipitation effects are much higher. The present chapter describes these effects as well as the channel models for estimating the system performance due to frequency selective fading. Techniques described elsewhere in this Handbook should be used to counteract these effects.

### 6.1 Multipath propagation models

A method predicting the performance due to multipath propagation (MP) consists of:

- a model for the MP,
- a model for the statistical occurrence of MP,
- a model on how the equipment can resist the MP.

The multipath propagation is usually described in terms of two or more discrete rays, given by amplitude and delay, and combined at the receiver. The number of rays may sometimes be large, but a deep fade occurs when two rays of comparable amplitude add destructively. It may well be that the deep fade (and frequency selective fading) are normally caused by one single ray arriving at a noticeable delay and adding to the other ray(s) that arrive earlier in time.

The complex transfer function of the radio channel for a physical multi-ray model is given by:

$$H(\omega) = \sum_{i=1}^N A_i e^{-j(\omega T_i + \phi_i)} \quad (46)$$

where:

$$\omega = 2\pi f$$

$A_i$ ,  $T_i$  and  $\phi_i$ : amplitude, delay and phase of the  $i$ -th ray, respectively.

To represent a limited bandwidth radio channel (40-100 MHz), simpler mathematical models may be used. These models may be classified as *polynomial* or *hypothetical* ray models.

### 6.1.1 Hypothetical ray models

The multipath transfer function can also be described using different models with a limited number of rays. These models are not physical because of the simplifications assumed in the expression of the transfer function. They are therefore referred to as hypothetical ray models.

The simplified three ray model, also called the Rummler model [Rummler, 1978], is given by:

$$H(\omega) = a \left( 1 - b e^{\pm j(\omega - \omega_M)\tau_f} \right) \quad (47)$$

The model has four parameters;  $a$  and  $b$  are the coefficients related to the amplitude and the shape of the selective fading respectively,  $\tau$  is the delay of the second hypothetical ray, and  $\omega$  is the angular frequency of the maximum fade depth. The number of parameters are often reduced to three by setting the delay to a fixed value, usually  $\tau = 6.3$  ns.

If the number of parameters are reduced to two,  $b$  and  $\omega$ , by setting  $a = 1$ , the model is called a normalized two ray model.

### 6.1.2 Polynomial models

Both real and complex polynomials can be used to represent the transfer function. The polynomial expression of amplitude and group delay is a function of frequency, with the general form of:

$$H(\omega) = \sum_{k=0}^N C_k \omega^k \quad (48)$$

where the coefficients  $C_k$  may be real or complex.

### 6.1.3 Parametric models

A different approach is to describe radio channel distortion using a parametric representation of the amplitude difference. The amplitude differences at two discrete frequencies are used to characterize the amplitude distortion. This method is generally called linear amplitude distortion method (LAD). Also, two fixed frequencies, preferably at equal distance from the centre of the radio channel, can be used, i.e., in-band amplitude dispersion (IBAD). Alternatively the two frequencies can correspond to the points of maximum and minimum fade depths relative to the free space level, referred to as in-band power dispersion (IBPD).

## 6.2 Performance calculation

The conventional method for calculating outage times for analogue systems is based on the concept of single-frequency fading and is therefore not directly applicable to high-capacity digital radio link systems. An increase in the fade margin, which in analogue systems will tend to reduce the effects of thermal noise, will not improve the performance of digital systems if frequency selective fading has already collapsed the eye-diagram amplitude to zero.

To use propagation models in performance calculations for high-capacity digital systems, it is necessary to have statistical descriptions of how all the different parameters behave during multipath fading. This issue can be separated into two parts: a characterization of the nature of the random fluctuations in the multipath transfer function model, ideally as a multidimensional joint probability distribution; a statement of the way in which the parameters of this distribution depend on the physical properties of the radio path, e.g., path length, radio frequency, path inclination, climate, etc.

Combined with statistics for the probability of occurrence of fading, this would give an unconditional joint probability distribution for the parameters determining system behaviour. The full set of parameters for a multipath model can be viewed as the dimensions of a multidimensional surface. Outage is caused when these parameters lie in a certain critical region of the multidimensional surface.

The outage of a digital radio system may be predicted using different methods such as:

- fade margin methods;
- signature curve methods;
- method using LAD statistics.

### 6.2.1 Signature curve methods

The signature curve method is not a single method, since several different approaches of this method exist. In this chapter, general principles for the method and some examples of solutions are given. For more details see the ITU-R Handbook – Digital Radio-Relay Systems.

The probability of outage ( $\text{BER} > 10^{-3}$ ) caused by multipath fading ( $P$ ) can be calculated from the outage probability due to frequency selective fading ( $P_s$ ) and the outage probability due to thermal noise ( $P_f$ ) using the following equation:

$$P = \left( P_f^{\alpha/2} + P_s^{\alpha/2} \right)^{2/\alpha} \quad (49)$$

$P_f$  can be calculated as indicated in Recommendation ITU-R P.530.

The outage probability due to frequency selective fading is given by the product of the probability of multipath fading  $\eta$  and the probability of outage given by intersymbol interference during multipath fading:

$$P_s = \eta \cdot (P_s|_{MP}) \quad (50)$$

The probability of multipath fading  $\eta$  can be linked to the deep fade occurrence factor  $P_0$  or to the parameters of the statistical distribution of concurrent slow fading. One suggested equation is:

$$\eta = 1 - e^{0.2 P_0^{3/4}} \quad (51)$$

The last term can be based on the simplified three ray model or on a two ray model. The outage probability is obtained by integrating the joint density distribution function of the random variables defined by the channel model over the critical region in the probability space. For the calculation one must make assumptions about the probability distributions for the different parameters, e.g. relative echo delay  $\tau$ , the relative echo amplitude  $k$  and the notch frequency  $\phi_0$ . A common way to describe the outage is to use the following equation is:

$$P_s|_{MP} = \int_0^{\infty} p(\tau) d\tau \int_{-1/2\pi}^{1/2\pi} \phi_0 d\phi \int_D p(k) dk \quad (52)$$

where  $D$  is the outage region defined by minimum and maximum phase signatures. If approximated signatures are used the result of the integration can be described by the following equation:

$$P_s|_{MP} = \frac{C \cdot W \cdot \lambda_a \cdot \{\tau^2\} \cdot P_b(1)}{\tau_r} \quad (53)$$

where:

- $C$ : constant factor
- $W$ : signature width (MHz)
- $\lambda_a$ : average critical height of the signature
- $\tau_r$ : reference delay for  $\lambda_a$  (ns)
- $P_b(1)$ : probability density function value corresponding to amplitude  $b = 1$
- $\{\tau^2\}$ : second order moment of the echo relative delay distribution ( $= 2\tau_m^2$ ) for exponential distribution and  $= \mu^2 + \nu^2$  for Gaussian distribution)
- $\tau_m$ : mean delay for the path that is related to the path length and the antenna pattern.

Different assumptions have been proposed for the pdf of the relative echo amplitude,  $P_b(b)$ : uniform, exponential [Saleh and Valenzuela, 1987], Weibull [Salous and Bajj, 1998], and Rayleigh-over-Rayleigh [Shafi, 1987]. The pdf of frequency minimum  $P_{f_0}(f_0)$  is uniform.

Two different echo delay distributions are assumed, for  $p(\tau)$ . In the first case the echo delay  $\tau$  has a negative exponential distribution with mean value  $\tau_m$  that depends on path length. The following empirical relation between  $\tau_m$  (ns) and  $d$  (km) is used for paths without strong surface reflections:

$$\tau_m = \tau_{m0} \cdot \left( \frac{d}{50} \right)^n \quad (54)$$

where  $n$  falls in the range 1.3 to 1.5 and  $\tau_{m0}$  is the mean relative delay for a standard path of 50 km.

In the second case, a Gaussian distribution with mean  $\mu$  and variance  $v^2$  is assumed. These parameters can be chosen independently, permitting a more accurate fit to measured (or calculated) density functions for individual hops than the sole parameter of the exponential density allows. In the absence of any hop-specific information, the model assumes:

$$\mu = 0.70 (d/50) \text{ ns} \quad (55)$$

$$v^2 = 0.49 (d/50) \text{ ns}^2 \quad (56)$$

The Gaussian distribution includes both positive and negative delays.

An approximation for the outage due to frequency selective fading can be obtained by using a rectangular approximation for the signature. In this case the following equation can be used:

$$P_S|_{MP} = \frac{C \cdot W \cdot 10^{-B/20} \cdot \tau_m}{\tau_r} \quad (57)$$

where:

- $B$ : signature depth
- $W$ : signature width
- $C$ : a constant
- $\tau_r$ : signature reference delay
- $\tau_m$ : mean delay.

Account must be taken of the relative occurrence of minimum phase and non-minimum phase conditions by computing outage probability separately when signatures for minimum and non-minimum phase are different.

#### **Calculation example:**

Location: Beijing, CHN

Latitude: 39° 55' N

Longitude: 116° 25' E

Frequency:  $f = 2$  GHz

Path length:  $d = 80$  km

Transmitter antenna height:  $h_t = 100$  m

Receiver antenna height:  $h_r = 55$  m.

*Step 1:* Calculate the mean time delay from:

$$\tau_m = 0.7 \left( \frac{d}{50} \right)^{1.3} = 1.29 \text{ ns} \quad (58)$$

*Step 2:* It is necessary to calculate the multipath activity parameter  $\eta$  (see § 7.2.2). The value of  $\eta$  is function of  $p_w$  and, in this case,  $\eta = 0.267$ .

*Step 3:* Let us assume that the modulation format is 8-PSK. According to Recommendation ITU-R F.1093, the normalized system parameter for this specific modulation is  $K_n = 7$ . Note that  $K_n$  depends on the signature width and depth and also on the reference delay.

*Step 4:* Assuming the same normalized system parameter for the minimum phase and the non-minimum phase fades, that is,  $K_{n,M} = K_{n,NM} = 7$  and a value of  $T = 105$  ns for the baud period (corresponding to a typical bit rate), the selective outage probability can be calculated by:

$$P_s = 2.15 \eta (K_{n,M} + K_{n,NM}) \frac{\tau_m^2}{T^2} = 0.0012 \quad (59)$$

### 6.2.2 Fade margin methods

The use of fade margins as system characteristics derives from the fading law for multipath fading at a single frequency. By substituting the net fade margin (or effective fade margin) for the flat fade margin, the outage on the hop can be calculated by using equation (15) or (28) in Recommendation ITU-R P.530. The net fade margin is defined as the single frequency fade depth exceeded for the same number of seconds as a threshold error ratio of, for example,  $10^{-3}$ .

Another approach for the fade margin method accounts for the dispersiveness of the fading by using dispersion ratios. In this method, the net fade margin is regarded as the composite of the effects of thermal noise, intersymbol interference due to multipath dispersion and interference. One way to obtain this is to determine the dispersive fade margin of a radio signal on a path with a known dispersion ratio of  $DR_0$ . This value is taken as a dispersive fade margin reference (DFMR). Then the dispersive fade margin that would be measured or predicted on a path with a dispersion ratio of  $DR$  is given by:

$$DFM = DFMR - 10 \log (DR/DR_0) \quad (60)$$

$DR$  is given by the following equation:

$$DR = \frac{T_{IBPD}}{T_{SFF} \cdot (BF)^2} \quad (61)$$

where:

$T_{IBPD}$ : amount of time that a chosen in-band power difference (IBPD) value is exceeded

$T_{SFF}$ : amount of time that a chosen single frequency fade (SFF) value is exceeded

$BF$ : bandwidth correction factor, which is the ratio of 22 MHz to the measurement bandwidth.

### 6.2.3 Method using linear amplitude dispersion (LAD) statistics

Propagation distortion includes both amplitude and delay distortion. Distortion caused by two path fading has a complex shape and cannot directly be composed completely by LAD. However, LAD is dominant. The effects of other distortions, such as delay distortion or higher degree amplitude distortion on outage are described accurately and appropriately by the threshold LAD. This means that outage probability caused by frequency selective fading can be estimated if equivalent LAD is given and LAD occurrence is known.

For each radio path, the cumulative distribution of in-band amplitude dispersion (IBAD) can be determined for the channel bandwidth using experimental results or with the calculation method described here [Martin *et al.*, 1993].

Knowing that the autocorrelation function  $\rho$  of fade depth at two fixed frequencies depends mainly on ground reflections, it is possible to calculate the cumulative distribution of IBAD for the channel bandwidth on a given radio path. The outage time during a given period will depend on  $D_c$ , the excess of carrier to noise ratio  $C/N$  above the flat fade margin MB, and on  $S$ , the value of IBAD statistically associated with  $D_c$ .

Without digital equalization, the equation for computing the  $S$  value of IBAD giving a BER equal to  $10^{-3}$ , for various values of  $D_c$  and for various modulation types, is as follows:

$$S = C_0^2 \left[ 1 - \frac{1}{(1 + D_C^{1/15})^n} \right] \cdot F^{0.2} \quad (62)$$

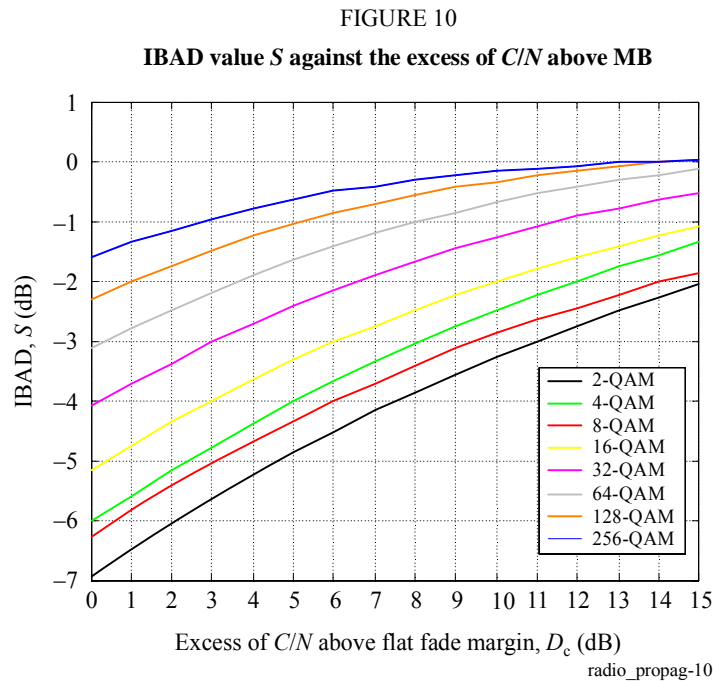
where:

$$n = \frac{\sqrt{N}}{10} \quad (63)$$

$$\log C_0^2 = -0.74 \log(N) + 1.91 \quad (64)$$

$F = 9 - N$  with  $F = 1$  if  $F < 1$ .  $N$  is the number of modulation levels.

As an example, the above procedure for calculating the IBAD value  $S$  against the excess of  $C/N$  above MB is illustrated in Fig. 10 for various modulation levels  $N$ .



When linear time domain equalization is used, the  $S_E$  value of IBAD giving a BER equal to  $10^{-3}$  is derived from the  $S$  value without equalization using the following equation:

$$S_E = S * k_E \quad (65)$$

where:

$$k_E = k + 2.46/N \quad (66)$$

and

$$\log k = 0.6636 \log N - 0.577 \quad (67)$$

The equation is valid values up to 256-QAM.

The correct value of outage time can be obtained using an iterative computing process adjusting the  $S$  value derived from the equation above to the  $S$  value derived from the equiprobability curve of  $S$  and fade depths  $F$  given from the autocorrelation function  $\rho$  characterizing the radio path.

## 7 Reduction in cross-polarization discrimination

To increase channel capacity without increasing bandwidth, orthogonal polarizations (either linear or circular) may be used independently for transmission at the same frequency channel over the same path. However, this technique may be impaired by the possibility that, in propagation through the atmosphere, some of the energy transmitted in one polarization can be transferred to the orthogonal polarization, thus causing co-channel interference in frequency re-use systems. To a lesser extent, the effect may also cause adjacent channel interference in frequency interleaved systems. When signals in two orthogonal polarizations  $a$  and  $b$  are transmitted at the same level, the ratio of the co-polarized received signal ( $ac$  or  $bc$ ) to the cross-polarized received signal ( $bx$  or  $ax$ ) in that channel, is known as cross-polarization isolation (XPI) and frequently used in systems design. These ratios  $ac/bx$  and  $bc/ax$  are not necessarily the same. Propagation experiments, on the other hand, usually provide measurements of cross-polarization discrimination (XPD), which is the ratio  $ac/ax$  when only the polarization  $a$  is transmitted. That is to say that the co-polar signal  $ac$ , and the cross-polar signal  $ax$ , are each measured independently and in the absence of any orthogonally-polarized signal  $b$ . Due to the characteristics of the antenna patterns in both terminals, a cross-polarized component will exist in the received signal even in normal propagation conditions through a standard atmosphere. The associated XPD can significantly deteriorate due to rain and hydrometeors other than rain, and also during periods of multipath propagation. In this chapter, the basis of prediction methods given in Recommendation ITU-R P.530 for estimation of XPD reduction in both clear-air and rain conditions are presented. Although conceptually different, as discussed above, the XPI and the XPD may be considered to be the same for practical applications [Oguchi, 1973].

### 7.1 Channel model

The discussion presented in the sections below follow the approach presented in the COST 235 [COST, 1996] Final Report.

The development of radio relay systems with frequency re-use of orthogonal polarisation has required the extension of the propagation channel model in order to take into account the transmission characteristics of the atmosphere in both polarisation planes. In this section, a general approach has been adopted in order to consider every possible effect (due to both propagation and antennas) and, as a further step, only the most relevant terms are kept; therefore a description of the depolarising phenomenon is supplied in terms of the (XPD) factor.

The transmission matrix  $M$  can be defined considering the antennas and the atmosphere (in between the two antennas) separately. To produce the matrix, some initial considerations have to be made.

If  $E_0$  is the field intensity at the receiver and  $E_i$  at the transmitter, it is possible to express these figures as a column matrix consisting of the vertical (V) and horizontal (H) components of the fields:

$$\begin{aligned} E_0 &= \begin{bmatrix} E_{H_0} \\ E_{V_0} \end{bmatrix} \\ E_i &= \begin{bmatrix} E_{H_i} \\ E_{V_i} \end{bmatrix} \end{aligned} \tag{68}$$

The effects of the transmitting and receiving antennas are represented by their co-polar and cross-polar radiation patterns in the V and H planes, denominated respectively  $g_{V,H}$  and  $x_{V,H}$ :

$$T = \begin{bmatrix} g_{TV} & x_{TV} \\ x_{TH} & g_{TH} \end{bmatrix} \quad (69)$$

$$R = \begin{bmatrix} g_{RV} & x_{RV} \\ x_{RH} & g_{RH} \end{bmatrix}$$

The transmission matrix of the propagation medium can be written as:

$$S = \begin{bmatrix} S_{VV} & S_{VH} \\ S_{HV} & S_{HH} \end{bmatrix} \quad (70)$$

The transmission matrix M can be obtained from the following matrix equation:

$$E_0 = R \cdot S \cdot T \cdot E_i = M \cdot E_i \quad (71)$$

Writing the transmission matrix explicitly, one obtains:

$$M = \begin{bmatrix} M_{VV} & M_{VH} \\ M_{HV} & M_{HH} \end{bmatrix} \quad (72)$$

An expression for each component can be derived from equations (74):

$$\begin{aligned} M_{VV} &= g_{RV} \cdot S_{VV} \cdot g_{TV} \\ M_{VH} &= g_{RV} \cdot S_{VV} \cdot x_{TV} + g_{RV} \cdot S_{VH} \cdot g_{TH} + x_{RV} \cdot S_{HH} \cdot g_{TH} \\ M_{HV} &= x_{RH} \cdot S_{VV} \cdot g_{TV} + g_{RH} \cdot S_{HV} \cdot g_{TV} + g_{RH} \cdot S_{HH} \cdot x_{TH} \\ M_{HH} &= g_{RH} \cdot S_{HH} \cdot g_{TH} \end{aligned} \quad (73)$$

Where the terms in which at least two out of three elements are diagonal have been omitted because the cross transmission terms are in general much smaller than the direct ones.

The received field for both polarisations can be derived from equation:

$$\begin{aligned} E_{V0} &= M_{VV} \cdot E_{Vi} + M_{VH} \cdot E_{Hi} \\ E_{H0} &= M_{HV} \cdot E_{Vi} + M_{HH} \cdot E_{Hi} \end{aligned} \quad (74)$$

The cross-polar discrimination is given according to the usual definition:

$$\begin{aligned} XPD_V &= -20 \log \left[ \frac{E_{H0}}{E_{V0}} \right]_{E_{Hi}=0} = -20 \log \left( \frac{M_{HV}}{M_{VV}} \right) \\ XPD_H &= -20 \log \left[ \frac{E_{V0}}{E_{H0}} \right]_{E_{Vi}=0} = -20 \log \left( \frac{M_{VH}}{M_{HH}} \right) \end{aligned} \quad (75)$$

while the isolation of the cross-polar channel is:

$$\begin{aligned} XPI_V &= -20 \log \left( \frac{M_{VH}}{M_{VV}} \right)_{E_{Hi}=E_{Vi}} \\ XPI_H &= -20 \log \left( \frac{M_{HV}}{M_{HH}} \right)_{E_{Hi}=E_{Vi}} \end{aligned} \quad (76)$$

Usually, the following assumption is well satisfied [Olsen, 1981]:

$$\begin{aligned} XPD_V &\cong XPI_V \\ XPD_H &\cong XPI_H \end{aligned} \quad (77)$$

### 7.1.1 Nominal received field

In the case of a normal received field, the propagation contribution is as follows:

$$\begin{aligned} S_{VV} &= S_{HH} = 1 \\ S_{VH} &= S_{HV} = 0 \end{aligned} \quad (78)$$

For simplicity purposes, it is assumed that the antennas have the same radiation pattern in the  $H$  and  $V$  planes, therefore the co-polar and cross-polar radiation patterns in the  $V$  and  $H$  planes are the same and denoted by  $g_{TR}$  and  $x_{TR}$ .

As a result, the isolation is given by:

$$XPI = -20 \log \left( \frac{x_R}{g_R} + \frac{x_T}{g_T} \right) \quad (79)$$

The discrimination properties of the antennas are the combined effects of the co- and cross-polar radiation patterns:

$$\begin{aligned} X_{RN} &= -20 \log \left( \frac{x_R}{g_R} \right) \\ X_{TN} &= -20 \log \left( \frac{x_T}{g_T} \right) \end{aligned} \quad (80)$$

Usually, in typical applications, the antennas are pointed at boresight which means that  $g_T = g_R = 1$ . Taking this into account, equation (80) becomes:

$$\begin{aligned} X_{RN} &= -20 \log (x_R) \\ X_{TN} &= -20 \log (x_T) \end{aligned} \quad (81)$$

Solving for  $x_{R,T}$  and substituting the results in equation (79), the following equation is obtained:

$$XPI = -20 \log \left( 10^{\frac{-X_{RN}}{20}} + 10^{\frac{-X_{TN}}{20}} \right) \quad (82)$$

This result does not include any additional propagation effects and should be used as nominal for equipment installation.

### 7.1.2 XPI due to propagation (1 ray approach)

The elements of the propagation transmission matrix in this case (non frequency selective fading) are:

$$\begin{aligned} S_{VV} &= l_V \exp(-j\phi_V) \\ S_{HH} &= l_H \exp(-j\phi_H) \\ S_{VH} &= d_V \exp(-j\gamma_V) \\ S_{HV} &= d_H \exp(-j\gamma_H) \end{aligned} \quad (83)$$

where:

- $l$  and  $\phi$ : additional attenuation and phase shift on the co-polar channel
- $d$  and  $\gamma$ : attenuation and phase shift on the cross-polar channel.

Using equation (76) and the aforementioned assumption of the antennas having the same radiation pattern in the  $H$  and  $V$  planes, the isolation is given by:

$$XPI = -20 \log \left[ \frac{g_T x_R + x_T g_R (l_H/l_V) \exp[-j(\phi_H - \phi_V)]}{g_T g_R} + \frac{d_H}{l_V} \exp[-j(\gamma_H - \phi_V)] \right] \quad (84)$$

The above equation can be used to model both clear air and rain conditions.

### 7.1.2.1 Clear air conditions

Assuming that the differential attenuation between the  $H$  and  $V$  components are negligible, then  $(l_H/l_V) \exp[-j(\phi_H - \phi_V)]$  is approximately unity and equation (84) becomes:

$$XPI = -20 \log \left[ \frac{x_R}{g_R} + \frac{x_T}{g_T} + \frac{d_H}{l_V} \exp[-j(\gamma_H - \phi_V)] \right] \quad (85)$$

Because of the variations of the atmospheric refractive index, the electromagnetic rays are, in general, received with an angle of arrival  $\delta$  not equal to the nominal one. As a result:

$$-20 \log \left[ \frac{x_R(\delta)}{g_R(\delta)} \right] = X_R(\delta) - G_R(\delta) \quad (86)$$

The radiation pattern in the cross-polar plane can be approximated by the following equation:

$$X_R(\delta) = X_{RN} - Q(\delta) \quad (87)$$

where  $Q(\delta)$  is the degradation of the cross polar discrimination due to the propagation induced misalignment.

The cross-polar contribution due to propagation is given by:

$$XPI_P = -20 \log \left[ \frac{d_H}{l_V} \exp[-j(\gamma_H - \phi_V)] \right] \quad (88)$$

Making the appropriate substitutions, and given the facts presented in the literature [Olsen, 1981] the cross-polar contribution due to propagation is about 200 dB below the nominal co-polar level, the isolation in equation (84) can be written as follows:

$$XPI = -20 \log \left[ 10^{-\frac{x_{RN} - Q(\delta) - G(\delta)}{20}} + 10^{-\frac{x_{TN}}{20}} \right] \quad (89)$$

### 7.1.2.2 Rain conditions

In this case, equation (84) cannot usually be simplified even if, for frequencies below 15 GHz, approximation  $(l_H/l_V) \exp[-j(\phi_H - \phi_V)] \cong 1$  still holds.

The isolation is then given by:

$$XPI = -20 \log \left[ 10^{-\frac{x_{RN}}{20}} + 10^{-\frac{x_{TN}}{20}} + 10^{-\frac{XPD_p}{20}} \right] \quad (90)$$

The median value of the propagation contribution  $XPD_p$  is given by the following equiprobability equation:

$$XPD_p = U - V \log(CPA) \quad (91)$$

where:

$$CPA = -20 \log |l_V \exp(-j\phi_V)| \quad (92)$$

is the co-polar attenuation ( $g_T = g_R = 1$ ), and the parameters  $U$  and  $V$  can be evaluated using the results in [Olsen, 1981].

### 7.1.3 XPI due to multipath propagation (2 rays)

In the case of interference among two or more ray components, the frequency selective effects become important. Considering a two-ray model (ray 1 and ray 2), the resulting received field is in general derived from equation (1) and it can be expressed by:

$$\bar{E}_0 = \bar{E}_{01} + \bar{E}_{02} = (\bar{M}_1 + \bar{M}_2) \cdot \bar{E}_i = \bar{M} \cdot \bar{E}_i \quad (93)$$

Making use of equation (93) and of the definition (75), the isolation is:

$$XPI = -20 \log \left[ \frac{\frac{x_{T1}}{g_{T1}} + \frac{x_{R1}}{g_{R1}} + b \left( \frac{x_{T2}}{g_{T2}} + \frac{x_{R2}}{g_{R2}} \right) \exp(-j\varphi) + \frac{d_{H1}}{l_{V1}} \exp(-j\varphi_1) + \frac{d_{H2}}{l_{V2}} b \exp(-j\varphi_2)}{1 + b \exp(-j\varphi)} \right] \quad (94)$$

where:

$$b = \frac{g_{T2} l_{V2} g_{R2}}{g_{T1} l_{V1} g_{R1}} \quad (95)$$

is the relative amplitude, and:

$$\begin{aligned} \varphi &= \varphi_{V2} - \varphi_{V1} \\ \varphi_1 &= \gamma_{H1} - \varphi_{V1} \\ \varphi_2 &= \gamma_{H2} - \varphi_{V1} \end{aligned} \quad (96)$$

where the approximation  $(l_H / l_V) \exp[-j(\varphi_H - \varphi_V)] \cong 1$ ,  $(l_H / l_V) \exp[-j(\varphi_H - \varphi_V)] \cong 1$  is used for both rays. It should be noted that the numerator and the denominator in equation (94) represent the elements of the transmission matrix  $M$  without the constant quantity:

$$a_1 = g_{T1} l_{V1} g_{R1} \exp(-j\varphi_{V1}) \quad (97)$$

equal to the non selective attenuation on the co-polar channel.

Assuming for the reference ray (ray 1) the same hypotheses and relationships derived in the preceding section for a single ray and considering both antennas (Tx and Rx) equal, equation (94) becomes:

$$XPI = -20 \log \left[ \frac{10^{-\frac{XPI_1}{20}} + b \left( 2 \times 10^{-\frac{X_{RN} - Q(\delta_2) - G(\delta_2)}{20}} + d_{H2} \right) \exp(-j\varphi)}{1 + b \exp(-j\varphi)} \right] \quad (98)$$

where  $XPI_1$  is given by equation (84),  $\delta_1$  and  $\delta_2$  are the angles of arrival of the reference and of the secondary ray with respect to the nominal pointing direction.

### 7.1.4 Co-polar attenuation dependence

The dependence of XPI on the co-polar signal attenuation can be expressed on average with a relation similar to the one reported by Recommendation ITU-R P.530:

$$XPI = C - CPA \quad (99)$$

where:

$$CPA = -20 \log [a_1 (1 + b \exp(-j\varphi))] \quad (100)$$

The constant parameter  $C$  can be derived from equation (98):

$$C = A_i - 20 \log \left[ 10^{-\frac{XPI_1}{20}} + b \left( 2 \times 10^{-\frac{X_{RN} - Q(\delta_2) - G(\delta_2)}{20}} + d_{H2} \right) \exp(-j\phi) \right] \quad (101)$$

Deep fades are usually dominated by selectivity and in equation (100) the flat fading contribution  $a_i$  can be neglected. Moreover given the following limits,  $b \rightarrow 1$  and  $\exp(-j\phi) \rightarrow 1$ ,  $C$  can be estimated through the following equation:

$$C = -20 \log \left[ 10^{-\frac{X_{TN}}{20}} + 10^{-\frac{X_{RN} - Q(\delta_1) - G(\delta_1)}{20}} - 2 \times 10^{-\frac{X_{RN} - Q(\delta_2) - G(\delta_2)}{20}} - d_{H2} \right] \quad (102)$$

It is worth noting that  $C$  is almost independent of the fading of the co-polar channel (parameters  $a_i$  and  $b$ ) and equation (101) becomes really consistent with the separation of variables. Equation (102) exhibits a further dependence on random variables such as the angles of arrival of the incoming rays and the depolarisation of the ground (if applicable).

In equation (99) it can also be noted that, particularly with equal transmitting and receiving antennas, the  $C$  parameter is almost equal to the value of  $d_{H2}$  (dB). In other words the discrimination properties of the propagation medium and not the antennas dominate the dual polarized channel behaviour during deep fade propagation conditions.

The value of  $C$  may be estimated either by simulating the random processes included in equation (102) or from experimental results.

## 7.2 Prediction of XPD statistics during clear air conditions

Still according to the results of the COST 235 Final Report, in order to evaluate the possibility of obtaining an acceptable transmission quality on dual polarisation, two main objectives must be reached. The first objective is to have an adequate prediction method for XPI (or XPD) degradation that can be applied to any radio link. The second objective is to obtain a performance prediction method capable of giving achievable transmission quality with and without cross-polar interference canceller (XPIC) devices.

As to the former objective, experimental results have shown that XPI and XPD distributions are statistically equivalent. This means that XPD measured distributions, as usually obtained from the received levels of the co-polarized and cross-polarized signals while transmitting on one single polarisation (defined as in equation (72)), can be used for evaluating XPI distributions. The basic starting point is equation (95), where an evaluation of the parameter  $C$  is required. If the co-polar signal cumulative distribution is assumed to have a slope of 10 dB/decade (Rayleigh distribution for deep fades), the cumulative distribution of XPD is as follows:

$$P_r(XPD < x) = P_0 \times 10^{-\frac{C-x}{10}} \quad \text{for } x < C - 15 \text{ dB} \quad (103)$$

where  $P_0$  is the multipath fading occurrence factor. The simplest approach is to consider the parameter  $C$  as a constant value derived from experimental data, the Recommendation ITU-R P.530 proposes in the following equation:

$$C = XPD_0 + Q \quad (104)$$

where  $XPD_0$  is the static XPD during non-fading conditions and  $Q$  is an improvement factor that shows a strong dependence on the slope of the cross-polarized antenna patterns ( $x_T$  and  $x_R$ ).

In the COST 235 Final Report, two separate prediction methods were considered, referred to as methods  $P$  and  $Q$ . As method  $Q$  was the one chosen as basis for the prediction procedure used in Recommendation ITU-R P.530, it will be discussed in some detail later in this section. More information about method  $P$  can be found in the COST 235 Final Report [COST, 1996]. Method  $Q$  is capable of deriving the parameter  $C$  from the general formulation reported in equation (101) performing a Monte Carlo simulation of the random processes involved. As far as the second objective is concerned, both methods consider the cross-polarized interfering signal as a noise source to be added to the thermal noise. Method  $Q$  is based on the assumption (based on experimental data) that there exists a high degree of decorrelation between the co-polarized and interfering cross-polarized signals, that is, XPI degradation occurs when the co-polarized signal is affected by high selective fading while, in general, the cross-polarized is not. In this case, XPI distributions can be used to evaluate the outage contribution due to XPI degradation and this quantity, together with the flat outage, defines the total non-selective outage. By using an appropriate, hardware depending, dependant cross-polar improvement factor (XPIF), the outage contribution due to XPI degradation in presence of an XPIC device can be evaluated.

### 7.2.1 Description of Method $Q$

Method  $Q$  was developed in the framework of the COST 235 project.

The model is presented in a step-by-step procedure in this section.

The first part of this procedure evaluates the parameters  $XPD_0$  and  $Q$  of equation (104).

$XPD_0$  is computed from:

$$XPD_0 = XPD_g + 5 \quad XPD_g < 35 \quad (105)$$

$$XPD_0 = 40 \quad XPD_g > 35 \quad (106)$$

Next, the fading occurrence factor,  $p_0$ , defined as corresponding to the percentage of the time of exceeding  $A = 0$  dB in the average worst month is calculated. From this amount, the fraction of fades corresponding to multipath is separated by the use of the multipath occurrence factor  $\eta$ , defined as the probability of a rather deep fade at a given frequency.

Recommendation ITU-R P.530, uses the following expression for the multipath fading factor:

$$\eta = 1 - e^{-0.2(P_0)^{0.75}} \quad (107)$$

Method  $Q$  then evaluates the  $Q$  factor using the following parametric approach:

$$Q = -10 \log \left( \frac{K \cdot \eta}{P_0} \right) \quad (108)$$

Recommendation ITU-R P.530 defines the  $K$  factor in equation (108)  $K_{XP}$ , and uses the following equation to derive its value for 1 or 2 transmitting antennas:

$$k_{XP} = \begin{cases} 0.7 & \text{one transmitting antenna} \\ 1 - 0.3 \exp \left[ -4 \times 10^{-6} \left( \frac{s_t}{\lambda} \right)^2 \right] & \text{two transmitting antennas} \end{cases} \quad (109)$$

where  $s_t$  is the antennas separation and  $\lambda$  the carrier wavelength in consistent units.

Finally, the  $C$  parameter is calculated from equation (101).

The probability of outage  $P_{XP}$  due to clear-air cross-polarization is calculated from:

$$P_{XP} = P_0 \times 10^{-\frac{M_{XPD}}{10}} \quad (110)$$

where  $M_{XPD}$ , expressed in dB, is the equivalent XPD margin for a reference BER and is given by:

$$M_{XPD} = \begin{cases} C - \frac{C_0}{I} & \text{without XPIC} \\ C - \frac{C_0}{I} + XPIF & \text{with XPIC} \end{cases} \quad (111)$$

Here,  $C_0/I$  is the carrier-to-interference ratio for a reference BER, which can be evaluated either from simulations or from measurements.

XPIF is a laboratory-measured cross-polarization improvement factor that gives the difference in XPI at sufficiently large carrier-to-noise ratio (typically 35 dB) and at a specific BER for systems with and without XPIC. A typical value of XPIF is about 20 dB.

The co-polar signal is assumed to be Rayleigh distributed for deep fades so that the contribution of XPD degradation for system outage is given by:

$$P_{XP} = P_0 \times 10^{-\frac{M_{XPD}}{10}} \quad (112)$$

### 7.2.2 Application examples

Location: Houston, TX, USA

Latitude: 29° 46' N

Longitude: 264° 78' E

Frequency:  $f = 8$  GHz

Path length:  $d = 45$  km

Transmitter antenna height:  $h_t = 500$  m

Receiver antenna height:  $h_r = 610$  m.

*Step 1:* For  $XPD_g = 42$  dB, i.e. the manufacturer's guaranteed minimum XPD for the transmitting/receiving antennas,  $XPD_0 = 40$  dB.

*Step 2:* Then, the multipath activity parameter is derived from:

$$\eta = 1 - e^{-0.2P_0^{0.75}} = 0.026 \quad (113)$$

where  $P_0 = p_w/100 = 0.0659$  is the multipath occurrence factor (percentage of time of exceeding  $A = 0$  dB).

*Step 3:* Determine  $Q = -10 \log \left( \frac{k_{XP} \eta}{P_0} \right) = 5.622$

where:

$$k_{XP} = 1 - 0.3 \exp \left[ -4 \times 10^{-6} \left( \frac{s_t}{\lambda} \right)^2 \right] = 0.7033 \quad (114)$$

assuming that the two orthogonally polarized transmissions are from different antennas, their vertical separation being  $s_t = 2$  m.

*Step 4:* The equivalent XPD margin for a reference BER is (assuming a cross-polar interference canceller is used with  $XPIF = 20$  dB):

$$M_{XPD} = C - C_0/I + XPIF = 33.62 \quad \text{dB} \quad (115)$$

where  $C = XPD_0 + Q = 45.622$  dB and  $C_0/I = 32$  dB is the carrier-to-interference ratio for the reference BER.

*Step 5:* Finally, the probability of outage due to clear-air cross-polarization is given by:

$$P_{XP} = P_0 \times 10^{-\frac{M_{XPD}}{10}} = 2.8 \times 10^{-5} \quad (116)$$

### 7.3 Prediction of XPD statistics during precipitation conditions

Experimental evidence shows that as the size of raindrops increases, their shapes depart from spherical and is similar to that of oblate spheroids with an increasingly pronounced flat base in which a concave depression develops for very large drop sizes [Pruppacher and Beard, 1970 and Pruppacher and Pitter, 1971]. Furthermore, raindrops may also be inclined to the horizontal [Saunders, 1971]. These two effects, that are the cause of cross-polarization during rain conditions, are discussed in greater detail in the Handbook on Radiometeorology. Most methods for the prediction of XPD statistics during precipitation conditions now in use are semi-empirical [Olsen, 1981]. They are modelled on general theories for rain with randomly-canted raindrops [Olsen, 1981] and with parameters chosen to give approximate agreement with experimental data. A two-parameter model based on a Gaussian distribution of raindrop canting angles is commonly assumed [Kobayashi, 1977 and Nowland *et al.*, 1977].

#### 7.3.1 Basis of prediction methods of XPD during precipitation

For most practical applications, the relationship between cross-polarized discrimination (XPD) and the co-polarized path attenuation (CPA) is of the utmost importance for predictions based on attenuation statistics.

Intense rain governs the reductions in XPD observed for small percentages of time. For paths on which more detailed predictions or measurements are not available, a rough estimate of the unconditional distribution of XPD can be obtained from a cumulative distribution of the co-polar attenuation (CPA) for rain using the equiprobability relation:

$$XPD = U - V(f) \log CPA \quad \text{dB} \quad (117)$$

The coefficients  $U$  and  $V(f)$  are in general dependent on a number of variables and empirical parameters, including frequency,  $f$ . For LoS paths with small elevation angles and horizontal or vertical polarization, these coefficients may be approximated by:

$$U = U_0 + 30 \log f \quad (118)$$

$$V(f) = 12.8 f^{0.19} \quad \text{for } 8 \leq f \leq 20 \text{ GHz} \quad (119)$$

$$V(f) = 22.6 \quad \text{for } 20 < f \leq 35 \text{ GHz}$$

An average value of  $U_0$  of about 15 dB, with a lower limit of 9 dB for all measurements, has been obtained for attenuations greater than 15 dB.

The variability in the values of  $U$  and  $V(f)$  is such that the difference between the CPA values for vertical and horizontal polarizations is not significant when evaluating XPD. The user is advised to use the value of CPA for circular polarization when applying equation (117).

Long-term XPD statistics obtained at one frequency can be scaled to another frequency using the semi-empirical equation:

$$XPD_2 = XPD_1 - 20 \log(f_2 / f_1) \quad \text{for } 4 \leq f_1, f_2 \leq 30 \text{ GHz} \quad (120)$$

where  $XPD_1$  and  $XPD_2$  are the XPD values not exceeded for the same percentage of time at frequencies  $f_1$  and  $f_2$ .

The relationship between XPD and CPA is influenced by many factors, including the residual antenna XPD, that might not have been taken into account. The equation above is the least accurate for large differences between the respective frequencies. It is, however, the most accurate if  $XPD_1$  and  $XPD_2$  correspond to the same polarization (horizontal or vertical).

### 7.3.2 Application examples

Location: Paris, FR

Latitude: 48° 52' N

Longitude: 02° 20' E

Frequency:  $f = 30$  GHz

Path length:  $d = 8$  km

Linear Polarization:  $\tau = 90^\circ$ .

*Step 1:* For the specified parameters, the equivalent path attenuation is determined from:

$$A_p = 10^{((U - C_0/I + XPIF)/V)} = 33 \text{ dB} \quad (121)$$

where  $U = U_0 + 30 \log f = 15 + 30 \log 30 = 59.31$ , the carrier-to-interference ratio  $C_0/I = 25$  dB and  $V = 22.6$  for this frequency range. No XPIC device is used.

*Step 2:* Then, the following parameters are determined:

$$m = 23.26 \log [A_p / 0.12 A_{0.01}] = 23.75 \quad (122)$$

$$n = \left( -12.7 + \sqrt{161.23 - 4m} \right) / 2 = -2.28 \quad (123)$$

*Step 3:* The XPD outage due to precipitation effects is given by:

$$P_{XPR} = 10^{n-2} = 5.25 \times 10^{-5} \quad (124)$$

## 7.4 Relative effects of XPD deterioration in clear-air and rain conditions

No general rule can be established to determine which of the two effects (rain and multipath) is dominant by considering the path characteristics. The user is then advised to estimate both the XPD reduction due to rain and the XPD reduction due to multipath when applying the above methods in systems design. However, it is usually observed that for dual horizontally and vertically polarized systems, with or without diversity, the dominant cause of deterioration is rain on short links and multipath on longer ones. The smallest path length for which multipath effects dominate depends on the frequency, climate, path clearance, and whether the link is over land or water and whether diversity is employed. In the non-diversity case, for example, measurements in the 10 to 12 GHz range in Europe for paths shorter than 20 km [Watson, 1976] show that rain is more significant. Measurements in the 6 to 13 GHz range for paths longer than 50 km [Rooryck and Battesti, 1976] show that multipath effects are more important. They also show that XPD degradation due to rain does not increase significantly the outage time, because reduction of XPD tends to occur at the same time as does severe attenuation.

## 7.5 Cross-polarization due to sand and dust storms

To date, no quantitative observations of cross-polarization during dust storms have been published in the open literature. All estimates of the cross-polarized performance of a microwave link during a sand or dust storm are, therefore, based on theoretical considerations of particle size, shape, number density and dielectric properties. Microscopic examinations [McEwan *et al.*, 1985 and Ghobrial and Sharief, 1987] have clearly shown that sand and dust particles carried in equatorial storms are non-spherical. Calculations further suggest that, in the absence of turbulence or wind shear, hydrodynamic forces would tend to orient the suspended particles with their major axis in the vertical plane [McEwan *et al.*, 1985]. As a result of this anisotropy, there may be significant degradation in XPD due to differential phase shift even though attenuation may not be severe. Similar conditions may apply to oblique linear polarizations [Bashir and McEwan, 1986]. Theoretical studies [Ghobrial and Sharief, 1987] suggest that in dry dust storms the XPD for circular polarization may be related to visibility by the equation:

$$XPD = 91.6 - 20 \log(fd) + 21.4 \log V \quad (125)$$

where:

- $f$ : frequency (GHz)
- $d$ : path length (km)
- $V$ : visibility (km).

The  $XPD$  is further reduced by approximately 1.7 dB for dust having 4% surface moisture content.

## 8 Multipath-propagation related alleviation techniques

The effect of slow relatively non-frequency selective fading (i.e., "flat fading") and selective fading must both be taken into account in the design of terrestrial LoS links. There are a number of techniques available for alleviating these effects, most of which alleviate both at the same time. The same techniques often alleviate the reductions in cross-polarization discrimination also. They can be categorized as techniques that do not require some kind of diversity reception or transmission, and techniques that do require diversity (purely system techniques such as adaptive equalization are discussed in the associated ITU-R Handbook on Digital Relay-Radio Systems).

Since it is desirable for economic reasons to avoid diversity whenever possible, strategies and techniques that do not require diversity are considered first in § 8.1. These strategies and techniques are also relevant for diversity systems, however, and should be employed when convenient even though they may be less necessary. Diversity techniques are discussed in § 8.2, with space diversity in § 8.2.1, angle diversity techniques in § 8.2.2, frequency diversity techniques in § 8.2.3, and polarization diversity in § 8.2.4. Diversity techniques for alleviating the reductions of cross-polarization discrimination in systems using dual-polarization frequency-reuse are discussed separately in § 8.3.

### 8.1 Non-diversity strategies and techniques

Non-diversity techniques for alleviating the most severe effects associated with multipath fading can be classified under one or more of three general strategies [Olsen, 1989]:

*Strategy A:* Reducing the occurrence of significant "flat fading" due to atmospheric mechanisms: Such mechanisms include beam spreading (commonly referred to as defocusing in the English scientific literature) and antenna decoupling, which commonly occur together, and atmospheric multipath. The purpose in reducing the occurrence of these mechanisms is to reduce the likelihood that the amplitude of the atmospheric wave (the direct wave unless atmospheric multipath occurs) will decrease to a level where it can interfere destructively with the ground reflected waves, resulting in severe multipath fading and distortion. Although atmospheric multipath can be itself slightly frequency selective across a band, it is usually

"flat" in its amplitude and delay characteristics compared to the surface multipath propagation that occurs when the atmospheric wave interferes destructively with one or more ground reflected waves.

*Strategy B:* Reducing the occurrence of significant surface reflections: Similar to the first strategy, the purpose of this strategy is also to reduce the likelihood of destructive interference between the atmospheric wave and the surface reflected waves, causing severe multipath fading and distortion.

*Strategy C:* Reducing the relative delay of the surface reflections with respect to the atmospheric wave: The purpose of this strategy is to reduce the severity of the amplitude and delay distortions that occur when there is destructive interference between the atmospheric wave and the surface reflected waves, which is normally not totally unavoidable.

The various techniques presented in Recommendation ITU-R P.530 elaborated below appear to accomplish one or more of these strategies.

### 8.1.1 Increasing path inclination

This technique, sometimes referred to as the "high-low technique" [Vigants, 1975 and Fehlhaber, 1976], should be employed whenever the terrain allows it. It tends to accomplish both Strategies A and B. First of all, the incidence of beam spreading loss and associated antenna decoupling tends to be reduced when the angle of the direct wave is increased relative to the severe refractive structures such as ducts causing these effects. Secondly, the level of the specularly and diffusely reflected wave or waves tends to be reduced since:

- less energy is spread from the direct wave in the direction of the surface,
- the combined directivities of the two antennas in the direction of a reflection is less, and
- the grazing angles of the reflected waves are usually increased.

In cases where atmospheric multipath is responsible for the fading of the atmospheric wave, there is also evidence from ray tracing analyses [Webster, 1983], i.e., increasing the path inclination reduces its incidence.

The improvement of the effects of multipath fading by increasing path inclination can be seen quantitatively in several of the prediction equations of Recommendation ITU-R P.530. In particular, equations (7) and (8) in that Recommendation demonstrate explicitly that the percentage of time exceeding a given fade depth is reduced. This relation is in fact the basis of the calculation of the multipath occurrence factor, which governs the amount of flat fading (see equation (24)), the amount of selective fading and the reduction in *XPD* in dual-polarization frequency-reuse systems (see equation (49)).

Clearly the type of terrain favouring the use of this technique is hilly or mountainous terrain. This type of terrain also tends to have the additional advantage that the roughness and altitudes involved are associated with a reduced incidence of extreme refractive layers such as ducts. Since an obvious disadvantage of the technique is that path lengths tend to be shorter, a trade-off should be found between the obvious economic advantage of long path lengths and the technical (and potentially economic) advantage in alleviating the most severe effects of multipath propagation. Unfortunately, there are currently no clear rules for carrying out such a trade-off.

Although the technique tends to reduce the strength of the surface reflections in general, instances can arise when the opposite occurs. The most obvious situation to avoid is one where the main surface reflections occur on water or flat ground. With some care, path geometries can be chosen in which the path is both inclined and has its significant surface reflections blocked by intervening terrain.

### 8.1.2 Reduction of the effect of surface reflections

Several techniques are given in Recommendation ITU-R P.530 for reducing the effect of surface reflections (strategy B) in order to reduce the occurrence of surface multipath fading. The basis of these techniques and additional salient points are discussed below.

### 8.1.2.1 Shielding of the reflection point

This technique of using the advantage of hills, mountains or buildings along the path to shield the antennas from the more specularly-reflective surfaces (e.g., water surfaces, plains, smooth hilltops not covered by trees, building tops) has been used since the early days of radio relay design. The availability of computer-based ray racing allows it to be applied efficiently and to take into account a wide range of effective  $k$  values. An example of the failure of this technique because of superrefraction of the surface-reflected wave over the ridge intended to block the reflection [Lam and Webster, 1985] illustrates the importance of such ray-tracing analyses.

### 8.1.2.2 Moving of reflection point to poorer reflecting surface

The technique here is to adjust the antenna height at one or both ends of the path to place reflections on a rougher terrain or vegetative surface than would otherwise be possible. It is particularly important to avoid reflections from water surfaces if this is possible.

### 8.1.2.3 Optimum choice of antenna heights

This technique, presented as a step-by-step procedure in Recommendation ITU-R P.530, does not necessarily reduce the level of surface reflections. It is designed instead to arrange for constructive interference between the direct wave and the major surface-reflected waves (usually one single wave) so as to avoid the harmful effects of multipath fading. For the range of effective  $k$  values of interest, this is only possible on short paths, or somewhat longer paths at lower frequencies. The step-by-step procedure in Recommendation ITU-R P.530 is presented in such a way as to allow the user to determine at what point some kind of diversity is necessary.

The basis of the technique is presented in two publications [Boithias, 1983 and Karl and Persson, 1998]. The only difference is that the former employs a closed-form solution whereas the latter a truncated series solution.

### 8.1.2.4 Choice of vertical polarization

It is advantageous to choose vertical polarization over horizontal polarization, particularly on overwater paths at frequencies below about 2 GHz. Step-by-step procedures are given in Recommendation ITU-R P.530 both for calculating the effective surface reflection coefficient and for measuring it.

Most of the mathematical basis of the techniques in Recommendation ITU-R P.530 has been described by [Boithias, 1983]. The one additional element is the introduction of a surface roughness factor. The original Gaussian approximation for this factor [Beckmann and Spizzichino, 1963] has been replaced by a modified Gaussian approximation based on experimental data for sea surfaces [Miller *et al.*, 1984]. The assumption made is that this modified form is also more accurate for terrain [Olsen *et al.*, 1987].

### 8.1.2.5 Use of antenna discrimination

On sufficiently inclined paths or paths with naturally large clearance, the angles between the direct and reflected waves become large enough to take advantage of the radiation pattern of one or both antennas to discriminate against the reflected wave(s). Even without this natural advantage, it is advantageous to tilt one or both antennas slightly upwards to increase the amount of discrimination available. The step-by-step procedure for this is presented in Recommendation ITU-R P.530. It tends to accomplish both strategies, B above and to some extent strategy A at the same time. Clearly the strengths of surface reflections are reduced as a result of the reduced antenna directivities in the directions of these reflections.

The value of upward tilting of antennas to ameliorate the effects of surface multipath has been demonstrated from measurements in several publications [Hartman and Smith, 1977; Sasaki *et al.*, 1987; Satoh *et al.*, 1989 and Prasad *et al.*, 1991] amongst others. Measurements of the three strongest rays on paths of 31, 41, and 51 km in length in eastern-central North America [Webster, 1991] confirm that upward tilting will discriminate against rays coming from the direction of the surface and demonstrate that the strongest ray (normally the direct ray) usually arrives with a positive angle-of-arrival during multipath conditions. The estimate of angle-of-arrival in Recommendation ITU-R P.530 [Karl and Persson, 1998] for  $k = \infty$  is in agreement with the most likely values (i.e., the modes) from these measurements.

Two complementary techniques for determining optimum tilt angles are given in Recommendation ITU-R P.530, one in which the maximum fade depth of surface multipath is minimized and the other in which amplitude distortion is minimized. The first is based on well-known equations for surface reflection [Boithias, 1983; Karl and Persson, 1998] an approximation of the antenna main lobe patterns by Gaussian beams [Olsen *et al.*, 1987] and current understanding of the physics of multipath propagation [Olsen *et al.*, 1987; Olsen, 1989 and Segal, 1999]. It should be noted, however, that the technique is not sensitive to the particular physical situations that are simulated. The second is based on another technique [Tanem, 1988] that applied to its fullest requires that the antenna patterns be known. As noted, if the loss in flat fade margin obtained by tilting both transmitting and receiving antennas is limited to about 6 dB, it is unnecessary to employ the antenna patterns. Also as noted, whether one technique is followed, the other, or a compromise, will depend on the characteristics of the system. Both techniques are consistent with a review of angle-diversity observations from several countries employing antenna tilting at the receiver only [Satoh *et al.*, 1989 and Sasaki *et al.*, 1991].

It should be noted that upward tilting of antennas to ameliorate the effects of surface multipath will in most cases also tend to ameliorate the effects of atmospheric multipath. This can be concluded from both ray-tracing analyses [Webster, 1983] and extensive analyses of measurements of amplitudes and angles-of-arrival of the three strongest rays on a 51 km path in eastern-central North America [Webster *et al.*, 1994]. The reason is that the stronger of the two strongest atmospheric multipath rays tends to have the larger angle-of-arrival also. Thus, if the antennas are uptilted by a larger angle than this larger angle-of-arrival, the difference in level between the two strongest atmospheric multipath rays will be most likely to increase. Measurements on paths of 31, 41, and 51 km in length [Webster, 1991] indicate that the strongest ray typically has an angle-of-arrival less than  $0.3^\circ$ . This is the reason for the statement in Recommendation ITU-R P.530 that upward tilting should be normally optimized to ameliorate the effects of surface multipath.

### 8.1.3 Reduction of path clearance

The technique of minimizing path clearance in order to alleviate the effects of multipath fading may be one of the best of those available, but published evidence for it as yet is unfortunately scanty [Olsen and Segal, 1992]. Most reports are anecdotal on the part of link designers. Since reductions in path clearance can result in an increased incidence of diffraction loss during sub-refractive conditions (see § 3.3), the technique is somewhat risky on paths without space diversity unless the amount of diffraction loss can be estimated reasonably accurately.

Techniques for estimating the diffraction loss have been suggested for some regions of the world, and the use of these would allow some diffraction loss to be tolerated [Giloi, 1979; Kalinin, 1979; Nadenenko, 1981; Vigants, 1981 and Olsen and Segal, 1992]. The path clearance rule in § 2.2.2.1 of Recommendation ITU-R P.530 [Olsen and Segal, 1992] is designed to avoid diffraction loss in normal refractivity conditions (i.e., median effective  $k$  factor), but to allow about 6 dB of diffraction loss in conditions corresponding to  $k_e$  (99.9%). In principle, for systems with sufficiently large flat fade margins, larger amounts of diffraction loss could be tolerated in both normal and sub-refractive conditions.

It is believed that the effectiveness of the technique results because paths with less clearance have fewer super refractive layers such as ducts that can exist below the path, thereby reducing the occurrence of severe beam spreading loss in the direct wave and consequently the likelihood of destructive interference with the surface-reflected waves [Olsen, 1989 and Olsen and Segal, 1992]. If this is the case then the technique would tend to accomplish both strategies A and C above. Reduction in the relative delay of the ground reflection would occur mainly because of a reduction in the large component of delay due to two-way transmission through the layer under the path but also in small part because of the reduction in the geometric component of delay [Olsen *et al.*, 1987 and Olsen, 1989].

## 8.2 Diversity techniques

Whenever the techniques given in the previous section do not alleviate the effects of multipath fading and distortion to reduce estimated system outages to acceptable levels, additional diversity techniques must be employed. Diversity techniques include space, angle, frequency, and polarization diversity. As noted in

Recommendation ITU-R P.530, frequency diversity should be avoided whenever possible so as to conserve spectrum. Whenever space diversity is used, it is also recommended that angle diversity be employed by tilting the antennas upward at different elevation angles. Angle diversity can be used in situations in which adequate space diversity is not possible or to reduce tower heights.

### 8.2.1 Space diversity

Space diversity systems normally employ two vertically-spaced antennas at one end of a link. Such configurations with standard spacing are usually sufficiently effective against the effects of multipath fading and distortion, but for some problem links other configurations have been employed. Increasing the spacing of the antennas has been suggested as a way to more effectively combat the effects of beam spreading and the associated surface multipath fading [Olsen, 1989]. The use of the lower path clearances in the range suggested for diversity antennas in Recommendation ITU-R P.530 should tend to produce this desirable result. For links in which beam spreading loss is even more extreme, spaced antennas at both ends of the link have proven effective [Boithias, 1979 and Hautefeuille *et al.*, 1980].

### 8.2.2 Antenna spacing in space diversity systems

Recommendation ITU-R P.530 gives a step-by-step procedure for determining the antenna spacing in two- and three-antenna space diversity systems. The procedure is a trade-off between:

- a) the need to keep clearance of the lower antenna as low as possible (within the clearance guidelines of § 2.2.2 of Recommendation ITU-R P.530) so as to minimize the occurrence of surface multipath fading (see § 8.1.3),
- b) the need to obtain a specific space diversity improvement factor for overland paths (see § 8.2.2), and
- c) the need to minimize the chance that the signal on one diversity antenna will be faded by surface multipath when that on the other antenna is faded.

It is based in part on a procedure for optimizing spacing to combat surface multipath [Karl and Persson, 1998] and in on part on knowledge of surface multipath physics [Olsen *et al.*, 1987; Olsen, 1989; Webster, 1991; Rana *et al.*, 1993, 1995 and Segal, 1999]. The approach for dealing with a two-leg passive reflector hop is partly based on 6 GHz measurements involving legs of 50.7 km and 15.3 km [Vigants, 1975].

### 8.2.3 Angular spacing in angle-diversity and combined space/angle-diversity systems

Angle diversity can be achieved through the use of:

- a) a single multifeed antenna with two or more beams separated by small angles in the vertical plane,
- b) the use of two antennas separated horizontally and tilted to different angles in the vertical plane, or
- c) the use of separate vertical space-diversity antennas that are tilted to different angles in the vertical plane.

The approach is effective because the respective beams discriminate differently against multipath signals with different angles-of-arrival in the vertical plane. Thus, two or more multipath signals which combine to cause a deep frequency-selective multipath fade on one beam will combine with different ratios on another beam, likely avoiding the same depth and selectivity of fading. Approaches a) or b) are useful when a diversity system must be installed on an already existing tower and the tower is not tall enough to allow space diversity. If the angle-diversity improvement achievable is adequate, these approaches may also be useful on new towers in order to minimize tower height. A slight disadvantage of the single-antenna technique besides the increased cost of such an antenna is that the beam spacing of "off-the-shelf" antennas may not be optimum for the particular path on which it is being used.

The use of angle diversity in combination with space diversity is encouraged whenever the latter is employed in order to maximize performance. This is most important on paths in which there are significant specular surface reflections. However, because there is some cost involved in tilting the antennas appropriately to

achieve angle diversity, it is recognized that it may be desirable to only employ space diversity on some paths where it is expected to be clearly adequate. Unfortunately, there are few measurements available for the combination of space diversity with antenna tilting [Satoh *et al.*, 1989; Vergeres *et al.*, 1990 and Sasaki *et al.*, 1991].

A review of the history and results of the early measurements has been given elsewhere [Lin *et al.*, 1988]. Another review [Olsen, 1989] discussed the measurements and their implications in terms of the multipath propagation physics. Since that time, there have been only a few other angle-diversity measurements and analyses reported [Satoh *et al.*, 1989; Vergeres *et al.*, 1990 and Sasaki *et al.*, 1991; Tjelta *et al.*, 1991; Alley *et al.*, 1992; Di Zenobio *et al.*, 1992 and Danielsson and Johansson, 1993].

Recommendation ITU-R P.530 gives a procedure for determining the tilt angles of the antenna beams in approaches b) and c). The procedure is based on the totality of experimental results available concerning, existing theory [Boithias, 1983; Tanem, 1988 and Karl and Persson, 1998] and knowledge of the multipath physics [Olsen *et al.*, 1987; Olsen, 1989 and Segal, 1999]. Particular attention, however, was paid to detailed angle- and space-diversity experiments involving multiple antenna tilt angles [Dombek, 1986 and Valentin *et al.*, 1987, 1989 and 1990], more than one path [Sasaki *et al.*, 1987; Satoh *et al.*, 1989; Valentin *et al.*, 1990 and Sasaki *et al.*, 1991], and with associated analyses of flat fading and selective fading components [Valentin *et al.*, 1990] or associated simulations [Satoh *et al.*, 1989 and Sasaki *et al.*, 1991]. Also, particular attention was paid to a series of long-term experiments involving the measurement of individual angles-of-arrival and levels of multipath signals on five different overland and overwater paths [Lam and Webster, 1985; Webster, 1991; Rana *et al.*, 1992, 1993 and 1995 and Webster *et al.*, 1994].

The basis for the procedure for determining the upward tilt angle of one antenna beam is described in § 8.1.2.5. Two techniques are given, one based on minimizing maximum fade depth and the other based on minimizing amplitude distortion. As noted, both techniques are consistent with a review of angle-diversity observations from several countries employing antenna tilting at the receiver only [Satoh *et al.* 1989 and Sasaki *et al.*, 1991].

The advantage of tilting the other antenna beam downwards on paths with sufficiently significant surface reflections to provide additional diversity protection in severe flat fading conditions caused by beam spreading of the direct wave has been demonstrated by experiments in which the flat fading component of the signal was extracted [Valentin *et al.* 1989 and 1990]. It also agrees with ray tracing analyses [Olsen *et al.*, 1987 and Sasaki *et al.* 1987] and with observations that surface multipaths are typically enhanced when a flat fade due to beam spreading of the direct wave occurs [Olsen *et al.*, 1987 and Rana *et al.*, 1992, 1993]. The tilt angle in the direction of the largest specular reflection is designed to maximize diversity protection in severe flat fading conditions. However, an additional advantage of this downward tilting beam is the reduction of antenna decoupling loss caused by a direct wave arriving with a negative angle-of-arrival due to subrefraction [Olsen, 1989]. As noted in Recommendation ITU-R P.530, the 3 dB limit in the design procedure is to avoid reducing the level of the direct signal (normally arriving with a positive angle-of-arrival in multipath conditions) on the downward tilting antenna beam by too much, particularly when the dominant specular reflection is in the foreground of the antenna.

The disadvantage of tilting one antenna beam downwards is that the occurrence of significant levels of frequency selective fading and distortion are known to be larger on this beam because of the enhanced levels of the multipath signals arriving from the direction of the path surface [Valentin *et al.*, 1989 and 1990 and Vergeres *et al.*, 1990]. However, when such fading and distortion occurs on this beam, it is unlikely to be occurring on the upward tilting beam simultaneously. This is because the ratio of direct and surface multipath signals will be significantly different on the upward tilting beam. Because of the more frequent large levels of fading and distortion occurring on the downward tilting beam, it is desirable to employ diversity switching rather than combining.

The decision to tilt one antenna beam downwards will be more difficult on paths for which there is no obvious specular surface reflection. However, it must be pointed out that diffuse surface scattering will occur on all paths and that the scattered signals can also be enhanced in level at the same time that the direct signal is undergoing a flat fade due to beam spreading. Thus, if the diffusely scattered signals are sufficiently large, there is a chance of significant fading and distortion. Also, there is some evidence that multipath from the

direction of the path surface can occur as a result of refraction by a thin sub-refractive layer at the surface [Segal, 1999]. The direction of such a reflection can be estimated by passing a regression curve through the path profile, or a portion of the path profile, and assuming a specular reflection from this. The equations for determining the reflection point and angle are given in Recommendation ITU-R P.530.

#### 8.2.4 Space-diversity improvement in narrow-band systems

Recommendation ITU-R P.530 gives a universal equation for predicting the space diversity improvement factor  $I$  for narrow-band systems. This equation was mainly based on an empirical fit to data listed in the ITU-R data bank (see Recommendation ITU-R P.311) and employs an approach designed to take into account large variations in flat fading occurring in different climates [Hosoya, 1991].

Another somewhat simpler prediction [CCIR, 1986-1990] equation which has been found to give results approaching in accuracy that of Recommendation ITU-R P.530 is:

$$I = 1 + 1.3 \times 10^{-5} (S f)^{1.3} \cdot d^{1.5/p} \quad (126)$$

where:

- $p$ : percentage of time fade depth  $A$  (dB) exceeded
- $S$ : vertical separation of receiving antennas centre-to-centre (m)
- $f$ : frequency (GHz)
- $d$ : path length (km).

This equation has been based on data for the parameter ranges  $2.1 < f < 6.2$  GHz,  $50 < d < 240$  km,  $63 < S/\lambda < 270$ , where  $\lambda$  is the wavelength. Further development of this approach is discussed elsewhere [Boithias, 1990].

The results of tests on these two methods and several others using the data in the ITU-R data bank are given by Hosoya [1991].

#### 8.2.5 Frequency diversity

Recognizing that frequency diversity systems should normally be avoided, Recommendation ITU-R P.530 gives a step-by-step procedure for determining the frequency spacing in such systems when it is of value out of necessity or convenience. One part of the procedure gives the minimum optimum frequency separation, as well as the possible wider optimum frequency separations, for main and protection channels for paths with obvious specular surface reflections. This part is based on the same approach used to develop the procedure for antenna spacing in space-diversity systems. It maximizes the chance that the most significant surface reflected wave will be in phase with the direct wave at one frequency while it is out of phase at the other frequency, where a deep fade occurs. The other part, applicable to paths without surface reflections is based on the calculation of the improvement factor from equation (107) of Recommendation ITU-R P.530.

As noted in that Recommendation, an optimally designed frequency diversity system does not offer as much protection as a similar optimally designed space diversity system. The latter gains all the protection of the former due to the phase difference between the signals in the main and protection channels, plus additional protection against the flat fading component due to beam-spreading loss of the direct signal, as a result of the vertical separation of antennas. This is particularly true if the path clearance of the diversity antenna is reduced based on the procedure of § 2.2.2.2 of Recommendation. In principle, space diversity should also offer more protection against atmospheric multipath.

##### 8.2.5.1 Frequency-diversity improvement factor for narrow-band 1 + 1 systems

There are few data available from which to develop and test a universal prediction equation for the frequency diversity improvement factor for narrow-band 1 + 1 systems.

The following commonly used equation for overland links, at least those on which there are no dominant ground reflections, was developed from the earlier data available [Barnett, 1970 and Vigants, 1975]:

$$I = (0.8/f/d) (\Delta f/f) 10^{A/10} \quad (127)$$

where:

- $f$ : band centre frequency (GHz)
- $d$ : path length (km)
- $(\Delta f/f)$ : relative frequency spacing as a percentage
- $A$ : fade depth (dB).

This equation applies only to the following range of parameters:

$$2 \leq f \leq 11 \text{ GHz}$$

$$30 \leq d \leq 70 \text{ km}$$

$$\Delta f/f \leq 5\% .$$

Extrapolation may lead to errors. The equation is considered valid only for values of  $I \geq 5$ .

Another prediction equation, developed from a combination of the earlier data base and some additional data for approximately the same range of parameters as those associated with equation (127) is given below [Boithias *et al.*, 1986]:

$$I = 1 + 0.015 (1/f) (\Delta f/f)^{1.25} \times 10^{A/10} \quad (128)$$

### 8.2.5.2 Frequency-diversity improvement factor for narrow-band multi-channel switched ( $n + 1$ ) etc. systems

The diversity improvement factor for an  $n + 1$  etc. analogue frequency-diversity system can be estimated from the following equation equivalent to that in equation (128) [Vigants and Pursley, 1979]:

$$I = 160 (f/d\Gamma) \times 10^{A/10} \quad (129)$$

where:

- $f$ : centre frequency of the RF band
- $\Gamma$ : parameter dependent on channel carrier frequencies, channel spacing, and variation in channel fade margins [Vigants and Pursely, 1979].

The other parameters have their previous significance.

### 8.2.5.3 Application examples

Example for a path with a significant surface reflection: let us consider a 10 km link at 4 GHz from the top of a building to a hill across a river that allows more than a full first Fresnel zone of reflection on its surface. The antenna on the building is 57 m above the river, and the antenna on the hill is 86 m above the river. (The length and widths of the first Fresnel zone on the water surface are 1.84 km and 27 m, respectively, see Recommendation ITU-R P.530).

The minimum optimum frequency separation is given in the last column of Table 5 for several values of  $k$ , along with the values of several other parameters of the above mentioned Recommendation, in order to illustrate the effect of surface reflection (a perfectly smooth water surface is assumed in this case, with  $R_r = 1$ ) on the fading when some beam-spreading loss due to the refractive structure of the atmosphere occurs to the direct wave. The fade variables  $A_{max}$ ,  $A_{min}$ , and  $A$  result from the assumption that the direct signal undergoes a

fade of  $0.5 \times 4.4 = 2.2$  dB due to beam spreading loss and that the surface reflected signal is enhanced by the same amount (i.e.,  $L_{add} = 4.4$  dB) for antenna half-power beamwidths of  $2.7^\circ$ . ( $A_{min}$  is the enhancement of the overall signal resulting from constructive interference of the direct and reflected waves, the value is obtained from Recommendation ITU-R P.530 with the negative sign in the parentheses replaced by a positive sign. Negative numbers imply an enhancement.) No uptilting of the antennas is assumed, but this would of course give additional protection to the frequency diversity. The optimum frequency spacing is only affected by the path lengths  $d$ ,  $d_1$ , and  $d_2$  and heights  $h_1$  and  $h_2$  of the antennas above the river, so that this example could take place at any frequency if the half-power beamwidths of the antennas remained the same.

As indicated in Recommendation ITU-R P.530, the minimum optimum frequency separation is about 160 MHz, a separation that could be achieved from most frequency plans. Such a separation of channel 2 would avoid the one deep fade that occurs at 4 GHz in the main channel (50.8 dB for a  $k$  value of about 10 and  $L_{add} = 4.4$  dB), giving an enhanced signal level instead in the diversity channel (about 3.8 dB for  $L_{add} = 4.4$  dB), which must be centred at about 4.16 GHz or 3.84 GHz.

If the path length were 30 km instead of 10 km, the minimum optimum frequency separation would be 692 MHz for a  $k$  value of  $4/3$ . In principle, cross-band diversity with the diversity channel at 6.076 GHz (i.e., three times the minimum optimum frequency separation, as specified in Recommendation ITU-R P.530) could protect against multipath fading caused by such beam-spreading loss of the direct signal combined with surface reflection.

TABLE 5

Values of minimum optimum frequency separation and other variables for various  $k$  values

$k$	$d_1$ (km)	$d_2$ (km)	$D$	$\rho$	$\rho_{eff}$	$L_s$ (dB)	$A_{max}$ (dB)	$A_{min}$ (dB)	$A$ (dB)	$\Delta f$ (MHz)
0.5	4.04	5.96	0.948	0.794	0.794	2.31	45.9	-3.8	-2.4	171.3
1	4.01	5.99	0.974	0.788	0.788	2.27	41.4	-3.8	-3.0	161.8
1.33	4.01	5.99	0.980	0.787	0.787	2.26	44.7	-3.8	-3.7	159.5
3	3.99	6.01	0.991	0.784	0.784	2.24	48.7	-3.8	2.2	155.8
5	3.99	6.01	0.995	0.784	0.784	2.24	49.8	-3.8	9.3	154.7
10	3.99	6.01	0.997	0.783	0.783	2.24	50.8	-3.8	49.6	153.8
100	3.99	6.01	1	0.782	0.782	2.23	51.8	-3.8	10.1	153.1
$1.0 \times 10^9$	3.99	6.01	1	0.782	0.782	2.23	52.0	-3.8	9.2	153.0

#### Example for a path with no obvious surface reflection:

Consider a 30 km path at 4 GHz, with a flat fade margin of 40 dB. If 80 MHz is the desired frequency separation in a particular system, the non-selective improvement factor  $I_{ns} = 133.3$  from Recommendation ITU-R P.530 can be used. This value can then be inserted in the method of Recommendation ITU-R P.530 to obtain a prediction of the outage. If the predicted outage is too large, a larger frequency separation can be considered. For example, a separation of 160 MHz would give  $I_{ns} = 266.7$ .

#### 8.2.6 Polarization-diversity improvement factor for wideband systems

The co-channel use of the frequency spectrum makes it important to know if there is a diversity effect and to qualify it. Especially the use of  $(n + m)$  switches requires the choice of the most adequate  $m$  protection channels in function of their frequency in the band and of their polarization.

Measurements have shown that fading events of the average power of 2 co-frequency channels (V and H) are extremely well correlated for values of fading up to, at least, 25 dB. So the improvement brought by polarization diversity mainly come from the fact that the dispersions in the 2 co-frequency channels are not well correlated.

### 8.2.7 Relative merits of the various diversity techniques and their combinations

One main advantage of space and angle diversity over frequency diversity is that it helps to preserve the available frequency spectrum.

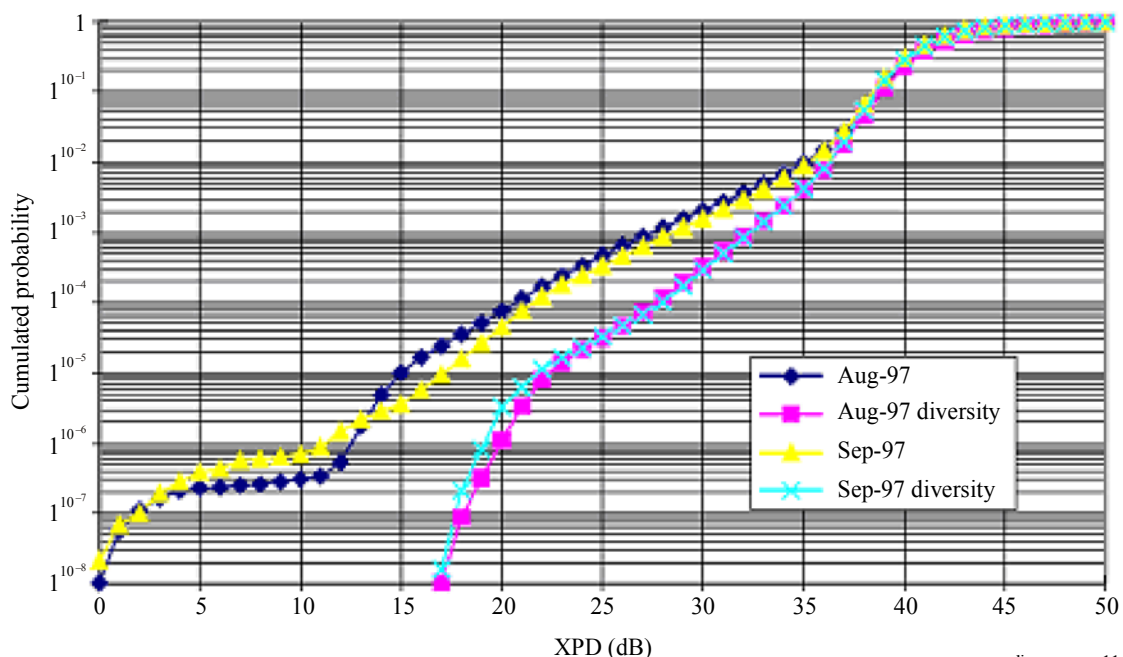
Comparisons of space and angle diversity are still at an early stage. Obvious advantages of single angle-diversity antennas with multiple beams are that of reduced cost, reduced tower loading, and their use on towers that are too short for space diversity. In terms of digital links relative performance, there is some indication that normal space diversity configurations may give the greatest diversity improvement for links where flat-fading-induced outages dominate and angle-diversity configurations may give the greatest diversity improvement for links where distortion-induced outages dominate [Lin *et al.*, 1988; Alley *et al.*, 1987; Valentin *et al.*, 1989 and Mohamed *et al.*, 1989].

Other experiments have also combined different diversity techniques. The statistics of single frequency fading, XPD, and in-band power difference were much improved by a combination of space and angle diversity reception with a non-tilted upper antenna and an upward tilted lower antenna. It was also confirmed that diversity reception between a non-tilted beam and a beam directed toward a sea-reflected wave is effective for reducing fading over paths where a stationary strong reflected wave exists and beam spreading occurs frequently [Sasaki *et al.*, 1987 and Satoh *et al.*, 1989].

### 8.3 Diversity techniques for alleviating reductions in XPD

An example of improvements obtained in cross-polar discrimination by the use of diversity is given in Fig. 11. It illustrates measurements during a year's worst months in a 4 GHz, 122.4 km link in Switzerland [Thorvaldsen, 2000].

FIGURE 11  
Improvement of cross-polar discrimination using diversity



## References

- ALLEY, G. D., BIANCHI, C. H. and ROBINSON, W. A. [1992] Angle diversity and space diversity experiments on the Salton/Browley hop. *IEEE Trans. Comm.*, Vol. 40, 2, p. 440-454.
- ALLEY, G. D., PENG, W. C., ROBINSON, W. A. and LING, E. H. [1987] The effect on error performance of angle diversity in a high capacity digital microwave radio system. *IEEE GLOBECOM*.
- BARNETT, W. T. [October 1970] Microwave line-of-sight propagation with and without frequency diversity. *BSTJ*, Vol. 49, 8, p. 1827-1871.
- BARNETT, W. T. [1972] Multipath propagation at 4, 6 and 11 GHz. *BSTJ*, Vol. 51, 2, p. 311-361.
- BASHIR, S. O. and McEWAN, N. J. [June 1986] Microwave propagation in dust storms: A review. *Proc. Inst. Elect. Eng.*, Vol. 133, p. 241-247.
- BATTESTI, J. and BOITHIAS, L. [1978] 6th Colloquium on Microwave Communications, Budapest, Hungary.
- BECKMANN, P. and SPIZZICHINO, A. [1963] *The Scattering of Electromagnetic Waves from Rough Surfaces*, Ed. Pergamon Press.
- BERTOK, E., DERENZIS, G. and DRUFUCA, G. [1977] Estimate of attenuation due to rain at 11 GHz from rain gauge. *CNET*, Issy-les-Moulineaux, France, p. 295-300.
- BOITHIAS, L. [1979] Protection contre les évanouissements dus aux conduits troposphériques sur les liaisons en visibilité. *Ann. des Télécomm.*, Vol. 34, 9-10, p. 513-514.
- BOITHIAS, L. [1981] Distribution statistiques des niveaux reçus en propagation par trajet multiple troposphérique. *Ann. des Télécomm.*, Vol. 36, 5-6, p. 329-337.
- BOITHIAS, L. [1983] *Propagation des Ondes Radioélectriques Dans L'Environnement Terrestre*. Ed. Dunod.
- BOITHIAS, L. [1987] *Radio Wave Propagation* (translated by D. Beeson). Ed. McGraw-Hill.
- BOITHIAS, L. [1989] Similitude en fréquences pour l'affaiblissement par la pluie. *Ann. des Télécomm.*, Vol. 44, 3-4, p. 186-191.
- BOITHIAS, L. [1990] La réception en diversité sur les liaisons de télécommunications. *L'Onde Electrique*, Vol. 70, 1, p. 65-75.
- BOITHIAS, L. and BATTESTI, J. [1967] Protection against fading on line-of-sight radio-relay systems (in French). *Ann des Télécomm.*, Vol. 22, 9-10, p. 230-242.
- BOITHIAS, L., BATTESTI, J. and ROORYCK, M. [1986] Prediction of the improvement due to diversity reception in microwave links. *Proc. MICROCOLL '86*, Budapest, Hungary.
- BULLINGTON, K. [1971] Phase and amplitude variations of multipath fading of microwave signals relating to atmospheric irregularities. *BSTJ*, Vol. 50, p. 2039-2053.
- CAPSONI, C., FEDI, F. and PARABONI, A. [1987] A comprehensive meteorologically oriented methodology for the prediction of wave propagation parameters in telecommunication applications beyond 10 GHz. *Radio Sci.*, Vol. 22, p. 387-393.
- CHU, T. [1974] Rain-induced crosspolarization at centimeter and millimeter wavelengths. *BSTJ*, Vol. 53, 8, p. 1557-1539.
- COST [1996] COST 235 – Radiowave propagation effects on next-generation fixed-services terrestrial telecommunications systems. European Commission, EUR 16992 EN, ISBN 92-827-8023-6.
- CRANE, R. K. [1976] *Refraction effects in the neutral atmosphere. Methods Experimental Physics*, Vol. 12B. M. L. Meeks, Ed. Academic Press.
- CRANE, R. K. [October 1979] Automatic cell detection and tracking. *IEEE Trans. Geosci. Electron.*, Vol. 17, Issue: 4.
- CRANE, R. K. [1980] Prediction of attenuation by rain. *IEEE Trans. Comm.*, Vol. 28, p. 1717-1733.
- CROMBIE, D. C. [1984] Prediction of multipath fading on terrestrial microwave links at frequencies of 11 GHz and greater. *NATO/AGARD Conf. Proc. CP-346*, p 10/1-8. North Atlantic Treaty Organization, Paris, France.

- DANIELSSON, B. and JOHANSSON, U. [1993] Measured improvements using angle and space diversity on a terrestrial microwave radio link. IEE Conf. Publ. No. 386 on Radio Relay Systems, p. 215-220.
- DERENNES, M. [1979] Etude statistique sur des trajets multiples. Note techniques CNET-TCR/APH/60. Centre national d'études des télécommunications, Issy-les-Moulineaux, France.
- DI ZENOBIO, D., SANTELLA, G., CANDEO, S. and MANDICH, D. [1992] Angle and Space Diversity: Experimental Comparison. Conf. IEEE Global Telecommunications Conference (GLOBECOM'92), Conf. Rec., Orlando, United States of America, p. 1851-1857.
- DISSANAYAKE, A. and ALLNUTT, J. E. [1992] Interpretation of radiometric measurements of sky-noise in terms of path attenuation. Proc. ICAP 1991, p. 374-378.
- DOMBEK, K. P. [1986] Reduction of multipath interference by adaptive beam orientation. Proc. European Conf. on Radio-Relay Systems, p. 400-106.
- DRUFUCA, G. [1974] Rain attenuation statistics for frequencies above 10 GHz from rain gauge observations. *J. Rech. Atmos.*
- FEDI, F., MERLO, U., and MIGLIORINI, P. [1977] Effect of the rain rate profile along a path on rain induced attenuation. Proc. URSI Open Symposium on Propagation in Non-ionised Media, La Baule, France.
- FEHLHABER, L. [1976] Influence of the path geometry on fading on line-of-sight radio-relay paths (in German). *Techn. Ber. FTZ, A 455 TBr 59.*
- FIMBEL, J. and JUY, M. [April 28-May 6, 1977] Differential attenuations at 13 GHz over 53 km - Comparison with simultaneous measurements at 20.5 GHz. Proc. Union Radio Scientifique Internationale, Open Symposium, La Baule, Loire-Atlantique, France.
- GARCIA LOPEZ, J. A. and PEIRO J. [1983] Simple rain attenuation prediction technique for terrestrial radio links. *Electron. Lett.*, Vol. 19, p. 879-881.
- GAVZILINA, V. D., KALININ, A. I., DADENENKO, L. V., PANOVA, R. K., SVJATOGOZ, V. V. and UDINA, T. A. [1986] The influence of multipath propagation on the performance characteristics of line-of-sight radio relay channels (in Russian). NIIR Proc., N1.
- GHOBRIAL, S. I. and SHARIEF, S. M. [April 1987] Microwave attenuation and cross polarization in dust storms. *IEEE Trans. Ant. Prop.*, Vol. AP-35, p. 418-425.
- GIBBINS, C. J. and WALDEN, C. J. [2003] A study into the derivation of improved rain attenuation regression coefficients. Radiocommunications Agency Report No. AY4359, available from <http://www.radio.gov.uk/topics/research/research-index.htm>.
- GILOI, H. G. [1979] Diffraction phenomena during multipath. AGARD Conf. Proc. No. 269, p. 32-1-32-14.
- GOSSARD, E. E. [1977] Refractive index variance and its height distribution in different air masses. *Radio Sci.*, **12**, p. 89-105.
- GUTTEBERG, O. [1983] Low elevation propagation in high-latitude regions. Telenor R&D Report No 7/83.
- HARDEN, B. N., NORBURY, J. and WHITE A. [1978] Use of a lognormal distribution of raindrop sizes in millimetric radio attenuation studies. IEE Conf. Publ 169, Part 2, p. 87-91.
- HARTMAN, W. J. and SMITH, D. [1977] Tilting antennas to reduce line-of-sight microwave link fading. *IEEE Trans. Ant. Prop.*, Vol. 25, **5**, p. 642-645.
- HAUTFEUILLE, M., BOYLE, A. W., TIMMERS, A. G. W., and SHANNON, J. D. [1980] Duct fading – is Senegal an isolated case? *Telecomm. J.*, Vol. 47, **VIII**, p. 517-525.
- HENDRY, A., ANTAR, Y. M. M., SCHLESACK, J. J. and OLSEN, R. L. [1981] Melting layer attenuation at 28.6 GHz from simultaneous Comstar beacon and polarisation diversity data. *Electron. Lett.*, **17(5)**, p. 190-191.
- HOSOYA, Y. [1991] A unified prediction method for space diversity improvement in received power on microwave links. *Electronics and Communications in Japan*. Part 1, Vol. 74, **9**, p. 73-81. Translated from Denshi Joho Tsushin Gakkai Ronbunshi, Vol. 73-B-II, **12**, December 1990.
- JAIN, Y. M. and WATSON, P. A. [1985] Attenuation in melting snow on microwave- and millimetre-wave terrestrial radio links. *Electron. Lett.*, **21(2)**.

- KALININ, A. I. [1979] Rasprostranenie radiovoln na trassakh nazemnykhi kosmicheskikh radioliny (Propagation on terrestrial and space links). *Sviaz*, Moscow, USSR.
- KARL, H. and PERSSON, R. [1998] The Planning and Engineering of Radio Systems. *K&K Engineering*, Stockholm, Sweden.
- KHARADLY, M., OWEN, N. VAN DER STAR, J., MICHELSON, D. and ENEGREN, T. [1983] Observations of abnormal microwave propagation phenomena during melting layer conditions. Proc. of International Conference on Antennas and Propagation (ICAP), Norwich United Kingdom.
- KHARADLY, M. M. Z. and OWEN, N. [1988] Microwave propagation through the melting layer at grazing angles of incidence. *IEEE Trans. Ant. Prop.*, 36(8).
- KOBAYASHI, T. [July 1977] Degradation of cross-polarization isolation due to rain. *Radio Res. Lab. J.*, Vol. 24, p. 101-107.
- KUZNETSOV, G. G., WALDEN, C. J. and HOLT, A. R. [2000] Attenuation of microwaves in sleet. Final Report to the Radiocommunication Agency AY 3564, Dep. of Mathematics, University of Essex, Colchester (Available from <http://www.ofcom.org.uk/>).
- LAM, W. I. and WEBSTER, A. R. [1985] Microwave propagation on two line-of-sight overseas paths. *IEEE Trans. Ant. Prop.*, Vol. 33, 5, p. 510-516.
- LIN, S. H. [1971] Probability amplitude analysis of statistical behaviour of fading signal envelope. *BSTJ*, Vol. 50, p. 3211-3270.
- LIN, S. H. [1975] A method for calculating rain attenuation distributions on microwave paths. *BSTJ*, 54, p. 1051-1086.
- LIN, S. H., LEE, T. C. and GARDINA, M. F. [1988] Diversity protections for digital radio – A review. SMBO Int. Microwave Symp. Proc., Vol. II, p. 1175-1182.
- MARTIN, L. [1983] Rates of change of propagation medium transfer functions during selective fading. Proc. URSI (Commission F) International Symposium on wave propagation and remote sensing, Louvain-la-Neuve, Belgium.
- MARTIN, L., GIRAUD, B. and BOUIDENE, A. [1993] General computation method of outage time for digital radio links. *Electron. Lett.*, Vol. 29, 22, p. 1913-1914.
- McEWAN, N. J., BASHIR, S. O., CONNOLLY, C. and EXCELL, D. [1985] The effect of sand and dust particles on 6/4 and 14/11 GHz signals on satellite-to-Earth paths. University of Bradford, Report 379.
- MEDHURST, R. [1965] Rainfall attenuation of centimeter waves: Comparison of theory and measurement. *IEEE Trans. Ant. Prop.*, p. 550- 564.
- MILLER, A. R., BROWN, R. M. and VEGH, E. [1984] New derivation for the rough-surface reflection coefficient and for the distribution of sea-wave elevations. *Proc. IEE*, Vol. 131, Pt. H, 2, p. 114-116.
- MINKIN, V. M. and NADENENKO, L.V. [1998] Influence of propagation conditions on the bringing into service procedure for digital radio-relay systems. Proc. of 6th ECRR' 98, Bergen, Norway.
- MISME, P. and FIMBEL, J. [1975] Theoretical and experimental determination of rain-induced attenuation on a radioelectric path. *Ann. des Télécomm.*, Vol. 30, p. 149-158.
- MOHAMED, S. A. RICHMAN, G. D., and HUIISH, P. W. [198] Results of angle diversity trials by British Telecom. Proc. 2nd European Conference on Radio-Relay Systems.
- MORITA, K. and HIGUTI, I. [1978] Statistical Studies on Rain Attenuation and Site Diversity Effect on Earth to Satellite Links in Microwave and Millimeter Wavebands. IEICE TRANS. (1976-1990), Vol. 61, 6, p. 425-432.
- MORITA, K. SHIMBA, M. and AKEYAMA, A. [May 1974] Radio propagation characteristics due to rain at 20-GHz band. *IEEE Trans. Ant. Prop.*, Vol. 22, 5, p. 507-509.
- MOUPFOUMA, F. [1984] Improvement of a rain attenuation prediction method for terrestrial microwave links. *IEEE Tran. Ant. Prop.*, Vol. 32, p. 1368-1372.
- NADENENKO, L.V. [1981] Raschet trass radioreleinykh liny pryamoi vidimosti (Calculations for line-of-sight radio relay paths). Spravochnik po radioreleinoi svyazi. *Radio I Sviaz*, Moscow, Russian Federation.

- NADENENKO, L. V. and SVIATOGOR, V. V. [1972] Dlitelnost zamiraniy signala na intervalakh radioreleynikh liniy pryamoy vidimosti (Duration of signal fading in the hops of line-of-sight radio-relay systems) (in Russian). *Elektrosviaz*, 5, p. 6-10.
- NISHITSUJI, A. [1971] Method of calculation of radio-wave attenuation in snowfall. *Electronics and communications in Japan*, 54-B(1).
- NOWLAND, W. L., OLSEN, R. L. and SHKAROFSKY, I. P. [October 1977] Theoretical relationship between rain depolarisation and attenuation. *Electron. Lett.*, Vol. 13, 22, p. 676-678.
- OLSEN, R. L. [1981] Cross-polarisation during precipitation on terrestrial links. *Radio Sci.*, Vol. 16, 5, p. 761-779.
- OLSEN, R. L. [1989] The role of atmospheric stratification and surface effects in multipath propagation over terrestrial line-of-sight links: A review of some recent results. SMBO Proc. Int. Microwave Symp., São Paulo, Brazil, p. 401-408.
- OGUCHI, T. [1973] Attenuation and phase rotation of radio-waves due to rain: Calculation of 19.3 and 34.8 GHz. *Radio Sci.*, Vol. 8, p. 51-58,
- OGUCHI, T. [1977] Scattering properties of Pruppacher-and-Pitter form raindrops and cross-polarization due to rain: calculations at 11,13, 19-3 and 34-8 GHz. *Radio Sci.*, 12, p. 41-51.
- OGUCHI, T. and HOSOYA, Y. [1974] Differential attenuation and differential phase shift of radio waves due to rain: Calculations of microwave and millimeter wave regions. *J. Rech. Atmos.*, Vol. 8, p. 121-128.
- OLSEN, R. L. [September-October 1981] Cross polarization during precipitation on terrestrial links: A review. *Radio Sci.* Vol. 16, p. 761-779.
- OLSEN, R. L. [1989] The role of atmospheric stratification and surface effects in multipath propagation over terrestrial line-of-sight links: A review of some recent results. Proc. SBMO International Microwave Symposium, São Paulo, Brazil, p. 401-408.
- OLSEN, R. L. and SEGAL, B. [1992] New techniques of predicting the multipath fading distribution on VHF/UHF/SHF terrestrial line-of-sight links in Canada. *Can. J. Elect. & Comp. Eng.*, Vol. 17, 1, p. 11-23.
- OLSEN, R. L. and TJELTA, T. [1999] Worldwide techniques for predicting the multipath fading distribution on terrestrial L.O.S. links: Background and results of tests. *IEEE Trans. Ant. Prop.*, Vol. 47, 1, p. 157-170.
- OLSEN, R. ROGERS, D. and HODGE, D. [1978] The aRb relation in the calculation of rain attenuation. *IEEE Trans. Ant. Prop.*, Vol. 26, 2, p. 318-329.
- OLSEN, R. L., MARTIN, L. and TJELTA, T. [1987] A review of the role of surface reflection in multipath propagation over terrestrial microwave links. Proc. of NATO/AGARD Symposium on Terrestrial propagation characteristics in modern systems of communications, surveillance, guidance and control, No. CP407, p. 2/1-23.
- OLSEN, R. L., TJELTA, T., MARTIN, L. and SEGAL, B. [January 2003] Worldwide techniques for predicting the multipath fading distribution on terrestrial L.O.S. links: comparison with regional techniques. *IEEE Trans. Ant. Prop.*, Vol. 51, 1, p. 23-30.
- PEARSON, K. W. [1965] Method for the prediction of the fading performance of a multisection microwave link. Proc. Inst. Elec. Eng., Vol. 112, p. 1291-1300.
- PERONI, B. and FEDI, F. [1974] The calculation of the hop length of digital radio relay systems at frequencies above 10 GHz. *Alta Frequenza*, Vol. 43, p. 634-639.
- PRASAD, M. V. S. N., DUTTA, H. N., SARKAR, S. K. and REDDY, B. M. [1991] Fading reduction in microwave LOS links using antenna beam tilting techniques. *Radio Sci.*, Vol. 26, 3, p. 751-758.
- PRUPPACHER, H. R. and BEARD, K. V. [1970] A wind-tunnel investigation of the internal circulation and shape of water drops falling at terminal velocity in air. *Quart. J. Roy. Meteor. Soc.*, Vol. 96, p. 247-256.
- PRUPPACHER, H. R. and PITTER, R. L. [1971] A semi-empirical determination of the shape of cloud and rain drops. *Atmos. Sci.*, 28, p. 86-94.
- RANA, D., WEBSTER, A. R. and SYLVAIN, M. [1992] Statistical characterization of line-of-sight microwave links. *Radio Sci.*, Vol. 27, 6, p. 783-796.
- RANA, D., WEBSTER, A. R. and SYLVAIN, M. [1993] Origin of multipath fading on a terrestrial link. *Ann. des Télécomm.*, Vol. 48, 11-12, p. 557-566.

- RANA, D., WEBSTER, A. R. and SYLVAIN, M. [1995] Surface reflection at low-angle propagation *IEEE Trans. Ant. Prop.*, Vol. 43, 7, p. 639-652.
- ROORYCK, M. and BATTISTI, J. [1976] Experimental investigation of a link at 13 GHz on 53 km: Attenuation and cross polarization. *ESA Probl. of Space and Terrest. Microwave Propagation*, p. 217-227.
- RUMMLER, W. D. [10-14 June 1978] A multipath channel model for line-of-sight digital radio systems. *IEEE International Conference on Communications (ICC'79)*, Boston, United States of America, Vol. 2, p. 32.2.1-5.
- RYDE, J. W. and D. RYDE [1945] Attenuation of Centimetre and Millimetre Waves by Rain, Hail, Fogs, and Clouds. Rpt. No. 8670, Research Laboratory of the General Electric Company, Wembley, England.
- SALEH, A. A. M. and VALENZUELA, R. A. [1987] A Statistical Model for Indoor Multipath Propagation. *IEEE J. Selected Areas Comm.*, Vol. 5, 2, p. 128-137.
- SALOUS, S. and BAJJ, N. [1998] Urban wideband measurements at 1.8 GHz with different chirp bandwidths. 48th IEEE Vehicular Technology Conference, Vol. 1, 18-21, p. 697-701.
- SASAKI, O., HOSOYA, Y. and YOSHIKAWA, M. [1987] A tilted-beam diversity reception system to reduce line-of-sight microwave fading. *Trans. Inst. Electron. Comm. Engrs.*, Vol. 70-B, 10, p. 1251-1253.
- SASAKI, O., MORITA, K. and KIKUSHIMA, M. [1976] 19 GHz rain attenuation characteristics on four tandem links. *IEEE Trans. Ant. Prop.*, Vol. 24, 2, p. 216-220.
- SASAKI, O., SATOH, A. and HOSOYA, Y. [1991] Multiple diversity reception techniques. *NTT Rev.*, Vol. 3, 1, p. 66-74.
- SATOH, A. and SASAKI, O. [1989] Tilted-beam-, beam-width- and space-diversity improvements on various paths. *IEEE Global Telecommunications Conf. (Globecom'89)*, p. 2.3.1.
- SATOH, A., SASAKI, O. and HOSOYA, Y. [1989] Improvement of in-band dispersion by beam tilting on radio links with strong ground reflection. *Proc. Int. Symp. on Antennas and Propagation (ISAP'89)*, p. 1073-1076.
- SAUNDERS, M. I. [1971] Cross polarisation at 18 and 30 GHz due to rain. *IEEE Trans.*, Vol. AP-19, p. 273-277.
- SCHIAVONE, J. A. [1981] Prediction of positive refractivity gradient for line-of-sight microwave radio paths. *BSTJ*, Vol. 60, 6, p. 803-822.
- SEGAL, B. [1979] High-intensity rainfall statistics for Canada. *Commun. Res. Centre, Ottawa, ON, Canada*, 1329-E.
- SEGAL, B. [1982] Rain Attenuation Statistics for Terrestrial. Microwave Links in Canada. *Comm. Res. Centre. Rep. No. 1351-E, Ottawa, Canada*, p. 14.
- SEGAL, B. [1999] Multipath propagation mechanisms deduced from tower-based meteorological measurements. *Proc. First International Workshop on Radiowave Propagation Modelling for SatCom Services at Ku-Band and Above, European Space Agency, Report No. 146*, p. 13-18, Noordwijk (The Netherlands).
- SETZER, J. E. [1970] Computed transmission through rain at microwave and visual frequencies. *BSTJ*, Vol. 49, p. 1873-1892.
- SHAFI, M. [April 1987] Statistical Analysis/Simulation of a Three Ray Model for Multipath Fading with Applications to Outage Prediction, *IEEE Journal on Selected Areas on Communication*, Special issue on Advances in Digital Communications.
- SILVA MELLO, L. A. R., GARCIA, N. A. P. and PONTES, M. S. [2005] Measurements and Prediction of Differential Rain Attenuation in Converging Links. *Electron. Lett.*, London, Vol. 41, 17, p. 942-942.
- STEPHANSEN, E. and MOGENSEN, G. [1979] Experimental Investigation of Some Effects of Multipath Propagation on a Line-of-Sight Path at 14 GHz. *IEEE Trans. Comm.*, Vol. 27, 3, p. 643-647.
- TAKADA, M. and NAKAMURA, S. [January 1966] Attenuation of 11 Gc Waves by Wet Snowfall. *Rev. Elec. Comm. Labs.*, 14(1-2), p. 27-42.
- TANEM, T. [1988] Forbedring av transmisjonskvaliteten i digital radiolinjesystemer over sjøhopp ved optimal tilting av antennene (in Norwegian). *Telekonikk*, Nr. 2/3. English translation available from author, Telenor, Oslo, Norway.
- TATARSKII, V. I. [1967] *Wave Propagation in the Turbulent Atmosphere*. Nauka, Moscow, Russian Federation.
- THORVALDSEN, P. [2000] Co-channels everywhere. *Proc. of ECRR 2000*.

- THURAI, M. and WOODROFFE, J. M. [1997] Precipitation induced co and cross-polar effects from a 9 km link operating at 38 GHz. Proc. of International Conference on Antennas and Propagation (ICAP), Conf. Publ. No. 436, **2**, p. 222-225.
- TJELTA, T., BRÅTEN L. E. and BACON D. [2005] Predicting the attenuation distribution on line-of-sight radio links due to melting snow. Proc. ClimDiff, Cleveland, United States of America.
- TJELTA, T., BRÅTEN L. E. and BREIVIK, T. O. [2006] Predicting the attenuation distribution on line-of-sight radio links due to melting snow. Telenor R&D Scientific. Doc. N 35/2005.
- TJELTA, T., HAYTON, T. G., SEGAL, B. and SALONEN, E. [1998] Correlation of observed multipath occurrence with climatic parameters derived from radiosondes, surface stations, and numerical atmosphere models. Proc. of URSI Commission F Symposium on Climatic Parameters in Radiowave Propagation, Ottawa, Canada, p. 85-92.
- TJELTA, T., NYSETH, A. and LIND, K. [1991] Simultaneous measurements of angle and space diversity improvement on a line-of-sight microwave link in Norway. Proc. 3<sup>rd</sup> European Conf. on Radio Relay Systems (ECRR).
- TJELTA, T. and OLSEN, R. L. [2-5 June 1998] Further development of methods for worldwide prediction of terrestrial radio link multipath fading distributions. Proc. of ECRR'98, Bergen, p. 330-335.
- TJELTA, T., OLSEN, R. L. and MARTIN, L. [1990] Systematic development of new multivariable techniques for predicting the distribution of multipath fading on terrestrial microwave links. *IEEE Trans. Ant. Prop.*, Vol. 38, **10**, p. 1650-1665.
- TJELTA, T. and TANEM, T. [1992] Measured and predicted enhancement on line-of-sight microwave links. URSI Comm. F Symposium, p. 9.1.1-6.
- VALENTIN, R., GILOI, H. G. and METZER, K. [1989] Space diversity versus angle diversity – Results of system analysis using propagation data. IEEE Int. Conf. Comm. (ICC'89).
- VALENTIN, R., GILOI, H. G. and METZGER, K. [1990] More on angle diversity for digital radio links.
- VALENTIN, R., METZGER, K., GILOI, H. G. and DOMBEK, K. P. [1987] Effects of angle diversity on the performance on line-of-sight digital radio-relay systems. IEEE Global Telcom. Conf. (Globecom'87), p. 1229-1232.
- VERGERES, D., JORDI, P. and LOEMBE, A. [1990] Simultaneous error performance of antenna pattern diversity and vertical space diversity on a 64 QAM-radio link. IEEE Global Telecom. Conf. (GLOBECOM'90), Conf. Rec., Vol. 2, p. 817-82 (see also Bulletin Technique PTT, Swiss PTT, Berne, Switzerland, 1, 28-33, 1991).
- VIGANTS, A [1971] Number and duration of fades at 6 and 4 GHz. *BSTJ*, Vol. 50, p. 815-841.
- VIGANTS, A. [1975] Space-diversity engineering. *BSTJ*, Vol. 54, **1**, p. 103-142.
- VIGANTS, A. [1981] Microwave radio obstruction fading. *BSTJ*, Vol. 60, **6**, p. 785-801.
- VIGANTS, A. and PURSLEY, M. V. [1979] Transmission unavailability of frequency-diversity protected microwave FM radio systems caused by multipath fading. *BSTJ*, Vol. 58, **8**, p. 1279-1796.
- WALDEN, C. J., WILSON C. L., GODDARD J. W. F., PAULSON K. S., WILLIS M. J. and EASTMENT J. D. [2003] A study of the effects of melting snow on communications links in Scotland. Proc. International Conference on Antennas and Propagation (ICAP).
- WATSON, P. A. [September 1976] Survey of measurements of attenuation by rain and other hydrometeors. *Proc IEE*, Vol. 123, **9**, p. 863-71.
- WEBSTER, A. R. [1983] Angle-of-arrival and delay times on terrestrial line-of-sight microwave links. *IEEE Trans. Ant. Prop.*, Vol. 31, **1**, p. 12-17.
- WEBSTER, A. R. [1991] Multipath angle-of-arrival measurements on microwave line-of-sight links. *IEEE Trans. Ant. Prop.*, Vol. 39, **6**, p. 798-803.
- WEBSTER, A. R., TIEU, T. and WONG, W. [1994] Simultaneous experimental studies of tropospheric microwave propagation. Dept. Electrical Engineering, University of Western Ontario, London, Ontario, Canada, Report CRC-CR-94-003.
- YAMADA, M., KARASAWA, Y. and YASUNAGA, M. [1987] An improved prediction method for rain attenuation in satellite communications operating at 10-20 GHz. *Radio Sci.*, Vol. 22.

**ITU-R texts**

- Recommendation ITU-R P.1510 (2001) Annual mean surface temperature.
- Recommendation ITU-R P.311-10 (2001) Acquisition, presentation and analysis of data in studies of tropospheric propagation.
- Recommendation ITU-R P.581-2 (1990) The concept of “worst month”.
- Recommendation ITU-R P.618-8 (2003) Propagation data and prediction methods required for the design of Earth-space telecommunication systems.
- Recommendation ITU-R P.676-5 (2001) Attenuation by atmospheric gases.
- Recommendation ITU-R P.835-3 (1999) Reference standard atmospheres.
- Recommendation ITU-R P.836-2 (2001) Water vapour: surface density and total columnar content.
- Recommendation ITU-R P.837-4 (2003) Characteristics of precipitation for propagation modelling.
- Recommendation ITU-R P.838-3 (2005) Specific attenuation model for rain for use in prediction methods.
- Recommendation ITU-R P.839-3 (2001) Rain height model for prediction methods.
- Recommendation ITU-R P.840-3 (1999) Attenuation due to clouds and fog.
- Recommendation ITU-R P.841-2 (2001) Conversion of annual statistics to worst-month statistics.
- Recommendation ITU-R P.676-3 (1997) Attenuation by atmospheric gases.
- ITU-R [2002] Development towards a model for combined rain and sleet attenuation. Document 3M/62E.
- ITU-R [1996] Handbook on Digital Radio-Relay Systems. Radiocommunication Bureau, Geneva.
- ITU-R [1996] Handbook on Radiometeorology. Radiocommunication Bureau, Geneva.
- CCIR [1986-1990] Doc. 5/287 (France).

## PART 2

### TRANS-HORIZON LINKS

#### 1 Introduction

This part of the Handbook relates to planning and design of trans-horizon radio-relay systems. Based on Recommendations ITU-R P.526 and ITU-R P.617, it provides background information on the various prediction methods for diffraction and tropospheric scatter losses, data and other material given in these Recommendations. This includes a brief presentation of the mathematical and empirical basis of the methods and citation of any associated references.

#### 2 Typical applications

The trans-horizon radiolinks are characterized by very long paths, typically from 100 km to almost 1 000 km. This gives very high path attenuation that must be compensated for by using very high RF radiated power, high gain antennas and sensitive low noise receivers. In addition, some kind of diversity may be needed. The frequency bands utilized are in the UHF and lower SHF range.

Compared with a conventional line-of-sight radiolinks, a trans-horizon system may, in some cases, lead to a more economical solution due to the possibility of avoiding repeaters. This feature is particularly useful for cases of difficult terrain such as connections between distant sites in rural areas, connections between the mainland and remote islands (or between the islands) and connections between the shore and oil platforms far out at the sea.

A trans-horizon link has good security against sabotage or disaster, as there are few repeater stations to protect. This is the main reason for the high military interest in such systems.

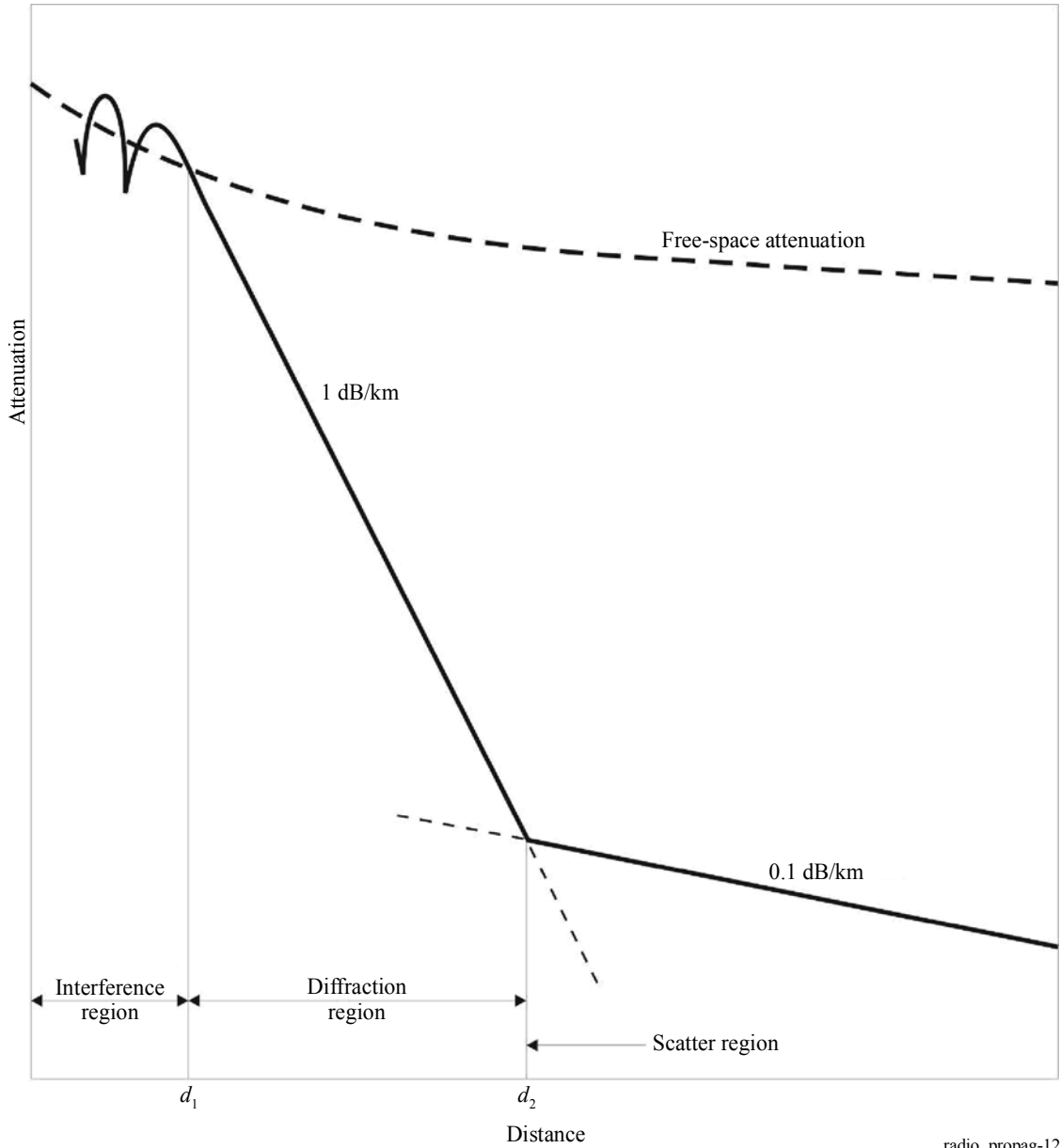
A peculiar characteristic of trans-horizon radio links is the problems of transmission, distortion that limits the useful bandwidth and traffic capacity, is a peculiar characteristic of trans-horizon radio links. This feature has been responsible for the exclusion of such systems from use in modern public telephone networks, except for some developing countries. In the future the main application of trans-horizon radio links is expected to be in governmental networks and, to some extent, in private communication networks e.g., the oil industry. Most of the new systems planned are designed to carry digital traffic. Special care must therefore be taken when managing the distortion problems.

#### 3 Basic theory

Trans-horizon propagation mechanism occurs over paths extending beyond the normal radio horizon. The only two permanent trans-horizon propagation mechanisms for frequencies above 30 MHz are diffraction and tropospheric scatter. The attenuation associated to these two mechanisms with distance is shown in Fig. 12.

It should be noted that just beyond the horizon the diffracted field has a rapid exponential decay, of the order of 1 dB/km at 1 GHz, while the scattered field decay is around 0.1 dB/km. Although not considered in the methods discussed here, also shown in Fig. 12 is the interference region, where the oscillation in the received field is due to the phasorial sum of the direct and reflected rays.

FIGURE 12  
Interference, diffraction and scatter regions



radio\_propag-12

### 3.1 Diffraction

As discussed in § 3.3 of Part 1, if the atmosphere is sufficiently subrefractive, radio waves are bent towards the Earth. Two main effects are related to this mechanism, the diffraction over the Earth curvature and over terrain irregularities.

#### 3.1.1 Diffraction over a smooth spherical Earth

The classical solution of the diffraction over a spherical Earth (smooth and homogeneous) is given by the residue series [Bremmer, 1949]. Over, or beyond, the horizon the first term of this series provides a valid approximation for the evaluation of the diffracted field [Bullington, 1947 and Rice *et al.*, 1967]. While this solution is a satisfactory approach for many applications, there are cases in which a more accurate determination is needed. One example is the prediction of the field strength for propagation over a path that is partly over land and partly over sea.

For the problem of diffraction over an inhomogeneous Earth, a semi-empirical solution has been given by Millington [1949a] and an integral equation solution was also derived by an application of the compensation theorem [Monteath, 1951]. Numerical results for both two- and three-section smooth Earth are presented in [Wait, 1974]. The agreement with experimental data in predicting the recovery effect in a land-sea boundary [Millington, 1949b and Millington and Isted, 1950] is an important confirmation of this theory.

### 3.1.2 Diffraction over isolated obstacles

A propagation path with a common horizon for both terminals may be considered as a single knife-edge. The classical approach to solve this problem is based on the Fresnel-Kirchhoff scalar theory for optics [Born and Wolf, 1970]. However, it has been verified that, in certain cases, the effect of obstacle dimension leads to results quite different from those predicted by the knife-edge model. A correction to this solution was developed in the 1950's by Fock, who demonstrated the existence of two parts in the diffracted field. One part is obtained by the Fresnel-Kirchhoff theory and the other, a function of obstacle dimension, corresponds to the appropriate correction factor. It should be also mentioned that, according to the principle of local action [Fock, 1965], the diffraction over a rounded obstacle is independent of the obstacle shape.

Based on Fock's work, the diffraction by a cylindrical smooth obstacle for grazing angles was investigated [Wait and Conda, 1959]. Through an integral equation solved by numerical methods, these authors avoided the problem of poor convergence of the series in the LoS region common to other existing solutions. Extensions to Wait and Conda's results were published in the sixties [Dougherty and Maloney, 1964 and Dougherty and Wilkerson, 1967], including engineering formulas and graphs for practical applications.

### 3.1.3 Diffraction over multiple obstacles

Rigorous solutions for the case of two knife-edges have been available for a number of years [Millington *et al.*, 1962 and Furutsu, 1963]. The theoretical solution for up to ten knife-edge obstacles requires the numerical evaluation of a multiple Fresnel-type integral of a dimension equal to the number of edges [Vogler, 1982]. For engineering purposes, approximate methods have been proposed [Epstein and Peterson, 1953; Deygout, 1966 and Giovaneli, 1984], all based on the single-edge diffraction theory.

No rigorous method exists for the prediction of field strength by diffraction over several round obstacles. An extension to the Deygout method has been suggested [Assis, 1971], employing a simplified solution based on the assumption that each obstacle can be represented by a cylinder with a radius equal to the radius of curvature at the obstacle top. A solution using the procedure adopted by Vogler [1982], for a cascaded arrangement of cylinders, has also been considered [Sharples and Mehler, 1989]. These authors use only the first term of Vogler's infinite series, producing a result similar to that of Epstein and Peterson [1953], but with a correction factor for the associated spreading losses.

Recommendation ITU-R P.526 presents two methods for the diffraction over multiple obstacles. The first method assumes that each obstacle can be represented by a cylinder with a radius equals to the radius of curvature at the obstacle top, being advisable when a detailed vertical profile through the ridge is available. The second one is based on knife-edge obstacles. This method uses Deygout construction limited to a maximum of three edges, plus an empirical correction derived from measurements carried out on 25 000 paths in the United Kingdom.

### 3.1.4 Diffraction over irregular terrain

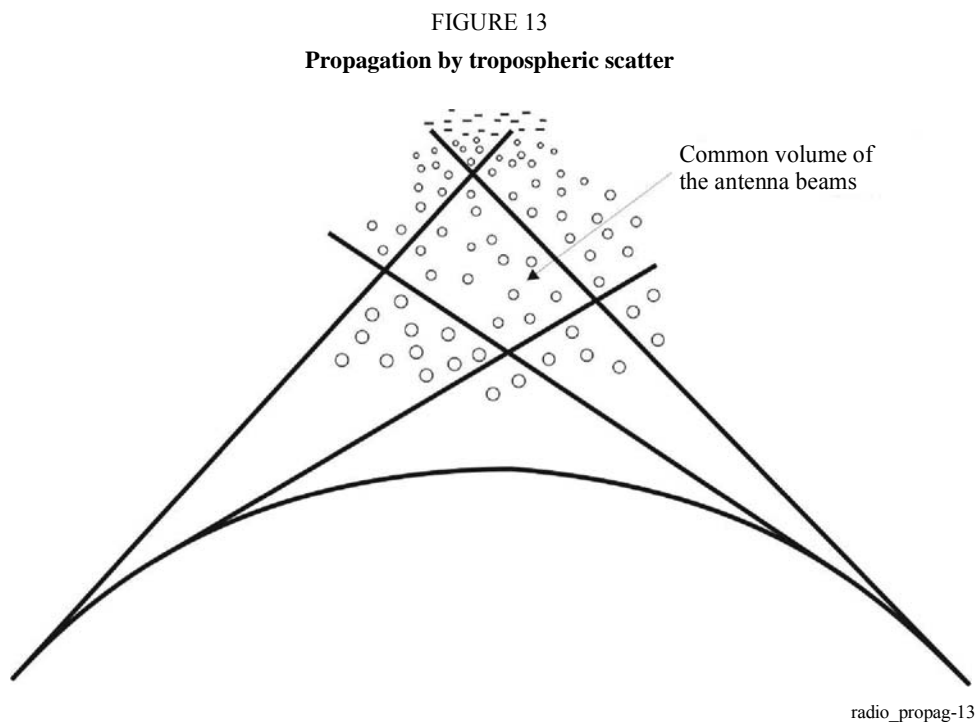
A fundamental theoretical approach to the problem of diffraction by terrain irregularities has been developed [Hufford, 1952] using an integral equation technique. Further work in this direction has been carried out by Ott and Berry [1970] and Ott [1971]. In their model, the terrain can be represented by a completely arbitrary profile along the great circle path, and the electrical properties of the Earth can vary continuously. Unfortunately, a great deal of computer storage space is needed if the fine scale structure of the terrain is to be accounted for.

A semi-empirical method [Furutsu and Wilkerson, 1970 and 1971] has been proposed for estimating the gain caused by a ridge on a spherical homogeneous Earth. This method uses graphs of the "terminal gain" of obstacles, which are defined by the asymptotic values of the theoretical obstacle gains for infinite propagation distance on one side of the obstacle, and assumes a finite distance on the other side. Similar results have been achieved by using the mode-matching approach [Wait, 1974].

A numerical method [Assis, 1982] has been developed for use in those cases where a terrain feature can be modelled as a single knife-edge and the terrain is irregular in a direction perpendicular to the plane of propagation (great circle path). Measurements in the frequency range from 270 to 330 MHz indicate that knife-edge calculations can result in  $\pm 10$  dB errors if lateral irregularities are not considered.

### 3.2 Tropospheric scatter

In this mechanism, the energy is scattered from tropospheric inhomogeneities in the common volume, which consists of that portion of the troposphere visible to both transmitting and receiving antennas, as can be seen in Fig. 13.



Since the first evidence of this mechanism appeared around 1950, for about 15 years a large number of theoretical studies were carried out and many scientific discussions occurred. The supremacy of one theory or other was never acknowledged. It is, however, recognized that the main mechanisms are turbulence scattering and incoherent layer reflection [Friis *et al.*, 1957], and that the relevant sub-mechanisms of both could behave as dominant, depending on climatological characteristics of the geographical region considered. Mathematical models to evaluate the troposcatter loss based on parameters such as turbulence scale and layer size were developed. However, due to difficulty to derive these parameters from meteorological measurements, these models are not used in practical applications. Nevertheless, the models may be useful to investigate frequency and distance dependence, the phenomenon of antenna gain loss, etc., [Du Castel, 1966]. On this basis, propagation measurements have been used to derive empirical or semi-empirical models to evaluate the transmission loss.

Currently, the prediction of tropospheric scatter paths is based on these empirical or semi-empirical methods. Two methods were published in 1965 and used as reference for ITU-R studies for more than 20 years. One of them corresponds to a simplified version of the US National Bureau of Standards (NBS) method, first published in May 1965 and, in a revised form, two years later [Rice *et al.*, 1967]. According to this method the annual median transmission loss is given by:

$$L(50) = 20 \log f - 20 \log d + F(\theta) + L_c - G_t - G_r - V(d_e) \quad (130)$$

where  $d$  is the distance (km),  $f$  is the frequency (MHz),  $\theta$  (rad) is the angle between radio horizon rays in the great circle plane containing the antennas for median atmospheric conditions (see Fig. 14), and  $G_t$  and  $G_r$  are the transmitting and receiving antenna gains (dB), respectively. The functions  $F(\theta)$  and  $V(d_e)$ , as well as the definition of the effective distance  $d_e$  are given in [Rice *et al.*, 1967].  $L_c$  is the aperture-to-medium coupling loss, given in Recommendation ITU-R P.617.

The scatter angle  $\theta$  is given by:

$$\theta = \theta_e + \theta_t + \theta_r \quad (131)$$

where  $\theta_t$  and  $\theta_r$  are the transmitter and receiver horizon angles, respectively. These angles can be calculated by:

$$\theta_e = d \times 10^3 / ka \quad \text{mrad} \quad (132)$$

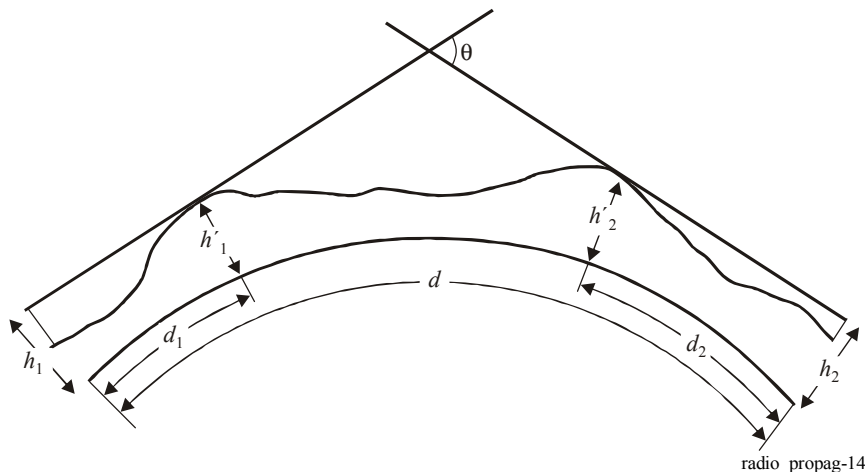
$$\theta_{t,r} = \frac{h'_{1,2} - h_{1,2}}{d_1} - \frac{d_{1,2} \times 10^3}{ka} \quad \text{mrad} \quad (133)$$

with:

- $d$ : path length (km)
- $a$ : 6370 km radius of the Earth
- $k$ : effective Earth radius factor for median refractivity conditions ( $k = 4/3$  should be used unless a more accurate value is known)

and the antenna heights ( $h_{1,2}$  and  $h'_{1,2}$ ) (m) and the distances ( $d_{1,2}$ ) (km) are shown in Fig. 14.

FIGURE 14  
Scatter geometry



For other annual percentages of time, a set of curves as a function of the effective distance and climate is provided in [Rice *et al.*, 1967]. In this method, to take into account the geographical variability around the world, nine radio climates were defined: Equatorial; Continental sub-tropical; Maritime sub-tropical; Desert; Mediterranean; Continental temperate; Maritime temperate, overland; Maritime temperate, overseas; Polar. This division is, of course, rather crude, and local geographical conditions may require substantial modifications. A brief description of these climates is given in Recommendation ITU-R P.617.

The second method was based on measurements carried out in Europe and Africa and is entirely graphical. A set of curves has been plotted for the following climates: Equatorial; Maritime sub-tropical; Desert; Continental temperate; Maritime temperate, overland. These curves show the transmission loss between isotropic antennas at 1 GHz for a number of time percentages (1%, 10%, 50%, 90%, 99% and 99.9%) for the worst month and for the whole year, which may be applied in designing radio-relay systems [Boithias and Battesti, 1965]. For frequencies other than 1 GHz the correction factor (dB) is  $30 \log(f/1\,000)$ , being  $f$  expressed in MHz.

In this method the curves assume that horizon is seen from each end of the link at a zero angle of elevation. If the angles of elevation are equal, respectively, to  $\theta_1$  and  $\theta_2$ , in radians, the real distance should be replaced by an equivalent distance  $d_q$  (km) given by:

$$d_q = d + 8.5 (\theta_1 + \theta_2) \quad (134)$$

In addition, the following term must be added to the loss thus calculated:

$$20 \log (d/d_q) \quad (135)$$

More recently, a simple and reasonably accurate method was developed in the People's Republic of China [Zhang, 1988]. Its initial form came from [Zhang, 1977] in which the scattering section was used in the form:

$$\sigma = A\lambda^n \theta m e^{-\gamma h} \quad (136)$$

where  $\lambda$  is the wavelength,  $\theta$  is the scattering angle,  $h$  is the height from the basis of the scattering volume to the Earth's surface, and  $A$ ,  $n$ ,  $m$ , and  $\gamma$  are meteorological parameters. The factor with  $\lambda$  and  $\theta$  characterizes the scattering mechanism, which can be turbulence scattering when  $n = m - 4$ , and can also be an incoherent layer reflection when  $n$  and  $m$  take other values. The exponential factor characterizes the dependence of the inhomogeneity strength on the height. The initial theoretical form of the transmission loss was modified by adjusting its meteorological parameters first through Chinese propagation data and then by using the data bank of Radiocommunication Study Group 3. This procedure led to a very simple equation for the annual median transmission loss. Moreover, as a characteristic of annual variation, the difference between transmission losses not exceeded for 50% and 90% of the time was believed to have the form:

$$Y(90) = a' + b' e^{-c'h} \quad (137)$$

where  $a'$ ,  $b'$ , and  $c'$  are constants to be determined and  $h$  is the height from the basis of the scattering volume to the Earth's surface. Constants  $a'$  and  $c'$  depend on climate, while constant  $b'$  depends on the annual variation range of  $\Delta N_s$  (surface refractivity), frequency, and climate.

#### 4 Prediction of transmission loss

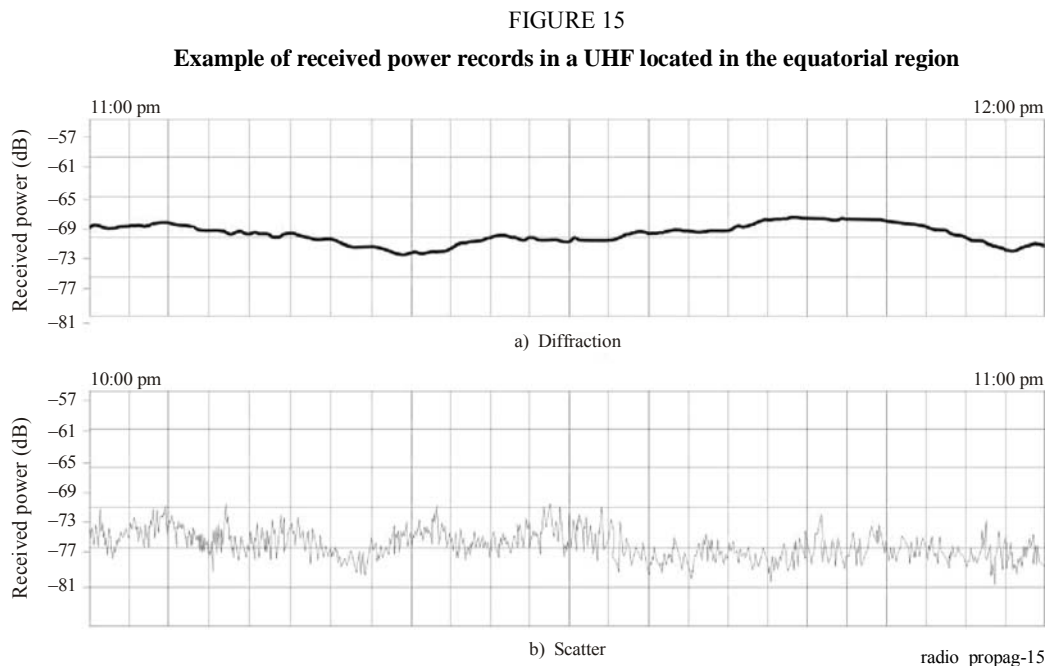
The material presented in this section is mainly based on Recommendations ITU-R P.526, particularly in the ITU-R P.526-3 and ITU-R P.526-9 versions for diffraction, and ITU-R P.617 for scattering. As these Recommendations cover a limited number of practical cases, the reader is referred to the list of references cited in the previous section. On the other hand, details about the concept of transmission loss used here can be found in Recommendation ITU-R P.341.

##### Path profile analysis

The first step in this analysis is to plot the path profile on a linear scale graph by modifying the terrain elevations to include the effect of tropospheric refraction. In the absence of information about the appropriate equivalent earth radius to be used, the standard value of 8 500 km may be taken as reference.

Once the path profile is conveniently plotted, the next step is to verify the main propagation mechanism (diffraction or scattering). As shown in Fig. 12, even in a line-of-sight path the diffraction may be effective. The separation between interference and diffraction regions ( $d_1$  in Fig. 12) corresponds to the point where the path clearance in terms of the first Fresnel zone radius is equal to 0.6 (see Recommendation ITU-R P.530).

The separation between diffraction and scattering regions ( $d_2$  in Fig. 12) is not easily defined. Experimental data show that there is an intermediate region where both diffraction and scattering mechanisms must be considered. This region is generally located 100 to 150 km far from the transmitting antenna site. In such a case, it is advisable to evaluate the attenuation loss by both mechanisms and to use the one most adequate for a given application (higher attenuation for planning and lower attenuation for interference calculation). To illustrate this situation, Fig. 15 [Assis, 1986] shows two samples of the variation of power received in a 300 MHz link, 135 km long, located in the Amazon region (equatorial climate).



During the day, the tropospheric scatter propagation mechanism is dominant and the received power fluctuates at a high rate within a range of about 10 dB. During night hours, the signal behaviour is quite different. Under the action of tropospheric stratification, the received power varies slowly without the fast fluctuations observed during daytime.

## 4.1 Diffraction loss

For propagation over the Earth's surface, diffraction paths are often encountered, and it is necessary to estimate the transmission loss due to diffraction either over a spherical Earth's surface or over irregular terrain, including with different types of obstacles. In both cases, the reference for diffraction loss is attenuation relative to free-space.

### 4.1.1 Diffraction over a spherical Earth

For the evaluation of diffraction loss in the case of over-the-horizon paths, Recommendation ITU-R P.526 presents a numerical method and a graphical method, both derived from the same approximation, i.e., the dominance of the first term of the residue series. The numerical method was mainly based on a contribution from the Administration of United States of America, while the graphical one was taken from a contribution presented by the French Administration. In both methods, the approximations referred above allow the evaluation of contributions from distance and antenna heights separately.

It should be noted that, in and above the VHF band, with horizontal polarization over any type of soil or vertical polarization over land, the effect of electrical characteristics of the Earth's surface may be disregarded. However, for vertical polarization over the sea at frequencies up to 300 MHz this effect must be taken into account. To do so, the numerical method described in Recommendation ITU-R P.526 includes a parameter  $\beta$  [Boithias, 1983] which depends on the effective relative permittivity  $\epsilon$  and the effective conductivity  $\sigma$  of the Earth. The same consideration is applied to the graphical solution, where a different pair of nomograms must be used in each situation.

In the case of line-of-sight paths with sub-path diffraction, it is recommended a linear interpolation between the limit of diffraction zone (clearance of 0.6 of the first Fresnel zone radius), where the attenuation relative to free-space is zero, and the radio horizon.

#### 4.1.2 Knife-edge diffraction

This highly idealized model is relevant only in those cases where the radius of curvature of the obstacle can be neglected as, for instance, in a path with a common horizon for both terminals. An approximate equation [Boithias, 1983] to evaluate the propagation loss relative to free-space due to a knife-edge, valid in the diffraction region, is given in Recommendation ITU-R P.526.

#### 4.1.3 Single rounded obstacle

The solution adopted by Recommendation ITU-R P.526 is based on the work of Dougherty and Maloney [1964] and of Dougherty and Wilkerson [1967]. According to these authors, the diffraction loss is given by:

$$A = J(\nu) + T(m, n) \quad (138)$$

where  $J(\nu)$  is the Fresnel-Kirchoff loss which supposes a single sharp obstacle (knife-edge) and  $T(m, n)$  a correction function to take into account the obstacle's dimensions ( $m$  and  $n$ ). The parameter  $\nu$  is defined by:

$$\nu = [2]^{1/2} h/F_1 \quad (139)$$

where  $h$  is the path obstruction measured from the line joining transmitting and receiving antennas and  $F_1$  is the first Fresnel zone radius evaluated where the obstacle is located. On the other hand, in the original notation of the above authors, the function  $T(m, n)$  is as follows:

$$T(m, n) = T(\rho) + Q(X) \quad (140)$$

where:

$$T(\rho) = 7,2\rho - 2\rho^2 + 3,6\rho^3 - 0,8\rho^4 \quad (141)$$

and

$$Q(X) = \begin{cases} 12,5 X & \text{for } 0 < X < 4 \\ 17 X - 6 - 20 \log X & \text{for } X \geq 4 \end{cases} \quad (142)$$

being  $m = \rho^2$ ;  $mn = X$ ;  $\rho = (\lambda^2 R)^{1/3} / \pi^{1/6} F_1$ ;  $X = (\pi R)^{1/3} \lambda^{2/3} h / F_1^2$  and  $R$  the obstacle radius of curvature.

An important problem in the application of this solution is the determination of the obstacle radius of curvature. A practical solution, which enables an acceptable accuracy [Crysdale, 1958; Assis, 1971], is to use the radius of curvature at the apex of a parabola fitted to obstacle profile in the vicinity of the top. If digital maps with information on ground topography are available, this procedure can be easily implemented.

#### 4.1.4 Double knife-edges

Two methods are proposed in Recommendation ITU-R P.526. The method by Epstein and Peterson [1953] is the simplest one. However, a correction based on [Millington *et al.*, 1962] is suggested to take into account the separation between edges. If one edge is predominant, it is recommended to use the Deygout method [Deygout, 1966]. In this case, the correction is not necessary.

#### 4.1.5 Multiple isolated obstacle

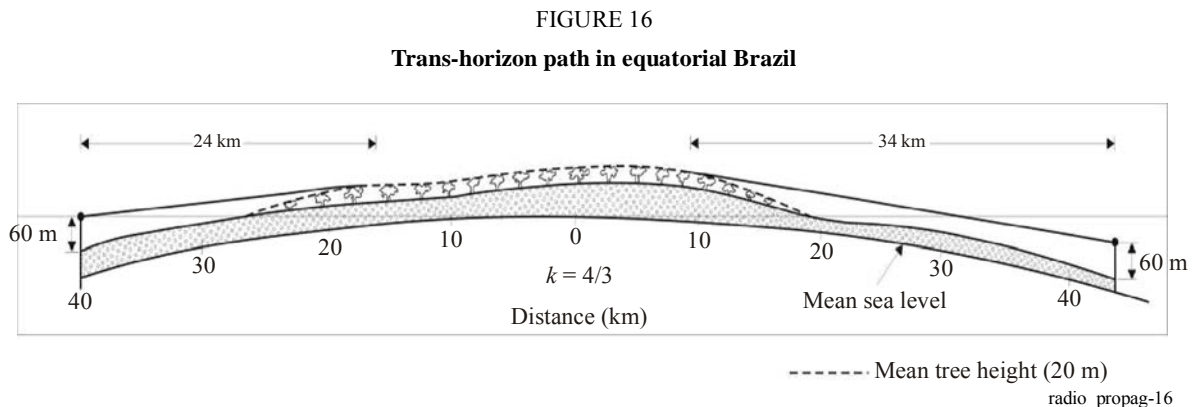
As it was pointed out before, for this case two methods are available in Recommendation ITU-R P.526. One is based on a cascaded arrangement of cylinders and the other based on knife-edge obstacles. The cascaded cylinder method has a solid mathematical basis, being supported by quite a lot of experimental results [Sharples and Mehler, 1989 and Eliades, 1993]. The knife-edge method is based on the approach proposed by Deygout [1966] limited to three edges plus an empirical correction. It can be shown that the Deygout model is compatible with the geometrical theory of diffraction [Pogozelski, 1980]. However, the empirical correction has no physical meaning, as the obstacle dimension is not taken into account.

It must be recognized that the knife-edge model is easier to implement in computer code and can be used as a first approach for planning purposes. However, when the accuracy is of paramount importance, preference should be given to the cascaded cylinder method.

#### 4.1.6 Application examples

##### 4.1.6.1 Spherical earth path

Figure 16 shows the profile of a 328 MHz path, 84 km long, located in the Amazon region, between the cities of Castanhal and Capanema, in the State of Pará, Brazil.



This path was plotted with an equivalent Earth radius of 8 500 km. Most of this path is covered by a dense forest, where the median tree height is around 20 m. Although not exactly a smooth spherical earth path, the procedure described in § 4.2.1 was used to calculate the diffraction loss. However, to guarantee the integrity of the physical problem, the distance between horizons (26 km), as well as the distance from each terminal to its horizon (24 km and 34 km) were maintained.

Within these assumptions, the following equivalent path was defined:

- path distance: 84 km;
- equivalent antenna height in terminal A:  $h_A = 34$  m;
- equivalent antenna height in terminal B:  $h_B = 68$  m.

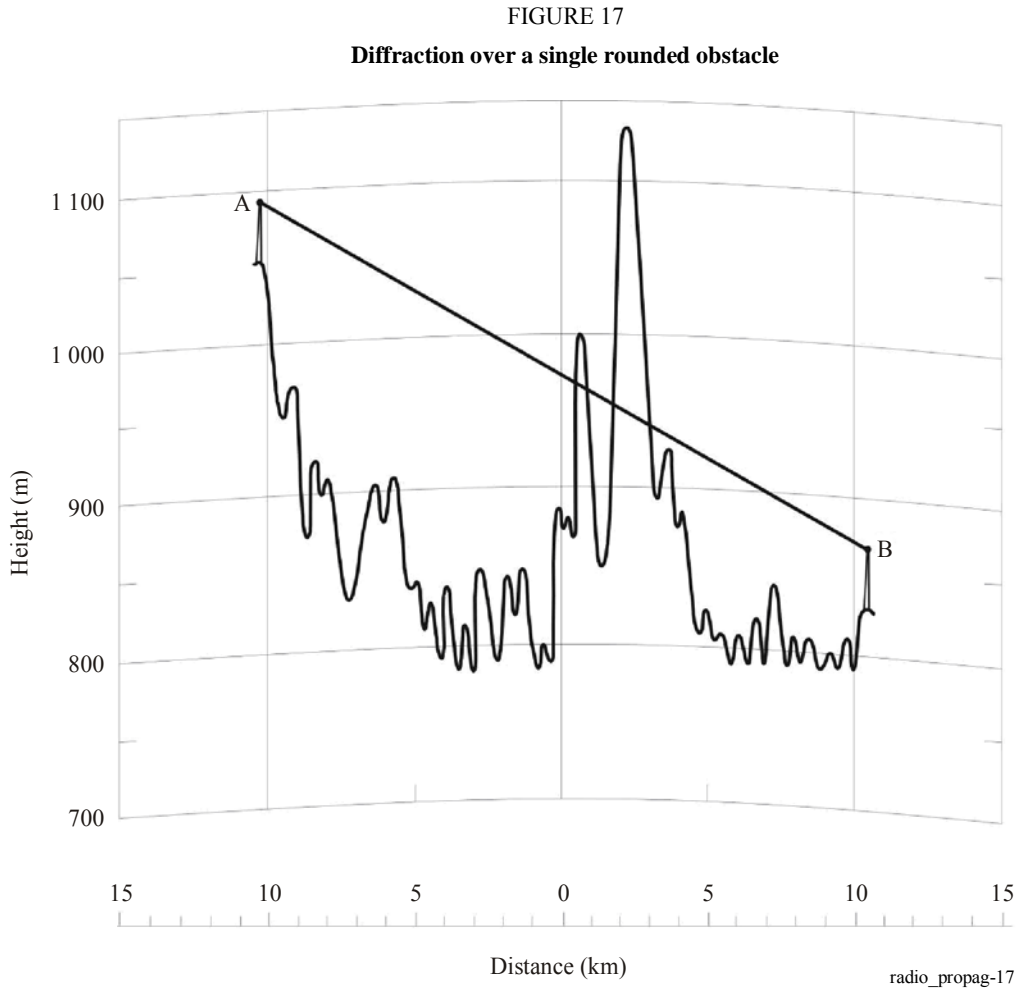
With these data the evaluation of diffraction loss is quite simple, i.e.:

- distance loss:  $-36.2$  dB ( $36.0$  dB with the nomogram);
- height gain in terminal A:  $-1.9$  dB ( $-1.5$  dB with the nomogram);
- height gain in terminal B:  $5.4$  dB ( $5.0$  dB with the nomogram).

Then the diffraction loss relative to free-space was 32.7 dB (or 36.5 dB with the nomograms). These values are well in accordance with the measured value (34.8 dB).

#### 4.1.6.2 Diffraction over a single obstacle

Figure 17 shows the profile of a 300 MHz diffraction path, 20.5 km long, between the cities of Bragança Paulista and Piracaia, in the State of São Paulo, Brazil. The path was plotted with an equivalent Earth radius of 8 500 km.



The basic parameters derived from the figure above are:

$$d_1 = 12.5 \text{ km}; \quad d_2 = 8.0 \text{ km}; \quad h_a = 1086 \text{ m}; \quad h_b = 865; \quad h_n = 1135 \text{ m}; \quad R = 1500 \text{ m}$$

when  $\lambda = 1 \text{ m}$ , according to Recommendation ITU-R P.526, the parameter  $\nu$  is obtained by:

$$h = h_n + d_1 d_2 / (2ka) - (h_a d_2 + h_b d_1) / d = 190 \text{ m} \quad (143)$$

$$\nu = h \sqrt{\frac{2}{\lambda} \left( \frac{1}{d_1} + \frac{1}{d_2} \right)} = 3.8 \quad (144)$$

with  $R$ ,  $d_1$ ,  $d_2$ ,  $h$  and  $\lambda$  in self-consistent units.

a) *Fresnel-Kirchoff loss*

From Recommendation ITU-R P.526:

$$J(v) = 6.9 + 20 \log \left( \sqrt{(v - 0.1)^2 + 1} + v - 0.1 \right) = 24.4 \text{ dB} \quad (145)$$

b) *Additional attenuation due to the curvature of the obstacle*

The application of Recommendation ITU-R P.526 leads to:

$$m = R \left[ \frac{d_1 + d_2}{d_1 d_2} \right] \Big/ \left[ \frac{\pi R}{\lambda} \right]^{1/3} = 0.018 \quad (146)$$

$$n = h \left[ \frac{\pi R}{\lambda} \right]^{2/3} \Big/ R = 35.5 \quad (147)$$

with  $R$ ,  $d_1$ ,  $d_2$ ,  $h$  and  $\lambda$  in self-consistent units.

$$T(m, n) = 7.2 m^{1/2} - (2 - 12.5 n)m + 3.6 m^{3/2} - 0.8 m^2 = 9.1 \text{ dB} \quad (148)$$

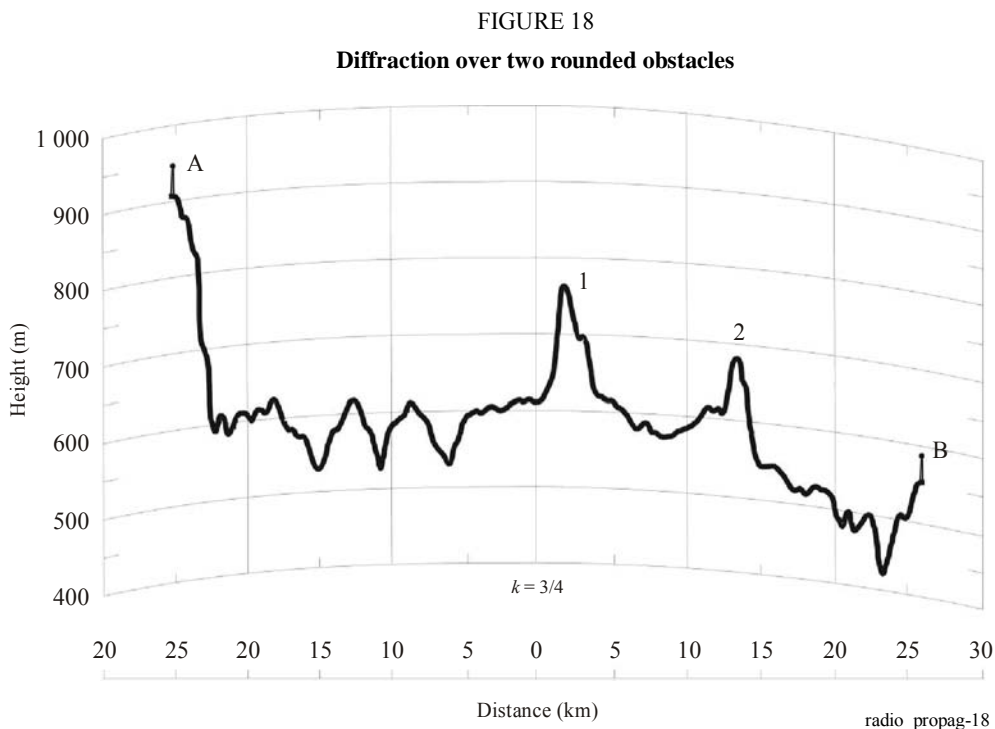
c) *Total diffraction loss*

$$A = J(v) + T(m, n) = 33.5 \text{ dB} \quad (149)$$

The measured value for the diffraction loss relative to free-space was 34.9 dB.

**4.1.6.3 Diffraction over several obstacles**

Figure 18 shows the profile of a 312.27 MHz ( $\lambda = 0.94 \text{ m}$ ) diffraction path, 50.6 km long, between two radio-relay stations in the vicinity of the city of Caçu, in the State of Goiás, Brazil.



The path was plotted with an equivalent Earth radius of 8 500 km. The basic parameters derived from the above figure are:

$$a = 26.6 \text{ km}; \quad b = 11.8 \text{ km}; \quad c = 12.2 \text{ km}; \quad h_a = 943 \text{ m}; \quad h_b = 591 \text{ m}; \quad h_{n1} = 762 \text{ m}; \quad h_{n2} = 684 \text{ m}$$

The radius of curvature of obstacles 1 and 2 are, respectively, 1 500 m and 1 000 m.

In the case of the cascaded cylinder method, the total diffraction loss in dB relative to free space is given in Recommendation ITU-R P.526:

$$L_d = L'_1 + L'_2 - 20 \log C_2 \quad (150)$$

where:

$L'_1$ : diffraction loss over the first cylinder calculated by the method given in Recommendation ITU-R P.526

$L'_2$ : the same for the second cylinder

$C_2$ : correction factor to account for spreading loss due to diffraction over successive cylinders.

The correction factor,  $C_2$ , is calculated using:

$$C_2 = (P_a/P_b)^{0.5} \quad (151)$$

$$P_a = abc(a + b + c) \quad (152)$$

$$P_b = ac(a + b)(b + c) \quad (153)$$

The parameters  $h'_{1,2}$  and  $v'_{1,2}$  for obstacles 1 and 2, calculated in the same way as in the previous example, are  $h'_1 = 17 \text{ m}$ ,  $v'_1 = 0.27$ ,  $h'_2 = 14.5 \text{ m}$ ,  $v'_2 = 0.27$ .

Then:

$$J(v_1) = J(v_2) = 8.4 \quad \text{dB} \quad (154)$$

The parameters  $m_1$ ,  $n_1$  and  $m_2$ ,  $n_2$  are calculated as in the previous example, giving  $m_1 = 0.011$ ,  $n_1 = 3.32$ ,  $m_2 = 0.011$  and  $n_2 = 3.24$ .

The additional losses due to the curvature of the obstacles are:

$$T_1(m_1, n_1) = T_2(m_2, n_2) \cong 1.2 \quad \text{dB} \quad (155)$$

The correction term to take into account the separation between the obstacles is given by:

$$C_2(\text{dB}) = 10 \log (P_a + P_b) = -1.9 \quad \text{dB} \quad (156)$$

and the excess loss becomes:

$$L = J(v_1) + T_1(m_1, n_1) + J(v_2) + T_2(m_2, n_2) - C_2 = 21.1 \quad \text{dB} \quad (157)$$

The measured excess loss in this link was 23 dB.

Alternatively, the cascaded knife-edge method can be used. The first step in the application of Deygout construction is to define the principal edge, i.e. the peak with the highest value of  $v$ .

For obstacle 1,  $d_1 = d_a = 26.6 \text{ km}$ ;  $d_2 = (d_b + d_c) = 24 \text{ km}$ ;  $h_n = 762 \text{ m}$ ;  $R = 1 500 \text{ m}$  giving:

$$h_1 = h_n + d_1 d_2 / (2ka) - (h_a d_2 + h_b d_1) / d = 41.6 \text{ m} \quad (158)$$

$$v_1 = h_1 \sqrt{\frac{2}{\lambda} \left( \frac{1}{d_1} + \frac{1}{d_2} \right)} = 0.54 \quad (159)$$

For obstacle 2,  $d_1 = (d_a + d_b) = 28.4$  km;  $d_2 = d_c = 12.2$  km;  $h_n = 684$  m;  $R = 1\,000$  m giving:

$$h_2 = h_n + d_1 d_2 / (2ka) - (h_a d_2 + h_b d_1) / d = 35.7 \text{ m} \quad (160)$$

$$v_2 = h_2 \sqrt{\frac{2}{\lambda} \left( \frac{1}{d_1} + \frac{1}{d_2} \right)} = 0.54 \quad (161)$$

As the value of  $v$  is the same for both obstacles, any of the two can be designated as principal. In this example, the obstacle 1 will be taken as the principal one.

The loss associated to the principal obstacle is given by:

$$J(v_1) = 6.9 + 20 \log \left( \sqrt{(v_1 - 0.1)^2 + 1} + v_1 - 0.1 \right) = 10.6 \text{ dB} \quad (162)$$

The loss associated to the secondary obstacle is a function of the new parameters  $h'_2$  and  $v'_2$  given with  $d_1 = d_b = 11.8$  km;  $d_2 = d_c = 12.2$  km;  $h_a = 762$  m;  $h_b = 591$  m;  $h_n = 684$  m;  $R = 1\,500$  m:

$$h'_2 = 14.5 \text{ m} \quad (163)$$

$$v'_2 = 0.27 \quad (164)$$

$$J(v'_2) = 6.9 + 20 \log \left( \sqrt{(v'_2 - 0.1)^2 + 1} + v'_2 - 0.1 \right) = 8.4 \text{ dB} \quad (165)$$

The empirical correction  $C$  is given in Recommendation ITU-R P.526:

$$C = 10.0 + 0.04 (d_a + d_b + d_c) = 12 \text{ dB} \quad (166)$$

The parameter  $T$  is given by:

$$T = 1.0 - \exp[-J(v_1)/6.0] = 0.83 \quad (167)$$

Finally, the diffraction loss is given in Recommendation ITU-R P.526:

$$L = J(v_1) + T [J(v_2) + C] = 27.5 \text{ dB} \quad (168)$$

## 4.2 Troposcatter transmission loss

The method given in Recommendation ITU-R P.617 for estimating the annual median transmission loss  $L(q)$  not exceeded for percentages of time greater than 50% is mainly based on the method developed by [Zhang, 1988], which itself is based in part on earlier methods [Rice *et al.*, 1967 and Boithias and Battesti, 1965] and whose basis were described in § 3.2. The general expression for the annual transmission loss not exceeded for  $q\%$  of the time is given by:

$$L(q) = M + 30 \log f + 30 \log \theta + 10 \log d + 30 \log \theta + L_N + L_c - G_t - G_r - Y(q) \quad (169)$$

where, besides the previously defined parameters ( $f$ ,  $d$ ,  $L_c$ ,  $\theta$ ,  $G_t$  and  $G_r$ ),  $M$  is a meteorological factor,  $L_N$  includes the transmission loss dependence on the height of the common volume and  $Y(q)$  is the difference between transmissions losses not exceeded for 50% and  $q\%$  of the time.

To elucidate the connection between the step-by-step procedure described in § 3 of the aforementioned Recommendation and the three empirical methods discussed in § 3.2 of this Handbook, it must be noted that:

- a) based on experimental data, values of the meteorological factor  $M$  and of the atmospheric structure parameter  $\gamma$  are given in Recommendation ITU-R P.617 for each climate cited in § 3.2;

- b) the height of the common volume above ground given in Recommendation ITU-R P.617 is an approximate expression as if the path section beyond the horizons of the two terminals is on a smooth Earth. In practice, the height can be accurately determined by the path geometry;
- c) the conversion factor  $Y(q)$  for  $q\%$  of the time was derived, as mentioned before, by a regression technique using the data bank of Radiocommunication Study Group 3 for climates 2, 6, 7a and 7b, and also based on three curves for  $Y(90)$  from [Rice *et al.*, 1967] for climates 1, 3 and 4 (no data were available to apply a regression technique for these three climates).

Additionally, the average worst-month median transmission loss distribution for time percentages greater than 50% is determined from the average annual distribution by means of a conversion factor based on the curves given by Boithias and Battesti [1965].

Finally, Recommendation ITU-R P.617 considers also the diversity reception. The equations given for horizontal and vertical space diversity are taken from [Fehlhaber and Grosskopf, 1967]. On the other hand, in the case of frequency diversity, the recommended separation is due to [Fehlhaber, 1967]. Angle diversity is also discussed. A simple system of this kind, employed at the receiver end, may provide a performance capability comparable to and considerably more economical than that of space diversity [Surenian, 1965]. Therefore, the performance of angle diversity is considered to be comparable to that of frequency diversity, although there is a slight increase in transmission loss.

#### 4.2.1 Path antenna gain

In a trans-horizon radio-relay system, the transmission of radio energy is due to the sum of re-radiations from all the atmospheric inhomogeneities illuminated by the transmitting antenna. Hence, a wave arriving at the receiving station is not a plane wave, so that the apparent gain of the receiving antenna is less than free-space gain (which is defined by a plane wave). For the same reason, the antenna beamwidth seems bigger than that in the case of a plane wave. This reduction in gain is known as "aperture-to-medium coupling loss" or "gain degradation".

A theoretical analysis of this phenomenon [Rice *et al.*, 1967], shows that the drop in gain will depend on the antenna gain and on distance. Contrary to this theoretical prediction, experience has shown that gain degradation is practically independent of distances between 150 km and 500 km [Boithias and Battesti, 1964], at least in temperate climates.

Based on experimental data, the following empirical equation [Boithias, 1983] was derived to calculate the total effective gain  $G_e$  over a troposcatter link as a function of the sum of free-space gains of both antennas:

$$G_e = (G_t + G_r) \exp\left(-\frac{a^4}{1 + a^4}\right) \quad (170)$$

where:

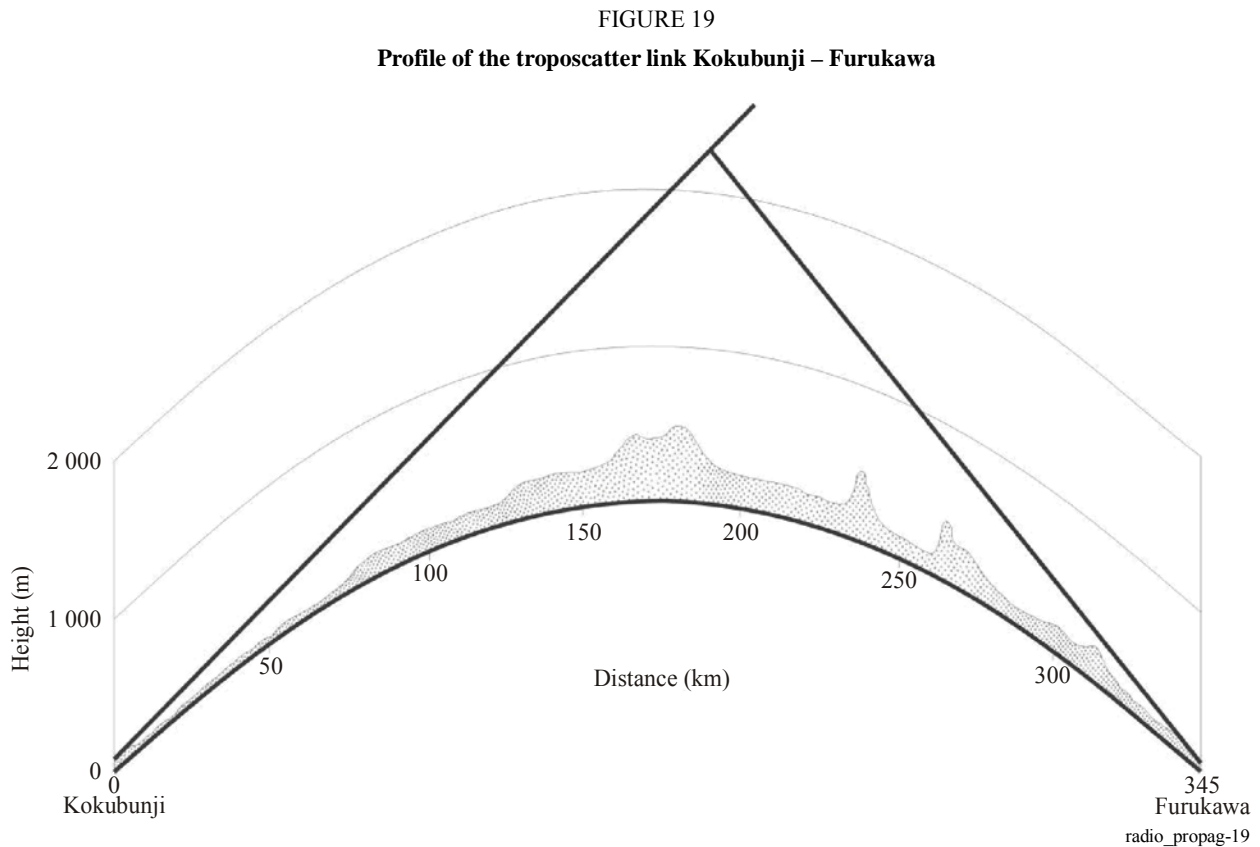
$$a = \frac{G_t + G_r}{148}$$

This formula is valid if  $G_t + G_r < 120$  dB and for similar gains of the two antennas.

A numerical analysis shows that the difference between the formula in [Boithias, 1983] and that given by equation (10) in Recommendation ITU-R P.617 has a mean value of -0.24 dB and a r.m.s. value of 0.61 dB for  $G_e$  between 50 and 100 dB.

### 4.2.2 Application example

Figure 19 shows the profile of a troposcatter link between Kokubunji and Furukawa in Japan.



The latitudes and longitudes are:

Kokubunji:  $35^{\circ} 42' 24''$  N;  $139^{\circ} 29' 18''$  E

Furukawa:  $38^{\circ} 34' 22''$  N;  $140^{\circ} 57' 51''$  E

The basic parameters are:  $f = 600$  MHz;  $d = 345$  km;  $h_1 = 103$  m;  $h_2 = 25$  m;  $h'_1 = 104$  m;  $h'_2 = 80$  m;  $d_1 = 4$  km;  $d_2 = 8$  km;  $G_t + G_r = 56$  dB.

The step-by-step procedure recommended in Recommendation ITU-R P.617 is used to calculate the transmission loss.

*Step 1:* Determine the appropriate climate for the link. This is an overland link between latitudes  $35^{\circ}$  N and  $39^{\circ}$  N. The surrounding terrain is rugged. The monthly mean surface refractivity was reported to have an annual range as large as about 60 N-units. According to the climate descriptions in Recommendation ITU-R P.617, the appropriate climate for the link should be of type 6, i.e., the continental temperate climate.

*Step 2:* Determine the meteorological and atmospheric structure parameters  $M$  and  $\gamma$ . From Recommendation ITU-R P.617, the two parameters for climate 6 are:

$$M = 29.73 \text{ dB}; \quad \gamma = 0.27 \text{ km}^{-1} \quad (171)$$

*Step 3:* Calculate the scatter angle  $\theta$ . The annual median decrease in refractivity over a 1 km layer from the surface for the region surrounding the link can be estimated using Recommendation ITU-R P.453 and found:

$$\Delta N \approx 40 N - \text{units} \quad (172)$$

Therefore, the effective Earth radius factor for median refractivity condition is:

$$k = 1/(1 - a \Delta N \times 10^{-6}) \cong 4/3 \quad (173)$$

where  $a$  is the true earth radius, i.e., 6370 km. The transmitter and receiver horizon angles are respectively:

$$\theta_t = (h'_1 - h_1)/d_1 - d_1 \cdot h_1/(2ka) \cong 0.2 \quad \text{mrad} \quad (174)$$

$$\theta_r = (h'_2 - h_2)/d_2 - d_2 \cdot h_2/(2ka) \cong 6.7 \quad \text{mrad} \quad (175)$$

According to Recommendation ITU-R P.617:

$$\theta = d \times 10^3 / (ka) + \theta_t + \theta_r = 47.7 \quad \text{mrad} \quad (176)$$

*Step 4:* Estimate the effect  $L_N$  of the height of the common volume. From Recommendation ITU-R P.617, with  $\gamma(\text{km}^{-1}) = 0.27$  (climate 6):

$$H = 10^{-3} \theta d/4 = 4.1 \quad \text{km} \quad (177)$$

$$h = 10^{-6} \theta^2 ka/8 = 2.4 \quad \text{km} \quad (178)$$

$$L_N = 20 \log(5 + \gamma H) + 4.34 \gamma h = 18.56 \quad \text{dB} \quad (179)$$

*Step 5:* Estimate the conversion factor  $Y(q)$  for non-exceedance percentage  $q$ .  $Y(q)$  can be estimate by the equation given in Recommendation ITU-R P.617:

$$Y(90) = -2.2 - (8.1 - 2.3 \times 10^{-4} f) \exp(-0.137 h) = -7.9 \quad \text{dB} \quad (180)$$

and according to the same Recommendation:

$$Y(q) = C(q) \cdot Y(90) \quad \text{dB} \quad (181)$$

with  $C(50) = 0$ ,  $C(99) = 1.82$  and  $C(99.9) = 2.41$ . Hence:

$$Y(50) = 0 \text{ dB}; \quad Y(99) = -14.41 \text{ dB}; \quad Y(99.9) = -19.1 \quad \text{dB} \quad (182)$$

*Step 6:* Estimate the aperture-to-medium coupling loss  $L_C$ . From Recommendation ITU-R P.617:

$$L_C = 0.07 \cdot \exp[0.055 (G_t + G_r)] = 1.52 \quad \text{dB} \quad (183)$$

*Step 7:* Estimate the average annual transmission loss  $L(q)$  not exceeded for  $q\%$  of the time. According to equation (169), with  $M = 29.73$  (climate 6):

$$L(50) = 152.9 \quad \text{dB}; \quad L(90) = 160.8 \quad \text{dB} \quad (184)$$

$$L(99) = 167.3 \quad \text{dB}; \quad L(99.9) = 172 \quad \text{dB} \quad (185)$$

For the annual transmission loss the measured results are:

$$L_{meas}(50) = 151.8 \quad \text{dB}; \quad L_{meas}(90) = 162.8 \quad \text{dB} \quad (186)$$

$$L_{meas}(99) = 169.8 \quad \text{dB} \quad (187)$$

and the prediction errors are 0.9 dB, -2 dB and -2.5 dB for 50%, 90% and 99% of the time, respectively.

Recommendation ITU-R P.617 also provides a step-by-step method for converting from the annual distribution to the worst month distribution.

*Step 8:* Determine the difference  $\Delta L(q)$  between the average annual transmission loss and the average worst-month transmission loss for  $q\%$  of the time. The equivalent distance can be obtained by:

$$d_e = \theta ka \times 10^{-3} = 400 \text{ km} \quad (188)$$

Recommendation ITU-R P.617 indicates the following values for  $\Delta L(q)$  in climate 6 and at an equivalent distance of 400 km:

$$\Delta L(50) = 5.9 \text{ dB}; \quad \Delta L(90) = 5.1 \text{ dB} \quad (189)$$

$$\Delta L(99) = 4.4 \text{ dB}; \quad \Delta L(99.9) = 4.0 \text{ dB} \quad (190)$$

*Step 9:* Estimate the average worst-month transmission loss  $L_w(q)$  for  $q\%$  of the time by adding the difference  $\Delta L(q)$  to the average transmission loss  $L(q)$ :

$$L_w(50) = 158.6 \text{ dB}; \quad L_w(90) = 165.9 \text{ dB} \quad (191)$$

$$L_w(99) = 171.5 \text{ dB}; \quad L_w(99.9) = 176 \text{ dB} \quad (192)$$

Data are not available for the worst-month.

### 4.2.3 Testing results

Tests were made for the various methods [Zhang, 1988; Rice *et al.*, 1967 and Boithias and Battesti, 1965]. Table 6 shows the testing results where, for simplicity, the above methods are referred to as I, II and III, respectively.

### 4.2.4 Combined loss and its variability

#### 4.2.4.1 Effect of frequency

It is generally agreed that the long-term median transmission loss between isotropic antennas (basic transmission loss) increases with the third power of the frequency up to 3 GHz, and linearly with the attenuation relative to free space. With a sampling period less than one hour, the frequency dependence of the attenuation relative to free space has been found to vary between  $f^2$  and  $f^{1/3}$  [Eklund and Wickerts, 1968]. Additionally, measurements made in France at 460 and 2 220 MHz over two distances, 325 km and 165 km, show that the law of dependence on frequency to be about  $f^2$  for 1% of the time and  $f$  for 99% of the time, on the long link and  $f^{1.5}$  for 1% of the time and  $f^{0.5}$  for 99% of the time, on the short link. This dependence was slightly higher in summer than winter, especially for the short link [Boithias and Battesti, 1983].

#### 4.2.4.2 Long-term and short-term transmission loss variations

Both slow and rapid field strength variations are observed. Slow fading is due to overall changes in refractive conditions of the atmosphere, and rapid fading to the movement of small-scale irregularities. The slow variations are well described by distributions of the hourly median transmission loss which are approximately log-normal with standard deviations between 4 dB and 8 dB, depending on climate.

The rapid fading is the result of the superposition of a number of variables, incoherent components, the amplitude of which is Rayleigh distributed. This is found to be nearly true when the distribution is analysed over periods of up to five minutes. If other types of signals contribute to the received signal, there is a modification of this distribution. Sudden, deep and fast fading events have been noted when a frontal disturbance passes over a link. Reflections from aircraft can give pronounced fast fading.

The fast fading has a frequency of a few fades per minute at VHF and a few Hertz at UHF. The frequency of the fast fading has been studied in terms of the time autocorrelation function, which provides a mean fading frequency for short periods of time for which the signal is stationary. The median value of the mean fading frequency was found to increase nearly proportionally to path length and carrier frequency, and to decrease slightly with increasing antenna diameter. The rapidity of fading is particularly important in digital signal transmission. The effect of rapid fading may be alleviated with diversity reception.

The subdivision of the fading into two components (slow and fast) is rather arbitrary and only intended to facilitate the mathematical analysis of this phenomenon. The fast fluctuations must be added to the slow variations of the received level. The resulting law for the received signal can thus be deduced, keeping in mind that the average value of the Rayleigh variable is, itself, a random variable obeying a log-normal law. For practical applications, a graphical method to combine slow and rapid fading distributions is available [Panther, 1972].

TABLE 6  
Prediction errors for tropospheric scatter paths  
Percentage of time

Path No.	50%			90%			99.9%		
	I	II	III	I	II	III	I	II	III
908	2.4	0.1	6.9	2.1	-2.4	5.3			
1440	-5.5	-10.5	-5.7	-6.9	-11.1	-9.0	-9.0	-12.7	-12.7
1441	-0.9	-6.0	-1.1	-1.1	-4.9	-2.4	-0.8	-3.8	-3.0
2064	1.7	-3.2	1.9	3.5	0.7	2.4	4.7	3.6	2.6
2272	-4.4	-6.3	1.5	-5.6	-10.2	-1.5	-5.3	-12.2	-2.8
2273	5.0	3.3	10.8	5.5	1.2	9.8	5.5	-1.0	8.6
2304	0.7	0.4	11.1	-2.3	-5.2	6.6	-2.7	-7.7	4.9
2305	0.6	-3.8	3.7	-0.1	-5.5	1.2	0.6	-5.8	0.3
2306	-4.9	-5.1	5.5	-3.1	-5.9	6.0	-0.8	-5.6	7.3
2307	0.9	-3.3	4.1	3.9	-1.3	5.5	7.3	1.2	7.6
4901	2.9	-0.2	6.1	3.3	2.7	8.2	6.3	7.7	12.6
5006	3.5	-1.2	5.0	7.1	3.5	7.2	4.1	1.4	3.0
5009	-2.0	-6.0	3.9	-2.3	-4.8	2.5	-6.9	-8.4	-3.2
9009	0.9	-0.9	14.9	-0.7	-2.7	12.4	-1.4	-3.6	10.8
9018	2.5	-1.6	2.5	1.1	0.1	1.1	0.3	1.9	0.3
9019	0.7	-1.2	5.6	1.5	0.8	5.4			
9034	3.7	1.8	10.8	1.8	-1.4	7.6	1.5	-2.9	6.1
9041	0.0	-2.6	6.4	7.4	5.9	10.0	10.5	10.0	10.0
9042	0.0	-1.1	-0.5	-4.1	-4.6	-4.7	-7.9	-7.9	-8.6
9043	0.0	0.7	4.6	6.9	7.6	-9.4			
9045	-0.4	-2.8	4.0	-3.2	-7.7	-0.7	-2.7	-8.9	-1.7
9046	0.1	-2.0	4.5	0.6	-3.2	3.9	2.5	-2.6	4.8
A	-3.7	-9.1	-2.7						
B	-0.6	-4.3	1.4						
C	-3.6	-7.6	-0.5						
Mean errors	0.0	-2.9	4.2	0.7	-2.2	3.9	0.3	-3.0	2.5
r.m.s. errors	2.7	4.4	6.2	4.0	5.2	6.5	5.2	6.8	7.0

#### 4.2.4.3 Seasonal and diurnal variations

In most climates transmission loss have significant seasonal variations along the year. Regarding diurnal variations, maximum transmission loss occurs in the late afternoon and the minimum in the morning.

In temperate climates, monthly median losses tend to be higher in winter than in summer. The range is 10 to 15 dB on 150 to 200 km overland paths, but decreases as the distance increases. Diurnal variations are most pronounced in summer, with a range of 5 to 10 dB on 100 to 200 km overland paths. Overseas paths are more likely to be affected by super-refraction and elevated layers than land paths, and so show larger variations. This may also apply to low, flat coastal regions in maritime zones.

In dry, hot desert climates attenuation reaches a maximum in the summer. The annual variation of the monthly medians may range from 15 to 20 dB for 200 to 300 km links, but also decreases as the distance increases. Variations exceeding 20 dB between hourly median values are observed in these climates.

In equatorial climates, the annual and diurnal variations are considerably smaller, the greatest values of transmission loss being in the rainy season.

In monsoon climates where measurements have been carried out (Senegal and Barbados), there are two high levels per year, one during the dry season and another during the rainy season. It should be mentioned that in these climates the maximum values of  $N_S$  (refractivity near the Earth's surface) occurs during the rainy season.

## 5 Propagation induced distortion

The distortion generated by multipath delays produces an intermodulation noise in analogue links and intersymbol interference in digital links. Multipath delay  $T_m$  is a measure of the width of the received waveform in the time domain when a single impulse function is transmitted through the channel. Its inverse is called coherence bandwidth  $B_c$ , which, from a practical point of view, defines the available or transmissible bandwidth [Hall, 1979; Boithias, 1983]. There are no significant effects if the bandwidth of the transmitted signal  $B$  is well within  $B_c$  or if the pulse duration of a transmitted digital signal is much longer than  $T_m$ . However, when the signal bandwidth is progressively broadened or the bit rate of the digital signal is progressively increased, the received signal becomes more and more distorted so that an increasing intermodulation noise appears in analogue systems and an increasing error rate, due to intersymbol interference, appears in digital systems.

The multipath delay in troposcatter propagation typically ranges from 0.1 to 1.0  $\mu\text{s}$ , depending on the path geometry and antenna beamwidth. This parameter can be calculated through a theoretical approach [Bello, 1969]. However, apart from the mathematical complexity, its agreement with the experimental data is only partial [Roda, 1988]. A rough estimation of  $T_m$  can be derived considering the phase shifts related to the size of the common volume of antenna beams, i.e., the path difference  $\Delta d$  given by:

$$\Delta d(m) = (\Omega^2 + \Omega\theta) \frac{d \times 10^3}{2} \quad (193)$$

where  $\Omega$  is the antenna 3 dB beamwidth and  $\theta$  and  $d$  are shown in Fig. 14, the angles being measured in mrad and the distance in km. Consequently,  $T_m$  ( $\mu\text{s}$ ) can be determined as follows:

$$T_m(\mu\text{s}) = \Delta d / (3 \times 10^2) \quad (194)$$

Regarding analogue links, the evaluation of the intermodulation noise is a quite difficult problem, which has not been fully solved. Some approximate methods are available [Medhurst, 1959; Beach and Trecker, 1963 and Sunde, 1964]. Experimental studies carried out in France [Battesti and Boithias, 1971] show that:

- an increase in the antenna gain widens the transmissible bandwidth to such an extent that the gain degradation also increases (i.e., for gains exceeding approximately 30 dB);
- all other things being equal, the transmissible bandwidth depends on the atmospheric structure and hence on the climatic zone in question;
- the usable bandwidth becomes narrower as the distance increases, but this is governed by a law which is not the same for all climates;

- the usable bandwidth becomes narrower when there are positive angles of departure, and wider, when these angles are negative.

In digital links, for bit rates up to 2 Mbit/s, multipath distortion usually is not a problem. However, for higher bit rates, there is an increase of bit errors as a function of the ratio  $T_m/T$ , where  $T$  is the duration of the transmitted symbols. The increase of the bit error rate (BER) is negligible for  $T_m/T$  up to values of 0.2 ~ 0.3 and increases rapidly above this limit. The most effective countermeasure against multipath distortion is the combination of diversity reception and adaptive equalization. This problem can be also reduced if the scatter angle and the antenna beamwidth are kept as small as possible, minimizing the largest path difference in the common volume.

## 6 Diversity techniques

The term diversity refers to the simultaneous reception of two or more signals carrying the same information. Diversity reception is mandatory in troposcatter radio links to overcome the effect of the variability of the received signal. In order to improve the reception, diversity signals must be the least correlated possible. Typical diversity configurations are: space diversity; frequency diversity; angle diversity; polarization diversity and time diversity.

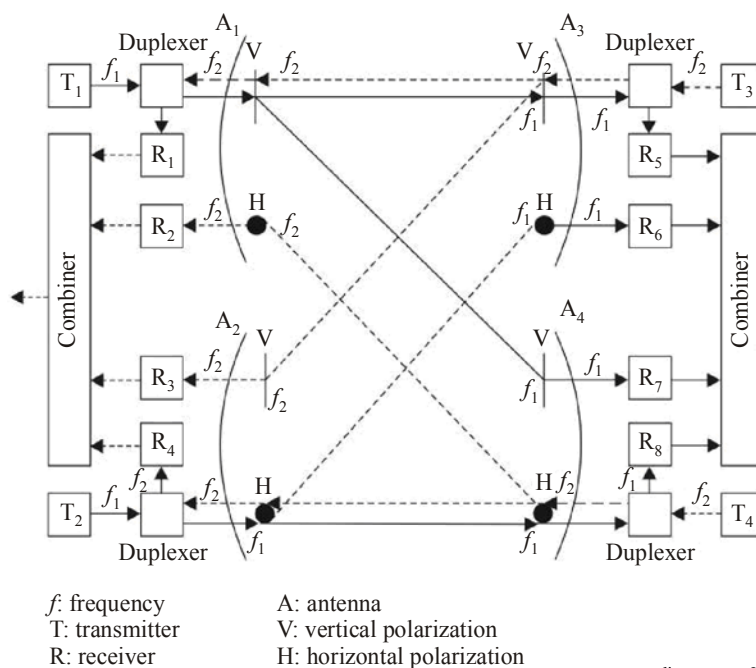
### 6.1 Space diversity

It is the most commonly used configuration. Current systems usually employ quadruple space-polarization diversity, with two cross-polarized antennas at each terminal to separate the two signals arriving at each receiving antenna, as can be seen in Fig. 20.

The design of this quadruple diversity system is somewhat critical, because the radio paths are only partially independent and a careful choice of antennas separation is necessary to obtain acceptable decorrelation [Larsen, 1980]. Dual space diversity is sometimes used. The cost saving of a dual diversity terminal compared to a quadruple diversity one is achieved at the expense of reliability, since the latter will still operate (with a reduced performance) should one of its transmitters fail [Roda, 1988].

FIGURE 20

Four-fold space diversity configuration



The effect of space diversity has been studied by Fehlhaber and Grosskopf [1967]. Adequate spacing  $\Delta h$  of two receiving antennas in a space diversity system depends on the scale length as defined by the space correlation function and on the antenna diameter of the receiving antenna. Because of the statistical character of the scale length, a value exceeded during 1% of time should be used. Recommendation ITU-R P.617 gives empirical formulas for  $\Delta h$ , for both horizontal and vertical separations.

## 6.2 Frequency diversity

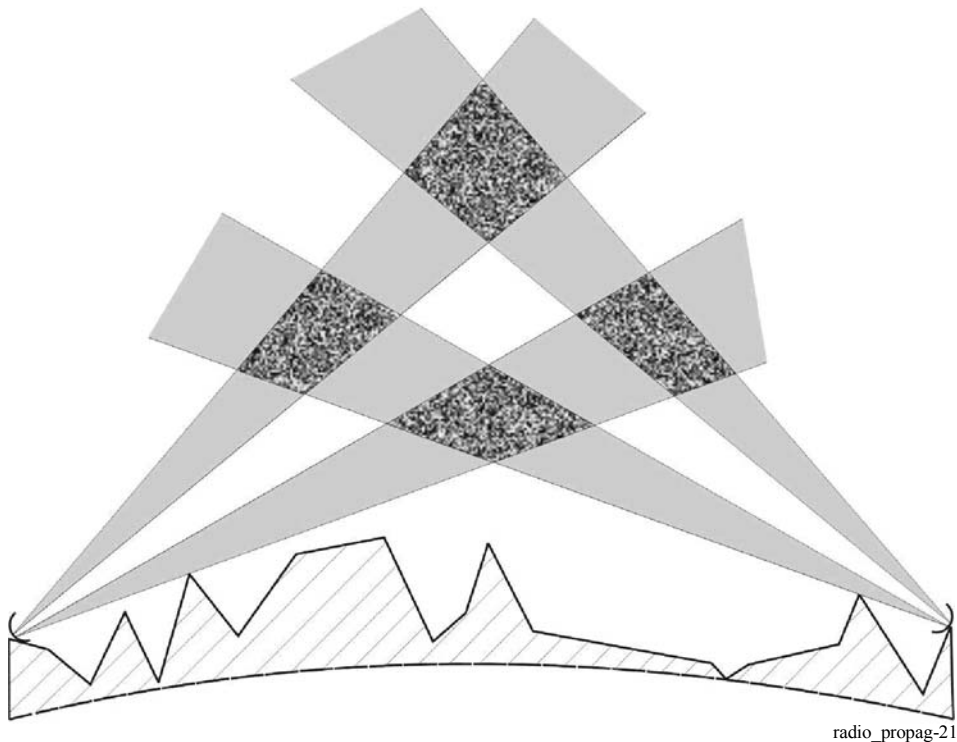
This configuration is not generally recommended because of the congestion of the radio spectrum. The variation in the frequency correlation coefficient with path length has been studied [Fehlhaber, 1967]. The same author has also investigated the appropriate frequency separation  $\Delta f$ . As a result of this study, a practical formula is given in Recommendation ITU-R P.617, as a function of frequency, antenna diameter, scatter angle and scale length in the vertical direction.

## 6.3 Angle diversity

Vertically displayed feeds are used at the receiving antenna to produce different vertically spaced common values as in the vertical space diversity. In dual diversity systems the signal is transmitted in one beam and received in two separated beams at different arrival angles. Although the two beams may also be horizontally separated, it has been found that vertical separation gives far better results [Roda, 1988]. In quadruple diversity system the signal is sent at the same frequency on two different beams creating four common volumes as shown in Fig. 21.

The various paths are reasonably decorrelated, but caution must be exercised, once they have different attenuations. A practical formula for the angular spacing between beams is given in Recommendation ITU-R P.617.

FIGURE 21  
Angle diversity



radio\_propag-21

## 6.4 Polarization diversity

There is experimental evidence that this configuration does not provide diversity gain. However, when used in conjunction with space diversity (see Fig. 21), the polarization discrimination allows the separation of two signals, transmitted on the same frequency with orthogonal polarizations, and at the receiving antenna by using orthogonal probes in the feed.

## 6.5 Time diversity

The information signal is repetitively transmitted at intervals longer than the inverse of the average fading rate. A kind of time diversity can be achieved in multipath situations when sufficient wideband signals  $B > B_c$  are transmitted that the multipath may be viewed as creating a series of echoes. This multipath diversity, called implicit diversity by Roda [1988], can be obtained by utilizing special modulation techniques, signal coding, etc. Frequency hopping and adaptive equalization are practical examples of this technique.

## 6.6 Combining techniques

There are four practical types of diversity combining systems:

- a) *Scanning diversity*: a selector device scans the channels in a fixed sequence until finding a signal above a preset threshold, uses that signal until it drops below the threshold, and then scans the other channels in the same fixed sequence until it again finds a signal above the threshold.
- b) *Selection diversity*: it is a more sophisticated version of the switched technique described above, where the best available signal is selected.
- c) *Maximal-ratio diversity*: before combining, the diversity signals are amplified inverse proportionally to the noise power, aiming a combined signal-to-noise ratio, which is at any moment, equal to or better than the best signal-to-noise ratios.
- d) *Equal gain diversity*: all diversity signals are combined after obtaining the same amplification gain.

A comparison between selection, maximal-ratio and equal gain techniques is presented in Figs. 22 and 23 for dual and quadruple diversity, respectively [Brennan, 1959].

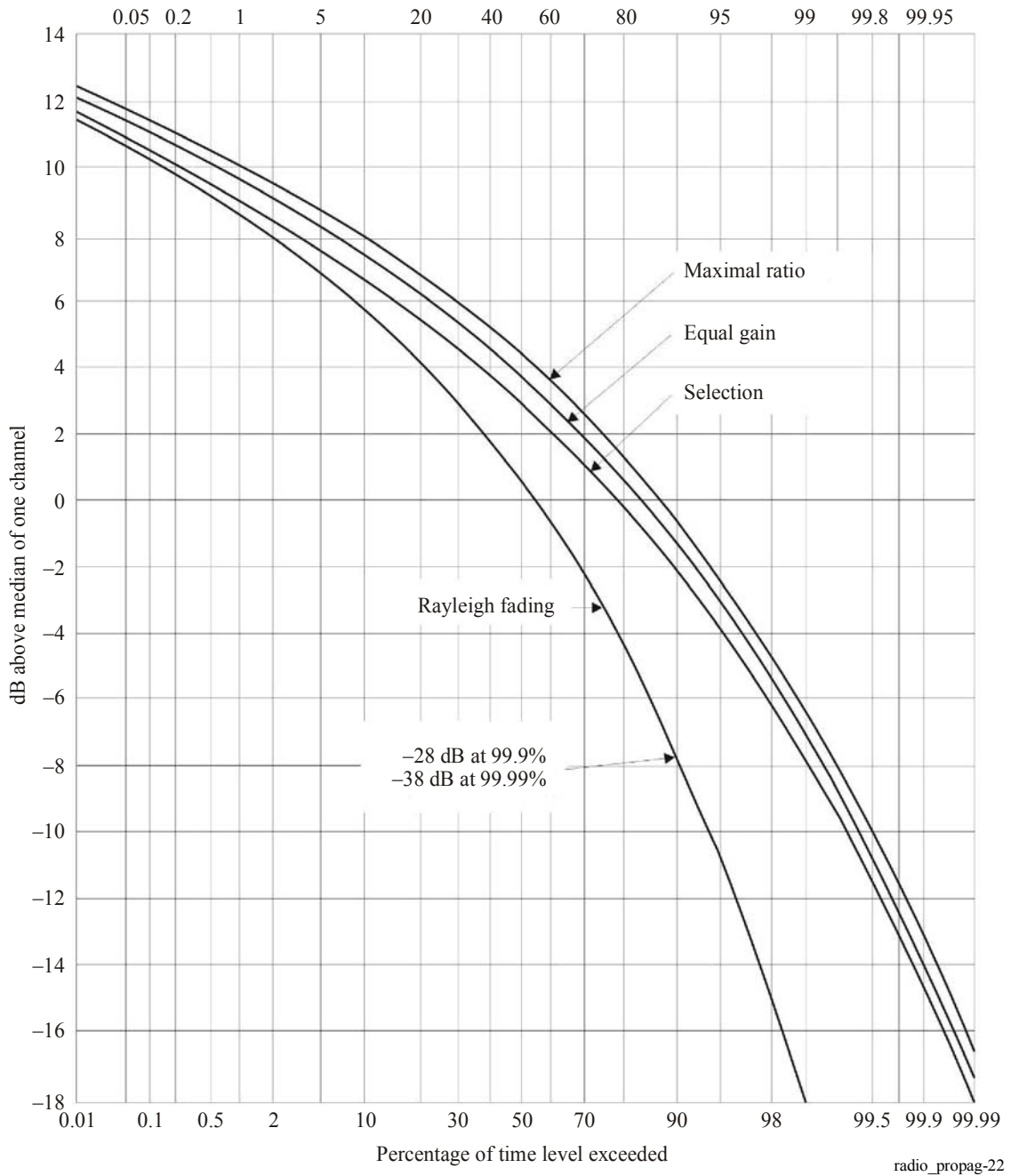
The maximal-ratio combiner is the most used, although the equal gain technique can result in equipment and maintenance simplification, at only a modest sacrifice (approximately 1 dB for quadruple diversity) in performance.

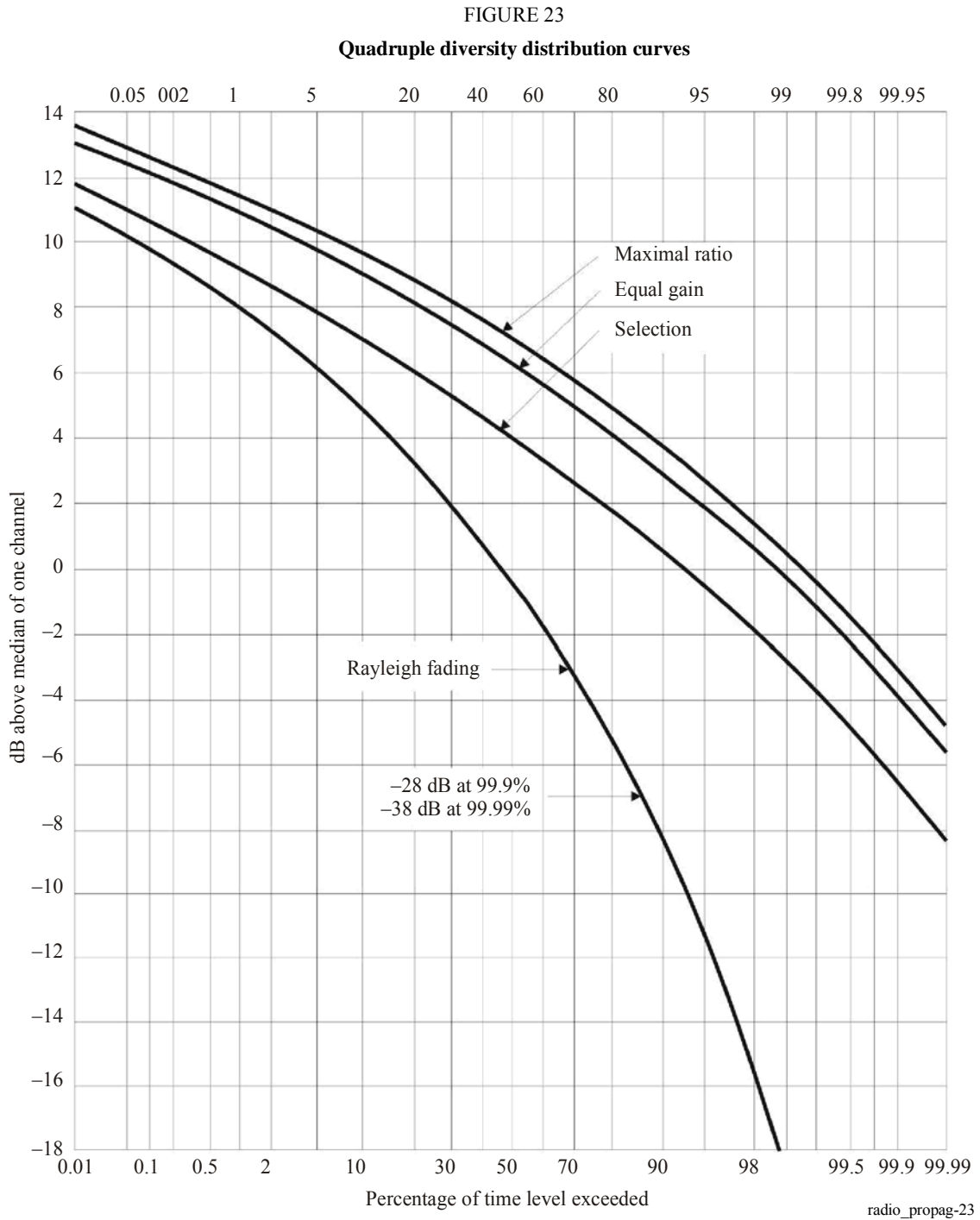
## 6.7 Diversity gain

It can be seen from Figs. 22 and 23 that the use of diversity results in a diversity gain for each percentage of time and that this gain increases as the time percentage increases. For example, with the selection type dual diversity there is a diversity gain of 15 dB for 99.9% of the time, since a signal of 28 dB below the median is raised to 13 dB below the median.

However, it must be pointed out that the term diversity gain, commonly employed to describe the effectiveness of various diversity configurations, is not a standard definition. For instance, in some cases, this term has the significance of diversity that reduces the fraction of time in which the signal drops to unusable levels.

FIGURE 22  
Dual diversity distribution curves





## References

- ASSIS, M. S. [1971] A simplified solution to the problem of multiple diffraction over rounded obstacles. *IEEE Trans. Ant. Prop.*, Vol. 19, p. 292-295.
- ASSIS, M. S. [1982] Effect of lateral profile on diffraction by natural obstacles. *Radio Sci.*, Vol. 17, 5, p. 1051-1054.
- ASSIS, M. S. [1986] Tropospheric propagation at low latitude areas. IEEE Global Telecommunications Conference, Houston, TX, United States of America.

- BARNETT, W. T. [1979] Microwave line-of-sight propagation with and without frequency diversity. *Bell BSTJ*, Vol. 49, **8**, p. 1827-1871.
- BATTESTI, J. and BOITHIAS, L. [1971] Nouveaux éléments sur la propagation par hétérogénéités de l'atmosphère. *Ann. des Télécomm.*, Vol. 26, p. 15-20.
- BEACH, C. D. and TRECKER, J. M. [1963] A method for predicting interchannel modulation due to multipath propagation in FM and PM tropospheric radio systems. *BSTJ*, Vol. 42, p. 1-36.
- BELLO, P. A. [1969] A troposcatter channel model. *IEEE Trans. Comm. Techn.*, Vol. 17, p. 130-137.
- BOITHIAS, L. [1983] *Propagation des Ondes Radioélectriques dans l'Environnement Terrestre*. Editions Dunod, Paris, France.
- BOITHIAS, L. and BATTESTI, J. [1964] Etude expérimentale de la baisse de gain d'antenne dans les liaisons transhorizon. *Ann. des Télécomm.*, Vol. 19, **9-10**, p. 221-229.
- BOITHIAS, L. and BATTESTI, J. [1965] Les faisceaux hertziens transhorizon de haute qualité. *Ann. des Télécomm.*, Vol. 20, **7-8**, p. 138-150.
- BOITHIAS, L. and BATTESTI, J. [1983] Propagation due to tropospheric inhomogeneities. *Proc. IEE*, Vol. 130, Part F, **7**, 657-664.
- BOOKER, H. G. and GORDON, W. E. [1950] A theory of radio scattering in the troposphere. *Proc. IRE*, Vol. 38, p. 401-412.
- BORN, M. and WOLF, E. [1970] *Principles of optics*. Pergamon Press, Oxford, United Kingdom.
- BREMMER, H. [1949] *Terrestrial Radio Waves*. Elsevier Publishing Co., Amsterdam, Netherland.
- BRENNAN, D. G. [1959] Linear diversity combining techniques. *Proc. IRE*, Vol. 47, p. 1075-1102.
- BULLINGTON, K. [1947] Radio propagation at frequencies above 30 Mc/s. *Proc. IRE*, Vol. 35, **10**, p. 1122-1136.
- CRYSDALE, J. H. [1958] Comparison of some experimental terrain diffraction losses with predictions based on Rice's theory for diffraction by a parabolic cylinder. *IRE Trans. Ant. Prop.*, Vol. 6, p. 293-295.
- DEYGOUT, J. [1966] Multiple knife-edge diffraction of microwaves. *IEEE Trans. Ant. Prop.*, Vol. 14, p. 480-489.
- DOUGHERTY, H. T. and MALONEY, L. J. [1964] Application of diffraction by convex surfaces to irregular terrain situations. *Radio Sci.*, J. Res. NBS, Vol. 68D, p. 239-250.
- DOUGHERTY, H. T. and WILKERSON, R. E. [1967] Determination of antenna height for protection against microwave diffraction fading. *Radio Sci.*, Vol. 2, p. 161-165.
- DU CASTEL, F. [1966] *Tropospheric radiowave propagation beyond the horizon*. Pergamon Press, New York, United States of America.
- EKLUND, F. and WICKERTS, S. [1968] Wavelength dependence of microwave propagation far beyond the radio horizon. *Radio Sci.*, Vol. 3, **11**, 1066-1074.
- ELIADES, D. E. [1993] Alternative derivation of the cascaded cylinder diffraction model. *Proc. IEE*, Part H, Vol. 140, p. 279-284.
- EPSTEIN J. and PETERSON, D. W. [1953] An experimental study of wave propagation at 850 Mc/s. *Proc. IRE*, Vol. 41, **5**, p. 595-611.
- FEHLHABER, L. [1967] Selektiver Schwund, übertragbare Bandbreite und Frequenzdiversity auf troposphärischen Scatterstrecken im Frequenzbereich zwischen 1 GHz und 10 GHz. *Tech. Ber. FTZ*, No. 5589.
- FEHLHABER, L. and GROSSKOPF, J. [1967] Das elektromagnetische Feld am Empfangsort einer troposphärischen Scatterstrecke. *NTZ*, Vol. 20, p. 511-520.
- FOCK, V. A. [1965] *Electromagnetic diffraction and propagation problems*. Pergamon Press, New York, United States of America.
- FRIIS, H. T., CRAWFORD, A. B. and HOGG, D. C. [1957] A reflection theory for propagation beyond the horizon. *BSTJ*, Vol. 36, p. 627-644.
- FURUTSU, K. [1963] On the theory of radio wave propagation over inhomogeneous earth. *J. Res. NBS*, Vol. 67D, p. 39-62.

- FURUTSU, K. and WILKERSON, R. E. [1970] Obstacles gain in radio-wave propagation over inhomogeneous earth. *Proc. IEE*, Vol. 117, p. 887-893.
- FURUTSU, K. and WILKERSON, R. E. [1971] Optical approximation for the residue series for terminal gain in radio-wave propagation over inhomogeneous earth. *Proc. IEE*, Vol. 118, p. 1197-1202.
- GIOVANELI, C. L. [1984] An analysis of simplified solutions for multiple knife-edge diffraction. *IEEE Trans. Ant. Prop.*, Vol. 32, p. 297-301.
- HALL, M. P. M. [1979] *Effects of the troposphere on radio communications*. Peter Peregrinus Ltd, Stevenage, United Kingdom.
- HUFFORD, G. A. [1952] An integral equation approach to the problem of wave propagation over an irregular surface. *Quart. J. Appl. Math.*, Vol. 9, p. 391-404.
- LARSEN, R. [1980] Quadruple space diversity in troposcatter systems. *Marconi Rev.*, p. 28-55.
- MEDHURST, R. G. [1959] Echo distortion in frequency modulation. *Electron. Radio Eng.*, Vol. 36, p. 253-259.
- MILLINGTON, G. [1949a] Ground wave propagation over an inhomogeneous smooth earth. *Proc. IEE*, Part III, Vol. 96, p. 53-64.
- MILLINGTON, G. [1949b] Ground wave propagation across a land/sea boundary. *Nature*, Vol. 163, p. 128.
- MILLINGTON, G. and ISTEAD, G. A. [1950] Ground wave propagation over an inhomogeneous smooth earth. *Proc. IEE*, Part III, Vol. 97, p. 209-222.
- MILLINGTON, G.; HEWITT, R. and IMMIRZI, F. S. [1962] Double knife-edge diffraction in field-strength prediction. *Proc. IEE*, Vol. 109C, p. 419-429.
- MONTEATH, G. D. [1951] Applications of the compensation theorem to certain radiation and propagation problems. *Proc. IEE*, Vol. 98, p. 23-30.
- OTT, R. H. [1971] An alternative integral equation for propagation over irregular terrain II. *Radio Sci.*, Vol. 6, p. 429-435.
- OTT, R. H. and BERRY, L. A. [1970] An alternative integral equation for propagation over irregular terrain. *Radio Sci.*, Vol. 5, p. 767-771.
- PANTHER, P. F. [1972] *Communications systems design – Line-of-sight and troposcatter systems*. McGraw-Hill, New York, United States of America.
- POGOZELSKI, R. J. [1980] A note on some common diffraction links models. *Radio Sci.*, Vol. 17, p. 1536-1540.
- RICE, P. L.; LONGLEY, A. G.; NORTON, K. A. and BARSIS, A. P. [1965 (Rev. 1967)] Transmission loss predictions for tropospheric communications circuits. NBS Tech. Note 101, Vols. 1 and 2, U.S. Dep. of Commerce. (Available as AD687-820, Natl. Tech Inf. Serv., Springfield, Va.)
- RODA, G. [1988] *Troposcatter radio links*. Artech House, Boston, United States of America.
- SHARPLES, P. A. and MEHLER, M. J. [1989] Cascaded cylinder model for predicting terrain diffraction loss at microwave frequencies. *Proc. IEE*, Part H, Vol. 136, p. 331-337.
- SUNDE, E. D. [1964] Intermodulation distortion in analog FM troposcatter systems. *BSTJ*, Vol. 43, p. 399-435.
- SURENIAN, D. [1965] Experimental results of angle diversity system tests. *IEEE Trans. Comm. Techn.*, Vol. 13, p. 208-219.
- VOGLER, L. E. [1982] An attenuation function for multiple knife-edge diffraction. *Radio Sci.*, Vol. 17, 6, p. 1541-1546.
- WAIT, J. R. [1974] Recent analytical investigations of electromagnetic ground wave propagation over inhomogeneous earth models. *Proc. IEEE*, Vol. 62, p. 1061-1072.
- WAIT, J. R. and CONDA, A. M. [1959] Diffraction of electromagnetic waves by smooth obstacles for grazing angles. *J. Res. NBS*, Vol. 63D, p. 181-197.
- ZHANG, M. [1977] Tropospheric scatter propagation. Monograph of China Research Institute of Radiowave Propagation.
- ZHANG, M. [1988] An Improved method for predicting the transmission loss due to troposcatter. International Symposium on Radio Propagation, Beijing, P. R. China.

## PART 3

### FREE-SPACE OPTICAL LINKS

#### 1 Introduction

This part of the ITU-R Handbook relates to planning and design of free-space optical (FSO) links. It provides background information on methods for calculating the various contributions for the total attenuation in such links, as given in Recommendation ITU-R P.1817. Also included are a brief discussion on additional issues to be taken into account in FSO system design and an application example.

#### 2 Initial considerations in designing an FSO link

In the design of FSO links several effects must be considered such as: loss due to atmospheric absorption, scattering and turbulence, microclimate environment and localized effects, link distance, mis-pointing, selection of wave length, data rates, eye–safety issues, and ambient solar attenuation.

FSO system operation requires line of sight (LOS). When testing for LOS, as FSO systems use beam expansion and a collimated beam, the clearance needed between the centre of the beam and any obstructions is equal to the beam radius. This is in contrast to RF systems where Fresnel clearance is needed.

The primary disadvantage of FSO systems is their vulnerability to atmospheric effects such as attenuation and scintillation, which can reduce link availability. Also, alignment of the laser communications terminal is more critical than is usual for RF systems, due to the narrow beam.

A key parameter in designing FSO links is the consideration of the power budget. The link margin,  $M_{link}$  (dB), which is the power available above the sensitivity of the receiver, can be given by the following equation:

$$M_{link} = P_e - S_r - A_{geo} - A_{atmo} - A_{scintillation} - A_{system} \quad (195)$$

where:

- $P_e$ : total power of the emitter (dBm)
- $S_r$ : sensitivity of the receiver, which depends on the bandwidth (data rate) (dBm)
- $A_{geo}$ : link geometrical attenuation due to transmit beam spreading with increasing range (dB)
- $A_{atmo}$ : atmospheric attenuation due to absorption and scattering (dB)
- $A_{scintillation}$ : attenuation due to atmospheric turbulence (dB)
- $A_{system}$ : represents all other system depending losses (dB) such as mis-pointing loss, receiver optical loss, beam wander loss, ambient light attenuation (solar radiation), etc.

The definition and computation of these terms and the initial considerations when planning an FSO link are given below.

The choice of a suitable link location is an important issue for the successful operation of an FSO system. The installation of FSO links has to take into account prevailing weather conditions, physical obstructions and surface types along the path, and transceiver mounting arrangements, to ensure optimum link performance.

#### **Weather**

- Weather conditions, and in particular the local climatology, in the vicinity of the chosen link path will influence the likely occurrence of snow, rain, drizzle fog, haze, aerosol and dust/sand that will lead to absorption and scattering of the transmitted signal.

**Path characteristics**

- Physical obstructions to the path between transmitter and receiver are clearly to be avoided. It is well worth bearing in mind that mature trees can increase in height by between 0.5 and 1 m in one year and vary in foliage density over the year.
- Links set up between buildings should take account of thermal vents that could result in hot air rising through the link path – resulting turbulence could lead to significant levels of scintillation at the receiver.
- The topography and the type of surface beneath an FSO line-of-sight path can significantly impact on the performance of the link. Those set up across river valleys, or across areas of open sea, will often experience increased incidents of fog. Building structures beneath the link may cause additional thermal activity in the air above them that may then lead to increased scintillation on the received signal.

**Transceiver mounting**

- Most FSO systems have very narrow beam widths and as a result the accurate set-up of the transceivers is critical; any misalignment causes significant loss of signal. The mount must be stable and direct mounting to substantial walls, or to the top of a single column, is considered essential for reliable performance over a period of time. Movement as the result of differential thermal expansion, or buffeting by wind, should be minimized.

**3 Geometrical attenuation**

Even in clear weather conditions, the beam diverges and the detector receives less power. The attenuation due to transmit beam spreading with increasing range is called geometrical attenuation and is given by equation (196):

$$A_{geo}(\text{dB}) = 10 \log_{10} \left( \frac{S_d}{S_{capture}} \right) = 10 \log_{10} \left( \frac{\frac{\pi}{4}(d\theta)^2}{S_{capture}} \right) \quad (196)$$

where:

- $S_d$ : surface area of transmit beam at range,  $d$
- $S_{capture}$ : receiver capture surface ( $\text{m}^2$ )
- $\theta$ : beam divergence (mrad)
- $d$ : transmitter-receiver distance (km).

**4 Atmospheric attenuation due to absorption and scattering**

Free-space optical (FSO) links are impaired by absorption and scattering of light by the Earth's atmosphere. The atmosphere interacts with light due to the composition of the atmosphere, which normally consists of a variety of different molecular species, small suspended particles (aerosol, fog) and precipitating particles (rain, snow and hail).

The attenuation of laser power is described by Beers's law [Weichel, 1990]:

$$\tau(\lambda, d) = \frac{P(\lambda, d)}{P(\lambda, 0)} = \exp\{-\gamma(\lambda) \cdot d\} \quad (197)$$

where:

- $\tau(\lambda, d)$ : transmittance at range  $d$  at wavelength  $\lambda$
- $P(\lambda, d)$ : laser power at the range  $d$
- $P(\lambda, 0)$ : laser power at the source
- $\gamma(\lambda)$ : attenuation or total extinction coefficient per unit length.

The extinction coefficient is composed of two parts:

$$\gamma(\lambda) = A_a + S_a \quad (198)$$

where  $A_a$  is the absorption coefficient ( $A_a$  represents the sum of all potential absorption coefficients i.e. molecular absorption, aerosol absorption) and  $S_a$  is the scattering coefficient ( $S_a$  represents the sum of all potential scattering coefficients i.e. molecular scattering, aerosol scattering, fog scattering etc.).

The atmospheric attenuation  $A_{atmo}$  can be written as the sum of two terms:

$$A_{atmo} = A_{clear\_air} + A_{excess} \quad (199)$$

where:

$A_{clear\_air}$ : attenuation under clear air (due to the presence of gaseous molecules)

$A_{excess}$ : attenuation due to the occasional presence of fog, mist, haze, drizzle, rain, snow, hail.

Atmosphere is a time varying transmission medium and as a result  $A_{atmo}$  is a stochastic process. However, imposing limits to system availability and thus its effects are generally treated on a statistical basis. The link margin,  $M_{link}$ , represents the amount of attenuation which can be tolerated by a given system at a given range.

#### 4.1 Clear air attenuation

Attenuation under clear air conditions is mainly the attenuation due to the absorption by the gaseous molecules. Absorption of radiations that propagate at specific optical wavelengths in the atmosphere results from the interaction between photons and atoms or molecules ( $N_2$ ,  $O_2$ ,  $H_2$ ,  $H_2O$ ,  $CO_2$ ,  $O_3$ , etc.) which leads to the disappearance of the incident photon and an elevation of the temperature. The absorption coefficient depends on the type of gas molecules and their concentration.

Molecular absorption is a selective phenomenon which results in a spectral transmission of the atmosphere presenting transparent zones, called atmospheric transmission windows, and opaque zones, called atmospheric blocking windows [Bouchet *et al.*, 2005 and Andrews and Phillips, 2005]. The important atmospheric molecules that have high absorption in the IR band include water,  $CO_2$ , ozone and  $O_3$ . Figure 24 presents the specific attenuation as calculated using LOWTRAN 7 software due to atmospheric gases in the frequency (wave number,  $1/\lambda$ ) range 20 to  $14,000\text{ cm}^{-1}$  – 600 GHz to 420 THz [Gibbins, 1999]. Because the size of the gaseous molecules is much smaller than the wavelength, scattering attenuation from the gaseous molecules is negligible [Pratt, 1969].

Usually the laser wavelengths are selected to fall inside atmospheric transmission windows, so  $A_{clear\_air}$  is negligible [Weichel, 1990]. The wavelengths generally used in FSO systems are near 690, 780, 850, and 1550 nm. However, applications in dense urban areas with high aerosol contents might slightly benefit from a different wavelength than relatively unpolluted suburban locations.

#### 4.2 Excess attenuation

Excess attenuation is regarded as the attenuation caused by the occasional presence of fog, mist, haze, drizzle, rain and snow particles. The presence of these particles causes an angular redistribution of the incident flux, known as scattering, and reduces the flux propagation in the original direction. However, there is no loss of energy like absorption. The physical size of the scatters with respect to the transmission laser wavelength determines the type of scattering. Table 5 shows the three different scattering regimes depending on the scatter's size and the approximate relationship between wavelength and the scatter's attenuation coefficient (effective-cross section). Also shown in Table 7 are the type of scatters falling in each regime for the visible and IR wavelengths [Kim *et al.*, 2000; McCartney, 1976 and Wallace and Hobbs, 1977].

FIGURE 24

Gaseous attenuation at infrared wavelengths

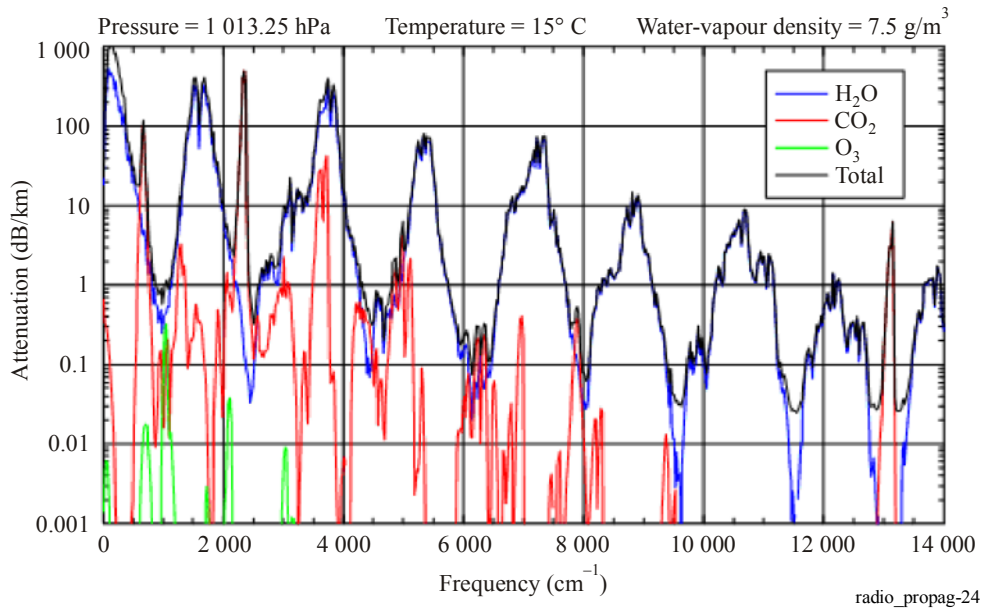


TABLE 7

Scattering regimes depending on the scatter size  $r$  with respect to wavelength  $\lambda$  and the approximate relationship between wavelength and scatter attenuation coefficient  $Q(\lambda)$

	Rayleigh scattering	Mie scattering	Non-selective or geometrical scattering
	$r \ll \lambda$ $Q(\lambda) \sim \lambda^{-4}$	$r \approx \lambda$ $Q(\lambda) \sim \lambda^{-1.6}$ to $Q(\lambda) \sim \lambda^0$	$r \gg \lambda$ $Q(\lambda) \sim \lambda^0$
Type of scatter	Air molecules Haze	Haze Fog Aerosol	Fog Rain Snow Hail

Because of the  $Q(\lambda) \sim \lambda^{-4}$  relationship of the Rayleigh regime the air molecular scattering contribution to the total attenuation coefficient is negligible [Pratt, 1969].

For particles that are much larger than the wavelength scattering can be described by geometric optics and there is no dependence on laser wavelength. Raindrops, snow, hail, cloud droplets and heavy fog will geometrically scatter laser light [Wallace and Hobbs, 1977].

For particles with size comparable to wavelength the Mie scattering regime can be applied. This theory is complicated but well understood. Fog and aerosol particles are the major contributors to the Mie scattering process.

An analytical approach can be used in which computation predictions of  $\gamma(\lambda)$  are made based on the theoretically derived effective cross-sections of atmospheric particles with assumed particle size distributions. However, particle size distribution of either aerosol or fog, which is a key parameter to determine their physical and optical properties, is not easy to model or even to measure.

#### 4.2.1 Mie scattering (estimation of fog attenuation)

Since using an analytical approach is not often very practical to compute the attenuation due to Mie Scattering empirical methods have been adopted by the FSO community. In these methods the attenuation coefficient due to Mie scattering is related to visibility.

The technical definition of visibility or visual range is the distance that light decreases to 2% of the original power or qualitatively visibility is the distance at which it is just possible to distinguish a dark object against the horizon [Middleton, 1952]. The visibility parameter is easily measured and stored in a meteorological station's or an airport's database, which allows geo-local performance evaluation of these telecommunication systems using the distribution of this parameter. However, it has to be pointed out that visibility data collected at airports may not necessarily represent conditions found either in urban environments, or in rural environments which can be very different in terms of topography and proximity to water.

An empirical simplified equation, which has been used in the FSO community for a long time to calculate the attenuation coefficient due to fog,  $\gamma_{fog}(\lambda)$  (dB/km), is found in [Weichel, 1990]:

$$\gamma_{fog}(\lambda) = \frac{3.91}{V} \left( \frac{\lambda}{550 \text{ nm}} \right)^{-q} \quad (200)$$

where:

$V$ : visibility (km)

$\lambda$ : wavelength (nm)

$q$ : coefficient which depends on the size distribution of the scattering particles.

It has been determined from experimental data [Kim, 1997; Middleton, 1952], but still is a subject of experimental work. It is given by [Weichel, 1990 and Pratt, 1969] as:

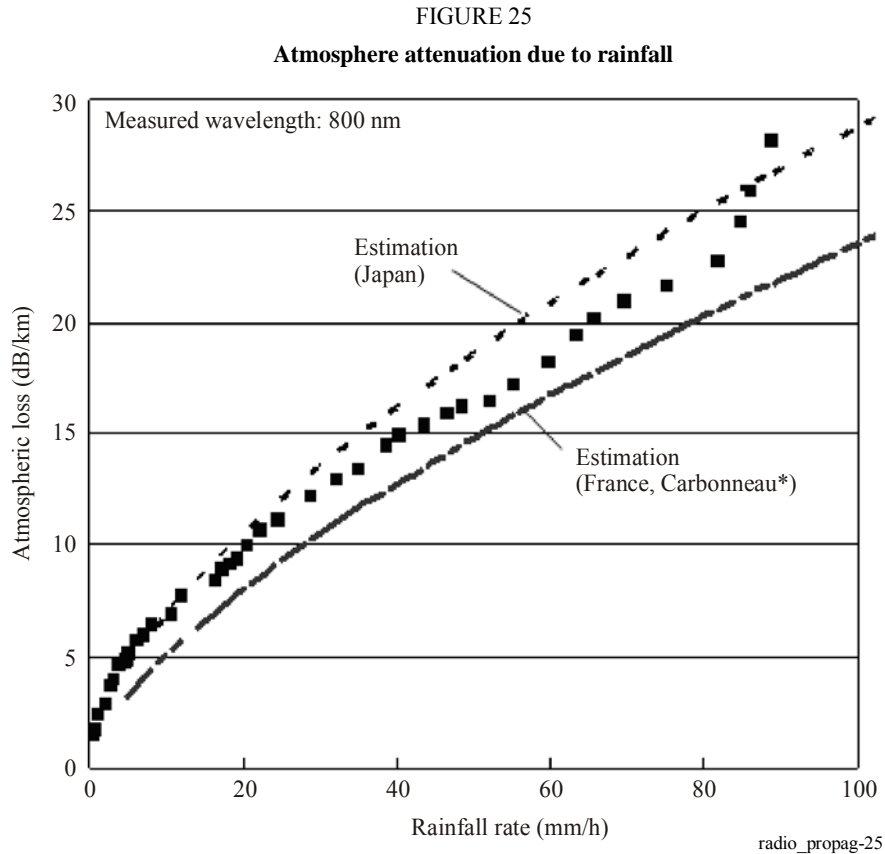
$$\begin{aligned} q &= 1.6 && \text{if } V > 50 \text{ km} \\ &= 1.3 && \text{if } 6 \text{ km} < V < 50 \text{ km} \\ &= 0.585V^{1/3} && \text{if } V < 6 \text{ km} \end{aligned} \quad (201)$$

To obtain the attenuation value exceeded for a given percentage of time  $p$  (i.e. for a given probability), the value of the visibility that was not exceeded for this percentage  $p$  is required according to equation (205). Recently improvements of the computation of fog attenuation have been proposed but are still subject to experimental work [Al Naboulsi *et al.*, 2004 and Kim *et al.*, 2000]. Table 8 shows the International Visibility Code (IVC) which correlates weather condition with a visibility range [Chu and Hogg, 1968 and McCartney, 1976].



Recommendation ITU-R P.837 gives the rainfall rate  $R(p)$  (mm/h) exceeded for given percentages of the average year,  $p$ , and for any location. Then equation (206) gives the value of the exceeded specific attenuation level for the percentage  $p$ .

Figure 25 illustrates the relation between  $\gamma_{rain}$  and rainfall rate  $R$  using the parameters in Table 7 for data measured in Japan.



### 4.2.3 Snow attenuation

Attenuation as a function of snowfall rate is given by the following relation:

$$\gamma_{snow} = a \cdot S^b \tag{203}$$

where:

$\gamma_{snow}$ : specific attenuation due to snow (dB/km)

$S$ : snowfall rate (mm/h)

$a$  and  $b$ : functions of the wavelength and are given by the following relation versus the wavelength  $\lambda$  (nm).

TABLE 10

**Parameters used for the estimation of the specific attenuation due to snow**

	<i>a</i>	<i>b</i>
Wet snow	$0.0001023\lambda + 3.7855466$	0.72
Dry snow	$0.0000542\lambda + 5.4958776$	1.38

**5 Scintillation effects**

A second major atmospheric process that affects the performance of laser communication systems is turbulence-induced atmospheric scintillation which causes severe fluctuations in received signal power.

Atmospheric turbulence produces temporary pockets of air with slightly different temperatures, different densities and thus different indices of refraction. Data can be lost due to beam wander and scintillation as the laser beam becomes deformed propagating through these index of refraction inhomogeneities. The significance of each effect depends on the size of these turbulence cells with respect to the laser beam diameter.

If the size of the turbulence cells is larger than the beam diameter, the laser beam as a whole randomly bends, causing possible signal loss if the beam wanders off the receiver aperture [Weichel, 1990 and Kim *et al.*, 1998]. For beam wander the longer wavelengths will have less beam wander than shorter wavelength although the wavelength dependence is weak. Although keeping a narrow beam on a track might be a problem, the fluctuation rate is slow (under a kHz or two), such that a tracking system can be used.

More commonly, if the size of the turbulence cells is smaller than the laser beam diameter, ray bending and diffraction cause distortions in the laser beam wave front [Weichel, 1990]. This results in temporal fluctuations, known as scintillations, in the laser beam intensity at the receiver which a frequency spectrum from 0.01 Hz to 200 Hz.

Tropospheric scintillations effects are generally studied from the logarithm of the amplitude  $\chi$  (dB) of the observed signal ("log-amplitude"), defined as the ratio in decibels between its instantaneous amplitude and its average value. The intensity and the speed of the fluctuations (scintillations frequency) increase with wave frequency. For a plane wave, a low turbulence and a specific receiver, the scintillation variance  $\sigma_x^2$  (dB<sup>2</sup>) can be expressed by the following equation:

$$\sigma_x^2 = 23.17 \cdot k^{7/6} \cdot C_n^2 \cdot L^{11/6} \quad (204)$$

where:

$$k = \frac{2\pi}{\lambda} : \text{ wave number (m}^{-1}\text{)}$$

$$L : \text{ length of the link (m)}$$

$$C_n^2 : \text{ refractive index structure parameter (m}^{-2/3}\text{)}.$$

The scintillations have peak amplitude of  $4\sigma_x$  and attenuation related to scintillation is equal to  $2\sigma_x$ . For strong turbulences, saturation of the variance given by the above relation is observed [Bataille, 1992]. The parameter  $C_n^2$  has a different value at optical wave lengths [Vasseur *et al.*, 1997] than at millimetre wavelengths. Scintillation at millimetre wavelengths is primarily due to humidity fluctuations, while at optical wavelengths scintillation is primarily a function of the temperature. One obtains in millimetre waves a value of  $C_n^2$  equal to about  $10^{-13} \text{ m}^{-2/3}$  what is an average turbulence (in general for millimetre waves we have  $10^{-14} < C_n^2 < 10^{-12}$ ) and in optical wave a value of  $C_n^2$  equal to about  $2 \times 10^{-15} \text{ m}^{-2/3}$  for low turbulence (in general for optic wave we have  $10^{-16} < C_n^2 < 10^{-13}$ ) [Bataille, 1992].

Figure 26 gives the variation of the attenuation of a 1.55  $\mu\text{m}$  wavelength optical beam for various types of turbulence at distances up to 2000 m. Clearly, attenuation increases as turbulence increases. Table 11 recapitulates the turbulence effect on optical and radio waves propagation. It should be noted that scintillations have effects definitely stronger on the optical beams lower wavelengths.

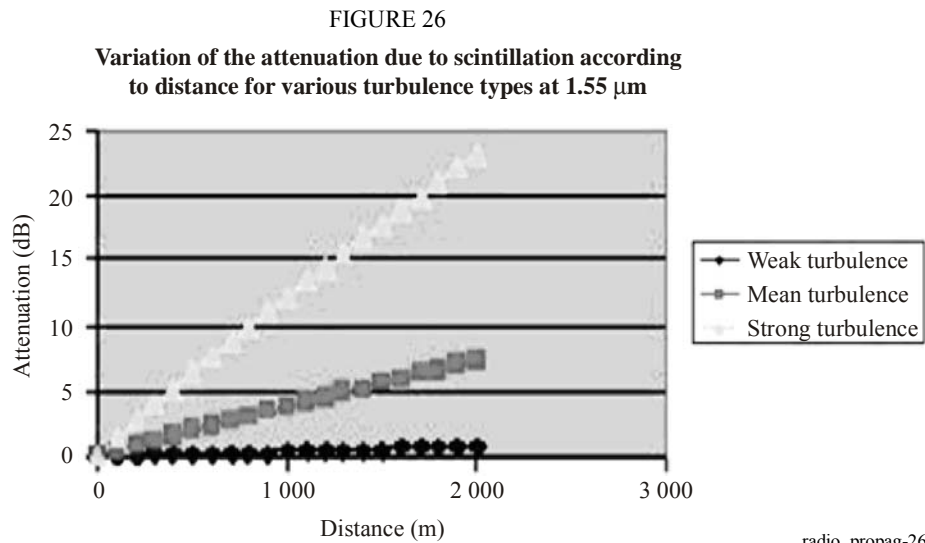


TABLE 11

### Summary of attenuation due to scintillation

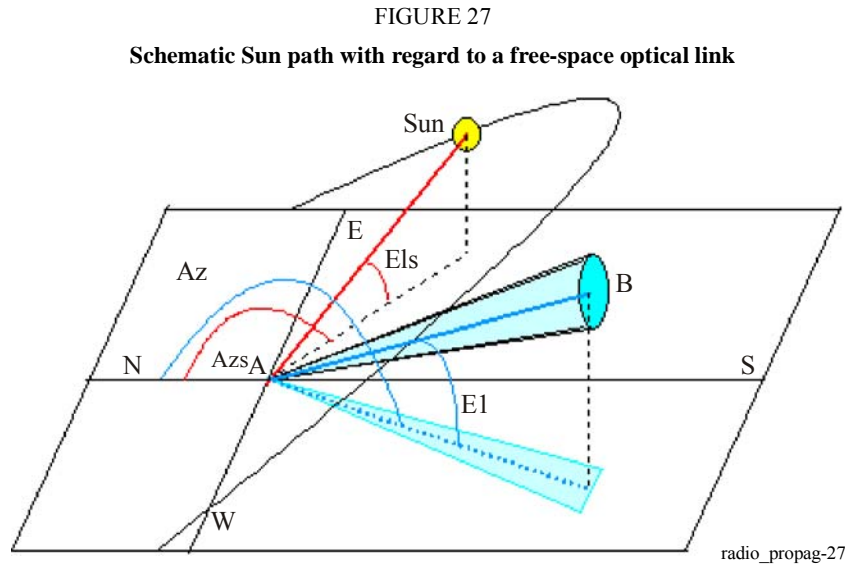
	Turbulence		
	Low	Moderate	High
$C_n^2$ optic waves ( $\text{m}^{-2/3}$ )	$10^{-16}$	$10^{-14}$	$10^{-13}$
Attenuation (0.98 $\mu\text{m}$ ) (dB)	0.51	5.06	16.00
Attenuation (1.55 $\mu\text{m}$ ) (dB)	0.39	3.87	12.25
$C_n^2$ millimetre waves ( $\text{m}^{-2/3}$ )	$10^{-15}$	$10^{-13}$	$10^{-12}$
Attenuation (40 GHz) (dB)	0.03	0.09	0.27
Attenuation (60 GHz) (dB)	0.03	0.11	0.35

Scintillation fluctuations can be reduced by using either multiple transmit beams or large receive apertures [Churnside, 1991 and Kim *et al.*, 1997]. Also to minimize the effects of scintillation on the transmission path, FSO systems should not be installed close to hot surfaces. Because scintillation decreases with altitude it is recommended that FSO systems must be installed a little bit higher above the rooftop (>1 m) and away from a side wall if the installation takes place in a desert-like environment.

## 6 Ambient light attenuation

Solar conjunction occurs when the sun or a reflected image of the sun is in or near the instantaneous field of view of an optical receiver (IFOV). The receive IFOV is generally at least as large as the transmit divergence. The problem becomes severe when the Sun's position is parallel to the optical link and the Sun power which penetrates inside the receiver is greater than the power received from the emitter.

Solar interference is usually reduced by arranging for the receiver to be positioned so that the Sun is always off axis. Figure 27 represents the geometry of the Sun path in the sky with regard to a free-space optical link (A is the receiver, B the emitter).



The power radiated by the Sun,  $P_{radiated}$  (W/m<sup>2</sup>) is defined by the following equation:

$$P_{radiated} = 1200 \cdot \cos\left(\frac{\pi}{2} - E_{ls}\right) \quad (205)$$

where  $E_{ls}$  is the Sun height (rad).

The received power is given by:

$$P_{solar} = F_{solar} \cdot P_{radiated} \cdot S_{capture} \cdot W_{receiver} / 100 \quad (206)$$

where:

- $F_{solar}$ : solar spectral power as a function of wavelength
- $S_{capture}$ : receiver capture surface area (m<sup>2</sup>)
- $W_{receiver}$ : receiver width band (nm).
- $F_{solar}$ : defined by the following relation:

$$\begin{aligned} F_{solar} = & 8.97162055148876 \times 10^{-13} \lambda^5 - 4.64912739129745 \times 10^{-9} \lambda^4 \\ & + 9.37072684333339 \times 10^{-6} \lambda^3 - 9.066632383289905 \times 10^{-3} \lambda^2 \\ & + 4.05479801934347 \lambda - 5.70237282654237 \end{aligned} \quad (207)$$

where  $\lambda$  is the wavelength (nm).

## 7 Other issues

Other factors that should be taken into account when an FSO system is designed include:

- International safety regulations strictly limit the maximum output power of optical systems. For 1550 nm, the regulatory agencies allow approximately 100 times higher power for “eye safe” lasers. The disadvantage of this laser type is mainly cost when compared to shorter wavelengths lasers operating around 850 nm.

- FSO transceivers can be located behind windows. The angle the beam makes with the window is critical. The angle should be as perpendicular as possible, yet slightly angled (5°) to reduce bounce-back of the beam to its receptor. Also some windows contain glass or glass coating that reduce glare. Because these windows are often specifically designed to reject infrared, the coatings can reduce the signal 60% or even more.
- Low visibilities will decrease the effectiveness and availability of FSO systems. Low visibility can occur during a specific time period within a year or day. Also low visibility can be a localized phenomenon (coastal fog). One solution to the negative impact of low visibility is to shorten the distance between the terminals which provides a greater link margin to handle bad weather conditions.

## 8 Application example

The step-by-step procedure recommended in Recommendation ITU-R P.1814 is used to calculate the link margin for systems with the following characteristics:

System parameters		
System A	System B	System C
Wavelength, $\lambda = 850$ nm	Wavelength, $\lambda = 850$ nm	Wavelength, $\lambda = 850$ nm
Total output power, $P_e = 100$ mW	Total output power, $P_e = 100$ mW	Total output power, $P_e = 100$ mW
Receiver sensitivity, $S_r = -46$ dBm	Receiver sensitivity, $S_r = -46$ dBm	Receiver sensitivity, $S_r = -46$ dBm
Receiver capture surface, $S_{capture} = 0.005$ m <sup>2</sup>	Receiver capture surface, $S_{capture} = 0.005$ m <sup>2</sup>	Receiver capture surface, $S_{capture} = 0.005$ m <sup>2</sup>
Beam divergence, $\theta = 2$ mrad	Beam divergence, $\theta = 2$ mrad	Beam divergence, $\theta = 2$ mrad
System loss, $A_{system} = 3$ dB	System loss, $A_{system} = 3$ dB	System loss, $A_{system} = 3$ dB
Location: France	Location: France	Location: France
Path length, $d = 500$ m	Path length, $d = 1\,000$ m	Path length, $d = 1\,000$ m

*Under clear air conditions:*

$$M_{link} = P_e - S_r - A_{system} - A_{geo} - \gamma_{clear\_air} \cdot d^*$$

System parameters		
System A	System B	System C
Geometrical attenuation $A_{geo} = 21.96$ dB	Geometrical attenuation $A_{geo} = 27.98$ dB	Geometrical attenuation $A_{geo} = 40.02$ dB
$M_{link} = 41.04$ dBm	$M_{link} = 35.02$ dBm	$M_{link} = 22.98$ dBm

\* Specific clear attenuation can be considered negligible.

**Under fog conditions:**

$$M_{link} = P_e - S_r - A_{system} - A_{geo} - \gamma_{clear\_air} \cdot d - \gamma_{fog} \cdot d$$

**Visibility  $V = 200$  m**

System parameters		
System A	System B	System C
$M_{link} = 32.61$ dBm	$M_{link} = 18.15$ dBm	$M_{link} = -44.49$ dBm

**Visibility  $V = 1000$  m**

$M_{link} = 39.52$ dBm	$M_{link} = 31.98$ dBm	$M_{link} = 10.83$ dBm
------------------------	------------------------	------------------------

**Under light rain conditions (rain rate  $R = 2.5$  mm/h):**

$$M_{link} = P_e - S_r - A_{system} - A_{geo} - \gamma_{clear\_air} \cdot d - \gamma_{rain} \cdot d$$

System parameters		
System A	System B	System C
$M_{link} = 40.05$ dBm	$M_{link} = 33.03$ dBm	$M_{link} = 15.02$ dBm

**Under heavy rain conditions (rain rate  $R = 25$  mm/h):**

$$M_{link} = P_e - S_r - A_{system} - A_{geo} - \gamma_{clear\_air} \cdot d - \gamma_{rain} \cdot d$$

System parameters		
System A	System B	System C
$M_{link} = 36.39$ dBm	$M_{link} = 25.72$ dBm	$M_{link} = -14.22$ dBm

## References

- AKIBA, M., WAKAMORI, K. and ITO, S. [2004] Measurement of optical propagation characteristics for free-space optical communication during rainfall. *IEICE Trans. Comm.*, Vol. E87-B, 7, p. 2053-2056.
- AL NABOULSI, M., SIZUN, H. and DE FORNEL, F. [2004] Fog attenuation prediction for optical and infrared waves. *Opt. Eng.*, Vol. 43, 2, p. 319-329.
- ANDREWS, L. C. and PHILLIPS, R. L. [2005] *Laser Beam Propagation through Random Media*. SPIE, Bellingham, Washington, United States of America.
- BATAILLE, P. [1992] Analyse du comportement d'un système de télécommunications optique fonctionnant à 0,83  $\mu\text{m}$  dans la basse atmosphère. Thèse de doctorat, Université de Rennes, France.
- BOUCHET, O., SIZUN, H., BOISROBERT, C., DE FORNEL, F. and FAVENNEC, P. N. [2005] *Free-Space Optics: Propagation and Communication*. Hermes, p. 214. ISBN: 978-1-905209-02-6 / 1-905209-02-9.
- CARBONNEAU, T. H. and WISELY, D. R. [1998] Opportunities and challenges for optical wireless; the competitive advantage of free space telecommunications links in today's crowded market place. SPIE Conference on optical wireless communications, Vol. 3232, Boston, Massachusetts, United States of America.
- CHU, T. S. and HOGG, D. C. [1968] Effects of precipitation on propagation at 0.63, 3.5 and 10.6 microns. *BSTJ*, Vol. 47, p. 723-759.
- CHURNSIDE, J. H. [1991] Aperture averaging of optical scintillations in the turbulent atmosphere. *Appl. Opt.*, 30, p. 1982-1994.
- GIBBINS, C. J. [1999] Propagation in the millimetric, submillimetric and infrared wavelength regions. A study for RACAL research. CCLRC RCRU-Rutherford Appleton Laboratory.
- HIROMOTO, N. [1997] Novel detector technologies for infrared communication and sensing. CRC International Topic Workshop on Space Laser Communication- Current Status and Future Perspectives, p. 90-95.
- KIM, I. I. *et al.* [1997] Measurement of scintillation and link margin for the TerraLink™ laser communication system. *Wireless Technologies and Systems: Millimeter Wave and Optical*. Proc. SPIE, 3232, p. 100-118.
- KIM, I. I., McARTHUR, B. and KOREVAAR, E. [2000] Comparison of laser beam propagation at 785 nm and 1550 nm in fog and haze for optical wireless communications. *Optical Wireless Communications III*. Proc. SPIE, 4214, p. 26-37.
- McCARTNEY, E. J. [1976] *Optics of the Atmosphere*. J. Wiley & Sons, New York, United States of America.
- MIDDLETON, W. E. K. [1952] *Vision Through the Atmosphere*. University of Toronto Press.
- ONTAR [1999] *Fascode Atmospheric code: PCLn/Fascode 3P*. Published by ONTAR Corporation, North Andover, Massachusetts, United States of America.
- PRATT, W. K. [1969] *Laser Communications Systems*. J. Wiley & Sons, New York, United States of America.
- VASSEUR H. V., OESTGES, C. and VANDER VORST, A. [1997] Influence de la troposphère sur les liaisons sans fil aux ondes millimétriques et optiques. Propagation électromagnétique du décimétrique à l'angström, 3<sup>èmes</sup> journées, Rennes, France.
- WALLACE, J. M. and HOBBS, P. V. [1977] *Atmospheric Science: An Introductory Survey*. Academic Press, Orlando, United States of America.
- WEICHEL, H. [1990] *Laser Beam Propagation in the Atmosphere*. SPIE Optical Engineering Press, Bellingham, WA, United States of America.
-







Printed in Switzerland  
Geneva, 2009  
ISBN 92-61-12771-1

Photo credits: Shutterstock